



UNIVERSIDAD DE INVESTIGACIÓN DE TECNOLOGÍA EXPERIMENTAL YACHAY

Escuela de Ciencias Químicas e Ingeniería

**Desarrollo e implementación de Delta Chem : Un nuevo
modelo geométrico para materiales porosos simétricos**

Trabajo de integración curricular presentado como requisito para la
obtención del título de Químico

Autor:

Castro Angamarca Jorge Luis

Tutor:

Ph.D. Thibault Terencio

Urcuqui, Julio 2020

Urcuquí, 9 de abril de 2020

SECRETARÍA GENERAL
(Vicerrectorado Académico/Cancillería)
ESCUELA DE CIENCIAS QUÍMICAS E INGENIERÍA
CARRERA DE QUÍMICA
ACTA DE DEFENSA No. UITEY-CHE-2020-00020-AD

A los 9 días del mes de abril de 2020, a las 14:15 horas, de manera virtual mediante videoconferencia, y ante el Tribunal Calificador, integrado por los docentes:

Presidente Tribunal de Defensa Dr. AVILA SOSA, EDWARD EBNER , Ph.D.
Miembro No Tutor Dr. CAETANO SOUSA MANUEL , Ph.D.
Tutor Dr. THIBAUT TERENCIO , Ph.D.

El(la) señor(ita) estudiante **CASTRO ANGAMARCA, JORGE LUIS**, con cédula de identidad No. **0105048458**, de la **ESCUELA DE CIENCIAS QUÍMICAS E INGENIERÍA**, de la Carrera de **QUÍMICA**, aprobada por el Consejo de Educación Superior (CES), mediante Resolución **RPC-SO-39-No.456-2014**, realiza a través de videoconferencia, la sustentación de su trabajo de titulación denominado: **A geometric approach of porosity: Development of Delta Chem, a new software for finding adsorption sites in microporous materials**, previa a la obtención del título de **QUÍMICO/A**.

El citado trabajo de titulación, fue debidamente aprobado por el(los) docente(s):

Tutor Dr. THIBAUT TERENCIO , Ph.D.

Y recibió las observaciones de los otros miembros del Tribunal Calificador, las mismas que han sido incorporadas por el(la) estudiante.

Previamente cumplidos los requisitos legales y reglamentarios, el trabajo de titulación fue sustentado por el(la) estudiante y examinado por los miembros del Tribunal Calificador. Escuchada la sustentación del trabajo de titulación a través de videoconferencia, que integró la exposición de el(la) estudiante sobre el contenido de la misma y las preguntas formuladas por los miembros del Tribunal, se califica la sustentación del trabajo de titulación con las siguientes calificaciones:

Tipo	Docente	Calificación
Presidente Tribunal De Defensa	Dr. AVILA SOSA, EDWARD EBNER , Ph.D.	10,0
Miembro Tribunal De Defensa	Dr. CAETANO SOUSA MANUEL , Ph.D.	10,0
Tutor	Dr. THIBAUT TERENCIO , Ph.D.	10,0

Lo que da un promedio de: **10 (Diez punto Cero)**, sobre 10 (diez), equivalente a: **APROBADO**

Para constancia de lo actuado, firman los miembros del Tribunal Calificador, el(la) estudiante y el(la) secretario ad-hoc.

Certifico que en cumplimiento del Decreto Ejecutivo 1017 de 16 de marzo de 2020, la defensa de trabajo de titulación (o examen de grado modalidad teórico práctica) se realizó vía virtual, por lo que las firmas de los miembros del Tribunal de Defensa de Grado, constan en forma digital.


CASTRO ANGAMARCA, JORGE LUIS
Estudiante

EDWARD EBNER Firmado digitalmente por
EDWARD EBNER AVILA SOSA
AVILA SOSA Fecha: 2020.05.08 17:25:02
+05'00'
Dr. AVILA SOSA, EDWARD EBNER , Ph.D.
Presidente Tribunal de Defensa

THIBAUT TERENCIO
Dr. THIBAUT TERENCIO , Ph.D.
Tutor
Firmado digitalmente por THIBAUT TERENCIO
Linea con THIBAUT TERENCIO en el
INSTITUTO NACIONAL CENTRAL DEL
Ecuador en 2020.05.08 17:25:02
Lectura de la firma de
THIBAUT TERENCIO en
Escuela de Ciencias Químicas e Ingeniería
Universidad Yachay Tech
Fecha: 2020.07.08 15:38:05.00

MANUEL
CAETANO SOUSA
Dr. CAETANO SOUSA MANUEL , Ph.D.
Miembro No Tutor

Digitally signed by MANUEL
CAETANO SOUSA
Date: 2020.07.08 15:07:53 -05'00'

 ANA MARIA
ESCOBAR
LANDAZURI

ESCOBAR LANDAZURI, ANA MARIA
Secretario Ad-hoc

AUTORÍA

Yo, **JORGE LUIS CASTRO ANGAMARCA**, con cédula de identidad 0105048458 ,declaro que las ideas, juicios, valoraciones, interpretaciones, consultas bibliográficas, definiciones y conceptualizaciones expuestas en el presente trabajo; así cómo, los procedimientos y herramientas utilizadas en la investigación, son de absoluta responsabilidad del autor del trabajo de integración curricular. Así mismo, me acojo a los reglamentos internos de la Universidad de Investigación de Tecnología Experimental Yachay.

Urququí, Julio 2020



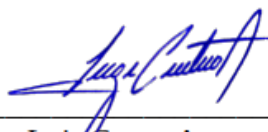
Jorge Luis Castro Angamarca
CI: 0105048458

AUTORIZACIÓN DE PUBLICACIÓN

Yo, **JORGE LUIS CASTRO ANGAMARCA**, con cédula de identidad 0105048458, cedo a la Universidad de Investigación de Tecnología Experimental Yachay, los derechos de publicación de la presente obra, sin que deba haber un reconocimiento económico por este concepto. Declaro además que el texto del presente trabajo de titulación no podrá ser cedido a ninguna empresa editorial para su publicación u otros fines, sin contar previamente con la autorización escrita de la Universidad.

Asimismo, autorizo a la Universidad que realice la digitalización y publicación de este trabajo de integración curricular en el repositorio virtual, de conformidad a lo dispuesto en el Art. 144 de la Ley Orgánica de Educación Superior

Urcuquí, Julio 2020.



Jorge Luis Castro Angamarca
CI: 0105048458

*To Jannys, you know, you remind me of a poem I can't remember, and a song that
may never have existed, and a place I'm not sure I've ever been to, but we both
know that everything about us was real, and will always be.*

Acknowledgements

I would like to thank my advisor Thibault for his great contribution to the development of this project and for having challenged me with a project that seemed impossible all the time until it was finally done. This was not an easy job for either of us and I definitely could not have arrived until the end of this adventure without his help. I definitely couldn't have had a better thesis advisor.

Thanks to the Yachay Tech professors who, despite all the problems the university has gone through have stayed with us, especially Manuel and Solmar for allowing me to learn from them and giving me their support and confidence at all times.

Thanks to my family, whose unconditional support has been my reason for never giving up. I also would like to thank

I can't put aside my friends and colleagues at Yachay Tech. A lot of my effort has been to be able to live up to it, and I really admire them.

Thanks to Alexandra Elbakyan for giving us Sci-Hub and free access to scientific knowledge from around the world. You're a hero, wherever you are, may the force be with you

Finally, I thank all the wonderful people that my experience in Yachay allowed me to meet in these five and a half years. Life is better friends, and my friends are the best of all. No matter what happens after this, coming to Yachay Tech was the right choice.

Jorge L. Castro

Abstract

The software Delta Chem works in the Computational Chemistry - Computational Geometry interface to implement a new approach of porosity for highly symmetric microporous materials. The proposed approach provides a double benefit. On one hand, it takes advantage of the symmetry of these materials to carry out a geometric approximation that significantly reduces the computational cost and the processing time for adsorption sites determination. On the other hand, the new approach provides a more realistic modeling of the internal surface of the porosities. Delta Chem performed a geometrical analysis of the structure of a microporous material using only the information of its .xyz to determine the irreducible volume of the porosities in the structure of a material. By construction, this region is representative of the whole cavity so the computational effort in adsorption sites determination can be concentrated in this region, using the critical points of the irreducible volume as candidates for the adsorption sites. Algebraic and Geometric operations like Delaunay Triangulation, Wythoff Construction, the fundamental algebraic transformations (Scaling, Translation, and Rotation), among others, are coordinately executed by Delta Chem through the use of the four subprograms or routines: Legando, Kerno, Mozaiko and Fragmento. Each of them is in charge of executing a wide variety of tasks including the implementation of several Python libraries and the external software PSD_solve [1], to perform the following fundamental processes: To read the input file provided by the user; determine porosity parameters: Center, size and contributing atoms for each porosity type; to model the internal surface of the porosities of the material and analyze their shapes; to find the polyhedron that best fits the shape of the porosity and use it to generate the irreducible volume. The approach has been tested for the determination of adsorption sites in MOF-5 using the package Quantum Espresso for periodic DFT calculations.

The code of Delta Chem was written in Python3.6 and it is available at the GitHub repository: https://github.com/jorgecastro316/Delta_Chem-.git

Keywords: Microporous materials, polyhedrons, Delaunay Triangulation, Wythoff Construction, adsorption sites, irreducible volume, PSD_solve, Delta Chem

Resumen

El software Delta Chem funciona en la interfaz de Química Computacional - Geometría Computacional para implementar un nuevo enfoque de porosidad para materiales microporosos altamente simétricos. El enfoque propuesto proporciona un doble beneficio. Por un lado, aprovecha la simetría de estos materiales para llevar a cabo una aproximación geométrica que reduce significativamente el costo computacional y el tiempo de procesamiento para la determinación de los sitios de adsorción. Por otro lado, el nuevo enfoque proporciona un modelado más realista de la superficie interna de las porosidades. Delta Chem realizó un análisis geométrico de la estructura de un material microporoso utilizando solo la información de su .xyz para determinar el volumen irreducible de las porosidades en la estructura de un material. Por construcción, esta región es representativa de toda la cavidad, por lo que el esfuerzo computacional en la determinación de los sitios de adsorción puede concentrarse en esta región, utilizando los puntos críticos del volumen irreducible como candidatos para los sitios de adsorción. Por construcción, esta región es representativa de toda la cavidad, por lo que el esfuerzo computacional en la determinación de los sitios de adsorción puede concentrarse en esta región. Operaciones algebraicas y geométricas como la triangulación de Delaunay, la construcción de Wythoff, las transformaciones algebraicas fundamentales (Scaling, Translation, Rotation), entre otros, son ejecutados de manera coordinada por Delta Chem mediante el uso de los cuatro subprogramas o rutinas: Legando, Kerno, Mozaiko y Fragmento. Cada uno de ellos está a cargo de ejecutar una amplia variedad de tareas, incluida la implementación de varias bibliotecas de Python y del software PSD_solve [1], para lograr los siguientes objetivos fundamentales: Leer el archivo de entrada proporcionado por el usuario; determinar los parámetros de porosidad: centro, tamaño y átomos contribuyentes para cada tipo de porosidad; modelar la superficie interna de las porosidades del material y analizar sus formas para encontrar el poliedro que mejor se adapte a la forma de la porosidad y usarlo para generar el volumen irreducible. El modelo de 'volumen irreducible' fue puesto a prueba para determinar los sitios de adsorción en MOF-5 utilizando el paquete Quantum Espresso para los cálculos de DFT.

El código de Delta Chem fue escrito en Python3.6 y está disponible en el repositorio de GitHub: [https://github.com/jorgecastro316/Delta_Chem-](https://github.com/jorgecastro316/Delta_Chem)

Palabras clave: Materiales microporosos, poliedros, triangulación de Delaunay, construcción de Wythoff, sitios de adsorción, volumen irreducible, PSD_solve, Delta Chem

Contents

Abstract	viii
Resumen	ix
1 Introduction	7
1.1 Preliminaries	9
1.1.1 Problem Statement	9
1.1.2 Justification	10
1.1.3 Document Organization	11
2 Objectives	12
2.1 General Objective	12
2.2 Specific Objectives	12
3 Theoretical Framework	13
3.1 Geometrical Section	13
3.1.1 Linear Algebra Concepts and Methods: The Power of the Matrix	13
3.1.2 Delaunay Triangulation: A Universe of Triangles	16
3.1.3 Wythoff Construction: Spherical Trigonometry to make it In-	
teresting	19
3.1.4 A journey to the Center of a Porosity	22
3.2 Chemical Section:	24
3.2.1 About MOFs and zeolites: Why microporous materials are so	
cool?	24
3.3 State-of-the-Art	26
3.3.1 Analyzed Microporous Materials	27
3.3.2 About Geometry applied to Chemistry: Triangles and Pores .	32
4 Methodology	34
4.1 From vectors to MOFs: Exploring Delta Chem.	34
4.1.1 Leganto: To understand Delta Chem is necessary to know how	
to read	35
4.1.2 'Kerno': an unexpectedly (hard) journey to Find the Center	
of the Porosities	37
4.1.3 Mozaiko: Modelling everything with Triangles	46
4.1.4 Fragmento: Let's find that Irreducible Volume	54

Contents	2
<hr/>	
4.2 Preliminary test of Delta Chem.	78
5 Results and Discussion	81
6 Conclusions and Perspectives	84
Bibliography	85

List of Figures

3.1	General Rotation	15
3.2	(a) Cloud of 46 points in 3D . (b) 3D Convex Hull of the triangulation in c (c)3D Delaunay triangulation of the cloud of points in a	17
3.3	Convex Hull H before (H_{i-1}) and after (H_i) adding point p	18
3.4	Incremental Algorithm for 3D Triangulation	19
3.5	Spherical triangle PQR, surface defined by the intersection of the great circles of a sphere.	20
3.6	Wythoffian constructions for the elemental triangle (4, 2, 3)	21
3.7	Graphic representation of the largest enclosing sphere optimization problem [1]	23
3.8	(a)Structure of MOF-5. (b)Pore size distribution obtained from PSD_solve for the structure given in (a)	24
3.9	HKUST-1 Structure: (a) $\text{Cu}_2(-\text{COO})_4$ SBU, (b) $(\text{C}_9\text{H}_3\text{O}_6)^{-3}$ BTC organic linker, (c) Cu-containing core structure, (d) HKUST-1 unit cell used for Delta Chem analysis	28
3.10	MOF-5 Structure: (a) $\text{Zn}_4\text{O}(-\text{COO})_6$ SBU, (b) $(\text{C}_8\text{H}_4\text{O}_4)^{-2}$ BDC or- ganic linker, (c) Zn-containing core structure, (d) MOF-5 unit cell used for Delta Chem analysis	29
3.11	UiO-66 Structure: (a) $\text{Zr}_6\text{O}_4(\text{OH})_4$ SBU, (b) $(\text{C}_8\text{H}_4\text{O}_4)^{-2}$ BDC organic linker, (c) Zr-containing core structure, (d)UiO-66 unit cell used for Delta Chem analysis	30
3.12	ZIF-8 Structure: (a) Imidazolate organic linker, (b) Zinc-coordinated core structure, (c)ZIF-8 unit cell used for Delta Chem analysis. <i>Color code: Zn-Brown, N-Blue, C-Black, H-White</i>	31
4.1	Structures of HKUST-1(a),UiO-66(b) and ZIF-8(c), read and repre- sented by Leganto(and Matplotlib)	37
4.2	PSD vs pore radius plots for (a)HKUST-1, (b)UiO-66 and (c)ZIF-8. The different types of porosities present in a material coincide with the number of peaks in the plots	38
4.3	Initial candidates for porosities centers in: (a)HKUST-1, (b)UiO-66, (c)ZIF-8.	40
4.4	Candidates after Filter 1 for: (a)HKUST-1, (b)UiO-66, (c)ZIF-8.	41

4.5	Neighbourhoods of Candidates created by Kerno through the function <i>grouping</i> . The structure used in the representation corresponds to the unit cell of MOF-5	42
4.6	Candidates after Filter 2: (a)HKUST-1, (b)UiO-66, (c)ZIF-8	43
4.7	Special geometrical situations in the structures of (a)MOF-5 and (b)HKUST-1	44
4.8	Final results provided by Kerno, includes centers of porosities, pore cavities' spheres, and contributing atoms of each porosity for (a)UiO-66, (b)ZIF-8, (c)HKUST-1	45
4.9	Convex Hulls of pore cavities for the structures of (a)UiO-66, (b)ZIF-8, (c)HKUST-1. Note the high symmetry of the resulting convex hulls.	47
4.10	Polygonalizations of the convex hull of (a) Small porosity(radius $\sim 2.382\text{\AA}$),(b) Medium porosity(radius $\sim 3.649\text{\AA}$),(c)Large porosity(radius $\sim 5.873\text{\AA}$) in HKUST-1 structure	50
4.11	Poligonalizations of the convex hull of (a)Small porosity(radius $\sim 3.828\text{\AA}$) (b)Large porosity(radius $\sim 4.425\text{\AA}$) in UiO-66 structure	51
4.12	Poligonalization of the convex hull of the single porosity(radius $\sim 5.773\text{\AA}$) in ZIF-8 structure	51
4.13	Example of Truncation in the small porosity (radius $\sim 5.911\text{\AA}$) in MOF-5 structure	53
4.14	Fitting with regular uniform polyhedrons for (a) Small porosity (radius $\sim 2.382\text{\AA}$),(b) Medium porosity (radius $\sim 3.649\text{\AA}$),(c) Large porosity (radius $\sim 5.873\text{\AA}$) in HKUST-1 structure	57
4.15	Fitting with regular uniform polyhedrons for (a) Small porosity(radius $\sim 3.828\text{\AA}$),(b) Large porosity(radius $\sim 4.425\text{\AA}$)	58
4.16	Fitting with regular uniform polyhedrons for the single porosity(radius $\sim 5.773\text{\AA}$) in ZIF-8 structure	58
4.17	Fitting with regular uniform polyhedrons for the structures of (a) UiO-66,(b) ZIF-8,(c) HKUST-1.Note the misalignment of some the polyhedrons.	59
4.18	Fittest polyhedron after first alignment transformation for structures of (a) UiO-66,(b) ZIF-8,(c) HKUST-1.	60
4.19	Example of alignment problem in regular polyhedrons: The cuboctahedron in the small porosity of MOF-5 structure.	61
4.20	Elemental Triangle (4,2,3)	64
4.21	Finding the incenter of a spherical triangle: Graphic Depiction	65

4.22	Wythoff construction of the triangle (4,2,3), with the generator vertex localized at the incenter (Part I)	66
4.23	Wythoff construction of the triangle (4,2,3), with the generator vertex localized at the incenter (Part II)	68
4.24	Finding the generator vertex on a side: Graphic depiction	68
4.25	(a) The elemental triangle (4,2,3). (b) Generator vertex(black dot) positioned on the hypotenuse (c) Generator vertex positioned in one of the legs of the elemental triangle. Note that the configuration A,B,C of the triangles in (b) and (c) is adapted so that the angle at B is bisected.	69
4.26	Wythoff Construction of the triangle (4,2,3), with the generator vertex localized at the Hypotenuse (Part I)	70
4.27	Wythoff construction of the triangle (4,2,3), with the generator vertex localized at the hypotenuse (Part II)	71
4.28	Wythoff construction of the triangle (4,2,3), with the generator vertex localized at one of the sides (Part I)	71
4.29	Wythoff construction of the triangle (4,2,3), with the generator vertex localized at one of the sides (Part II)	72
4.30	(a) The elemental triangle (4,2,3). (b) Generator vertex(black dot) positioned on the reference corner. (c) Generator vertex positioned in In a corner other than the reference. Note that the configuration A,B,C of the triangle in (b) is adapted so that the angle at B is bisected just like in the previous generator triangles.	73
4.31	Wythoff Construction of the triangle (4,2,3), with the generator vertex localized at reference corner (Part I)	74
4.32	Wythoff Construction of the triangle (4,2,3), with the generator vertex localized at reference corner (Part II)	74
4.33	Construction of the triangle (4,2,3), with the generator vertex localized at a corner other than the reference (Part I)	75
4.34	Construction of the triangle (4,2,3), with the generator vertex localized at a corner other than the reference (Part II)	76
4.35	Irreducible volumes obtained by Delta Chem for (a) HKUST-1, (b) UiO-66 and (c) ZIF-8	77
4.36	MOF-5 cluster used for DFT calculations with Quantum Espresso. <i>Color code: Zn-Brown, O-Red, C-Black, H-white</i>	79

5.1	Kerno's process results for MOF-5 structure, they include: Position of the centers of porosities, atoms contributing to the internal surface of each pore cavity, and sphere representing the pore cavities.	81
5.2	Triangulation, Polygonalization and Fitting processes results for MOF-5 structure: (a) Small porosity, (b) Big porosity.	82
5.3	Irreducible volumes of the porosities in MOF-5: (a) Side view,(b) Front view.	82
5.4	Position of the relevant point provided by Delta Chem, around the cluster model used for DFT calculations	83

Chapter 1

Introduction

Microporous Materials (also referred to as nanoporous by some authors) are those that, as their name implies, have in their structure pores, channels or cavities. They can be seen as 3D networks of atoms ordered so that they form arrays of uniformly-sized cavities with molecular dimensions [2]. Their pores are well-defined structures and their permanent porosity must be demonstrated by gas sorption isotherms [3]. For this reason, not all materials that have empty spaces in their structure can be called ‘porous’ or ‘microporous’.

Well delimited, molecule-sized, empty spaces can result in useful structures for applications in manipulating, separating, arranging and reacting molecules. Their usefulness lies in the permanent porosity provided by their structural stability in the absence of a guest¹ [4]. The precision with which the shape and size of these voids can be defined limits the control which can be exerted in their applications [3]. Inorganic Zeolites, Metal-Organic Frameworks(MOFs), Zeolitic Imidazolate Frameworks(ZIFs) and Covalent Organic Frameworks(COFs) are representative categories of these materials. The directionality of the bonds between their repetitive sub-units allows the formation of highly symmetric pore cavities. Naturally occurring microporous materials, like many Zeolites, are widely used as catalysts in the petrochemical industry [5]. However, synthetically obtained microporous materials result very attractive because it presents opportunities for the design of specific framework geometries and the assembly of crystalline materials which have up to 91.1% of the solid as the extra-framework volume, which can be rendered permanently porous, with pore sizes of up to 28.8Å [3].

A wide variety of shapes and volumes can be designed or find in nature, but all their structures share a common feature: a large surface area. The ordered arrays of atoms lining the pore walls can be thought of as defining a surface internal to the solid [3]. In these large surfaces, the adsorption phenomena become important. Indeed, since their particular structure allows access to large internal surfaces and cavities to a wide variety of molecules, important applications of these materials, like gas separation and storage, lie on their adsorption properties.

¹Solvent trapped inside the molecular framework that defines the cavity.

During adsorption a molecule, or ion, called adsorbate present in a fluid bulk (gas or liquid) is transferred and stuck on the surface of a solid known as adsorbent [6]. Often, the reverse process, desorption, may be present; therefore, not only the trapping of substances but also their release depends on these adsorption-desorption processes. They can be driven by physical interactions or chemical bonds [7].

If the adsorbate adheres to the surface because of physical forces, the process is called physical adsorption or physisorption. Physisorption involves Van Der Waals interactions only, these are attractive forces due to weak electrostatic interactions between the molecules of the adsorbate and the adsorbent. Chemical adsorption or chemisorption occurs if the adsorbate is chemically bound to the adsorbent's surface. The forces participating in chemisorption are much stronger than those of the physisorption, allowing the adsorbate to form a chemical bond with the structure of the adsorbent [7].

Adsorption based technologies exploit the ability of certain solids to selectively concentrate specific molecules in large quantities from solution or any bulk fluid [6]. Nowadays, adsorption of small molecules of gas or liquid is an important process for a wide variety of applications that include separation of air pollutants [8] and removal of volatile organic compounds, gas sensing, heterogeneous catalysis, wastewater treatment and storage of logistically important gases like hydrogen and methane [6].

The development of mesoporous materials with structures characterized by a high level of order during the 1990s motivated the emergence of experimental methods of structural characterization of the pores of a material based on adsorption isotherms [9]. The precise location of the adsorption sites was achieved with new characterization techniques such as Transmission Electron Microscopy (TEM) and Neutron and/or X-ray Diffraction [10]. These high precision techniques encouraged the discovery and creation of new nanomaterials with a wide range of novel applications. Therefore, the use and development of new theoretical and computational methods for the adequate analysis of data to describe the process of adsorption in the cavities of porous materials became necessary [10]. The methods of Computational Chemistry constitute important tools to investigate the adsorption of different adsorbate molecules in porous materials. Density Functional Theory or simply DFT stands out among other methods due to its compromise between data quality and computational cost. In addition, strict treatment at the Quantum-Mechanical level (QM) allows obtaining fundamental theoretical information about the system analyzed and the nature of the adsorption process [10]. The disadvantage of DFT (and basically every Ab Initio method) is that the computational cost scales as N^2 where N is the number of atoms present in the periodic cell [9]; considering that

the number of atoms in analyzed porous material can easily exceed 400 atoms, the computation time results really large, and can become even larger for adsorption studies where the adsorbed molecules must be included.

Highly symmetric structures of porosities in many of these materials clearly resembles the shape of uniform convex polyhedrons. This suggests that such symmetric systems can be represented using some elements and characteristics of these solids. The symmetry of a uniform polyhedron allows it to be wholly generated parting from a minimal section of its volume referred to in this project as irreducible volume. In this context, the present Capstone Project proposes a new approach of porosity that makes use of the symmetrical shape of these materials to generate a minimal representative region of the porosity, where high-level QM methods can be applied rigorously for the determination of the adsorption sites. The idea is to determine which uniform polyhedron (platonic or archimedean) that best resembles the shape of the internal surface of a porosity and use this *fittest polyhedron* to generate the Irreducible Volume. Then computational simulations of absorptive processes can be carried out placing the adsorbate molecules in this minimal region only. The reduction in the number of molecules used in the simulations of adsorption allows the reduction of the computational time consumed, and more importantly, to get all the QM effort focused in over a reduced region, right where it is needed. This idea was originally proposed by Thibault Terencio [11].

The program has been tested to obtain the irreducible volumes of the following materials: MOF-5, HKUST-1, UiO-66 and ZIF-8. They were chosen because they are considered ‘benchmark’ or ‘prototypical’ materials and the knowledge obtained from them is expected to apply to a broad range of microporous materials. Additionally, the Irreducible Volume approach was proven by using the information provided by Delta Chem in a simulation to determine the adsorption sites in MOF-5. The software package Quantum Espresso was used for the QM calculations with DFT.

1.1 Preliminaries

1.1.1 Problem Statement

Computational studies of microporous material face two main problems. The modeling of the internal surface of the porosities constitutes the first problem. The current model uses the atoms of framework’s joints, usually the metals, as vertices of a polyhedral representation of the pore cavities. However this model fails to represent the real internal surface of the materials where adsorption processes actually

take place.

As mentioned above, the DFT method's application is limited to systems with a small number of atoms (if the processing time is considered as an important factor). Given this situation, alternative methods and approaches have been proposed. The utilization of force-field based Grand Canonical Monte Carlo (GCMC) simulations have allowed a reasonable agreement with experimental data for some families of MOFs [10] [12]. However, different conditions of temperature, adsorbate molecules or families of materials may affect greatly the quality of the data, and the obtained values may considerably deviate from what is expected experimentally [10]. Some adjustments in the force field may produce a better agreement between the molecular simulations and the experimental isotherms, but they don't provide realistic adsorption mechanisms [10]. It is not convenient to completely ignore the QM methods since their applications in studies of microporous materials have contributed to the interpretation of experimental results and have led to predictions of properties even on materials that haven't been synthesized [10]. A desirable solution would be a computational model that presents a reasonable balance between the number of atoms in the model and computational cost, that could be transferable from one type of system to another, [3], and provides an accurate representation adsorption sites of small non-polarizable molecules at the interior of molecule-sized porosities.

1.1.2 Justification

In Ecuador, there has been little interaction between academia and the oil industry sector controlled by the State-owned Petroecuador and PetroAmazonas. Any of these companies have research and development departments [13]. This is worrisome considering the transcendental importance of the oil industry in the country's economy. This lack of scientific research has led to the national oil industry to a state where the crude oil treatment methods are almost rudimentary compared to those of the main oil-producing countries. Only in the region, in 2016 Colombia, an oil-exporting country with approximately one-fourth of Ecuador's oil reserves receives almost twice as much oil revenue per year than our country². While Colombian 'nanotechnology-based' developments have shown great potential for increasing the efficiency of different operations in the oil and gas industry, Ecuador imports all of its catalysts [13]. The need to modernize the oil industry (and many other industries in Ecuador) is obvious. Research in nanomaterials with direct application

²OPEC Annual Statistical Bulletin 2017: <http://www.worldstopexports.com/worlds-top-oil-exports-country/>

to improving the country's productive matrix should be a priority for ecuadorian government and academy. Computational Modeling is a powerful tool to provide insight into molecular-level details of the underlying mechanisms that can guide the current and future rational design and synthesis of microporous materials with significantly improved adsorption capability. [3]. To make feasible the use of DFT for adsorption studies in microporous materials, the irreducible volume approach is proposed as an alternative method to obtain accurate results with the advantage of requiring a minimum of adsorbate molecules, therefore reducing the computational cost and processing time. This approach also offers a new geometrical interpretation of the shape of the porosity that takes into account the atoms that directly contribute to the internal surface of the porosity instead of just the metals, providing a more realistic representation of the cavities in microporous materials. Since it is not depending on the nature of the atoms but only on the spacial disposition of the atomic spheres³, i.e the geometry of the system, this approach can be generalized for different types of microporous materials.

1.1.3 Document Organization

The present document has been divided into seven chapters: Introduction, Objectives, Theoretical Framework, Methodology, Results and Discussion, Conclusion and Perspectives.

Chapter 1 exposes briefly the scientific foundation of the project, then presents the problem statement, the justification of the project and the organization of the present document.

Chapter 2 shows the general and specific objectives of this research.

Chapter 3 presents the scientific base of the research. This is a brief review of the geometrical and computational methods used in the elaboration of Delta Chem and the State-of-the-Art on microporous materials and computational methods for studies of absorptive processes.

Chapter 4 provides a deep insight to the functioning of Delta Chem.

Chapter 5 is dedicated to the evaluation of Delta Chem by a comparative analysis of the positions provided by Delta Chem as candidates for adsorptions sites before and after geometric optimization.

Finally, Chapter 7 shows the conclusions of this work and presents some suggestions for enhancements in the accuracy of the program and future perspectives.

³Delta Chem treats the atoms geometrically as spheres with a given Van der Waals

Chapter 2

Objectives

2.1 General Objective

Propose a new approach of porosity for highly ordered microporous materials, to accurately represent the internal surface of these materials and allow a rigorous QM treatment to determine the position of their adsorption sites.

2.2 Specific Objectives

- Create a program written on Python that, given a .xyz file containing the structure of a microporous material, determines the irreducible volumes of the material's pore cavities.
- Evaluate the irreducible volume approach by comparing the results for the position of the adsorption sites obtained by Delta Chem against computational results upon geometric optimization of the studied system.

Chapter 3

Theoretical Framework

This project is the result of the coordinated application of methods taken from two different but slightly related disciplines: Computational Geometry and Computational Chemistry. It is therefore convenient to divide the description of these methods into two sections devoted to the geometrical and chemical components of the project. This separation has the purpose of making easier for the reader to understand (and for the author to explain) the role that the geometrical and algebraic operations below have in the complete work performed by Delta Chem. Let's get the theoretical bases required to do some geometry-based computational chemistry!

3.1 Geometrical Section

Most of this section is dedicated to describing the geometrical and algebraic operations that are performed on geometrical objects called polygons and their vertices. The most relevant operations, by its complexity, are Delaunay Triangulation, Wythoff Construction, and Localization of the center of a porosity. Each of them will be described in this section, but before we start to run, it is necessary to learn how to walk. Prior to delving into the description of the aftermentioned operations it is essential to insight the algebraic and geometrical operations that serve as gears for the complex machinery behind the functioning of every algorithm in Delta Chem.

3.1.1 Linear Algebra Concepts and Methods: The Power of the Matrix

Objects can be moved around in 3D space by manipulating their vertices, applying over them operations known as Transformations. The vertices of the object can be represented as vectors and the transformation is represented as a matrix. There are three basic types of transformations: Scaling, Translation, and Rotation [14].

Scaling

A scaling transformation can be used to make objects bigger or smaller. Mathematically, this transformation scales the coordinates of an object with respect to

the origin by multiplying each object's coordinate by a factor. It is represented by a 4x4 matrix with entries in the diagonal only [14]. Applying the transformation to the point P(u,v,w):

$$\begin{bmatrix} u & v & w & 1 \end{bmatrix} \begin{bmatrix} a & 0 & 0 & 0 \\ 0 & b & 0 & 0 \\ 0 & 0 & c & 0 \\ 0 & 0 & 0 & 1 \end{bmatrix} = \begin{bmatrix} au & bv & cw & 1 \end{bmatrix}$$

Translation

Translation transformation moves an object by a certain amount determined by a translation vector representing the coordinates of a destiny location. Mathematically, an object can be moved from an original position to another different by adding the coordinates of the translation vector to the originals. [14]. It also can be represented by a 4x4 matrix that has the translation movement put in the first three positions of the last row while the rest of the matrix looks the same as the identity matrix. Applying the transformation onto a point P(u,v,w):

$$\begin{bmatrix} u & v & w & 1 \end{bmatrix} \begin{bmatrix} 1 & 0 & 0 & 0 \\ 0 & 1 & 0 & 0 \\ 0 & 0 & 1 & 0 \\ T_x & T_y & T_z & 1 \end{bmatrix} = \begin{bmatrix} u + T_x & v + T_y & w + T_z & 1 \end{bmatrix}$$

Rotation

Rotation is a little bit more complicated than the past transformations since it involves trigonometry. In general, it consist in moving an object around a given rotation axis in an angle θ . Rotation can also be represented as a matrix but its entries can vary depending on the angle and the axis of rotation. The rotations around the coordinate axis for a given angle θ , are well identified and are the following for x,y and z axis respectively [15]:

$$\begin{bmatrix} 1 & 0 & 0 & 0 \\ 0 & \cos\theta & -\sin\theta & 0 \\ 0 & \sin\theta & \cos\theta & 0 \\ 0 & 0 & 0 & 1 \end{bmatrix} \begin{bmatrix} \cos\theta & 0 & \sin\theta & 0 \\ 0 & 1 & 0 & 0 \\ -\sin\theta & 0 & \cos\theta & 0 \\ 0 & 0 & 0 & 1 \end{bmatrix} \begin{bmatrix} \cos\theta & \sin\theta & 0 & 0 \\ -\sin\theta & \cos\theta & 0 & 0 \\ 0 & 0 & 1 & 0 \\ 0 & 0 & 0 & 1 \end{bmatrix}$$

The rotation only around these three vertices may seem a little limiting, especially if more complex movements are required. However, these elementary rotation

matrices used in combination with translation transformations allow rotating an object around any axis and on an arbitrary angle. Of course, this *general rotation* can be represented as a matrix, which is constructed with the method presented by Kenneth Joy [15].

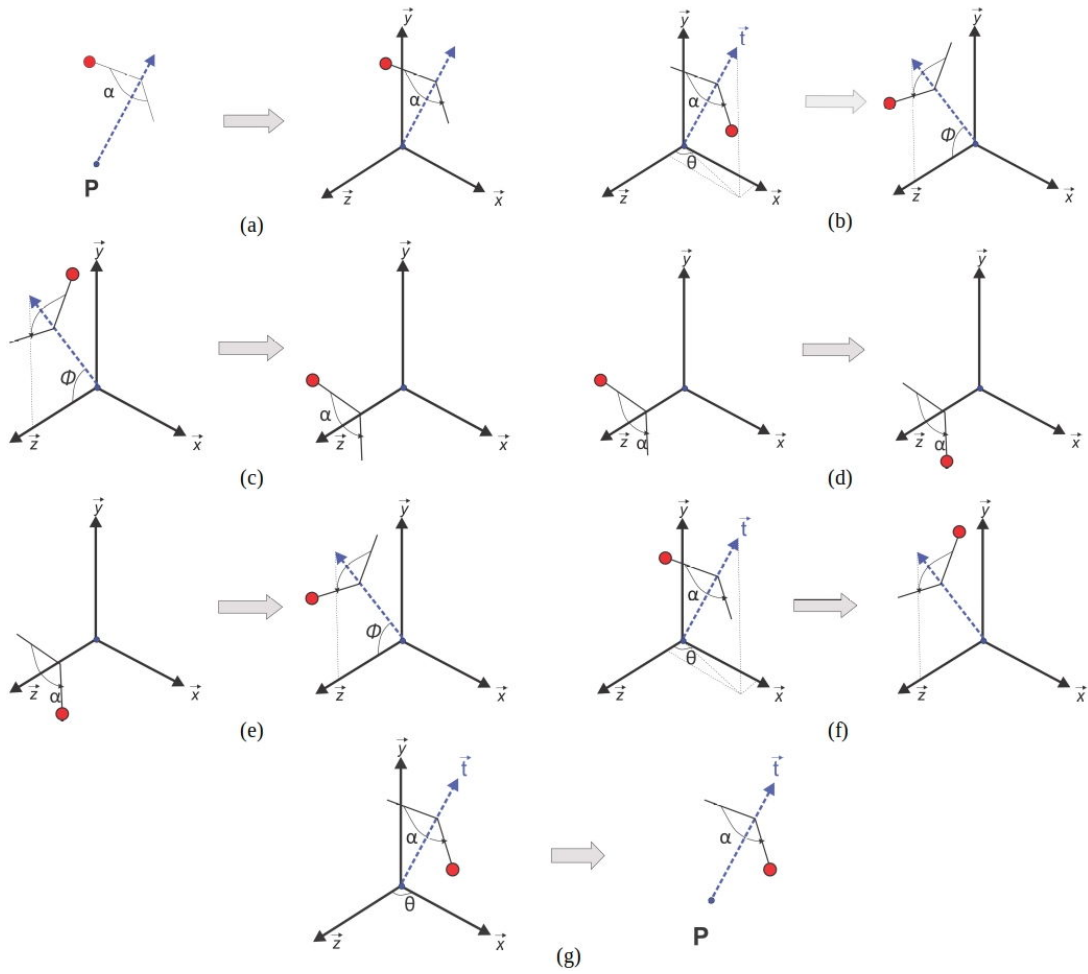


Figure 3.1: General Rotation

Suppose that an object on an arbitrary angle α must be rotated around a new axis that passes through an arbitrary point $P(x_p, y_p, z_p)$. This axis points in the direction given by a vector $t(x_t, y_t, z_t)$, then:

1. The point P is relocated by translation $T(-x_p, -y_p, -z_p)$ to the origin (Figure 3.1a).
2. The direction vector is rotated about the y-axis on an angle $\theta = \arctan(\frac{x_t}{z_t})$ using a rotation matrix $R_{y,-\theta}$, so that it coincides with the plane yz (Figure 3.1b).

3. The vector is then rotated about x-axis on an angle $\phi = \arctan\left(\frac{y_t}{\sqrt{x_t^2 + z_t^2}}\right)$ with $R_{x,\phi}$ so that it coincides with z-axis (Figure 3.1c).
4. The object is rotated about z-axis on the desired angle α with $R_{z,\alpha}$ (Figure 3.1d).
5. The first two procedures are reversed by using $R_{x,-\phi}$ and $R_{y,\theta}$ over the vector (Figure 3.1e and (Figure 3.1f)).
6. Finally, the point P is translated back to its original position with $T(x_p, y_p, z_p)$ (Figure 3.1g).

The total rotation matrix is the product of all the transformations used during this procedure:

$$T(-x_p, -y_p, -z_p)R_{y,-\theta}R_{x,\phi}R_{z,\alpha}R_{x,-\phi}R_{y,\theta}T(x_p, y_p, z_p)$$

Another useful transformation is the alignment of vectors, which implies rotating a vector so that it has the same direction of an objective vector. To align a vector a with a vector b the direction vector of the rotation is given by the cross product of both vectors while the angle of rotation is given by their dot product.

Transformation matrices can multiply by each other, and the resulting matrix represents the transformations that were encoded in the original matrices. In this way, whole processes like the one shown in Figure 3.1 can be assembled. Transformation after transformations can be concatenated and combined by simply multiplying matrices together, so that a single matrix can represent infinity unitary transformations. That is the real power of a matrix.

3.1.2 Delaunay Triangulation: A Universe of Triangles

Triangulation is the name given in Mathematics and Computer Graphics to the geometric operation that, applied over a set of points distributed in a space region of two or three dimensions, generates edges joining those points so that the created edges don't intersect. The Triangulation is said to be complete if there are no points left to be joined [16]. Once the operation is completed, the set of points has been divided into adjacent triangles for the 2D case and tetrahedrons for the 3D case. That is the reason why this operation is denominated Triangulation. The surface (perimeter) of the generated polytope(polygon) is known as the Convex Hull. The tetrahedrons generated by the 3D Triangulation constitute a triangle faced polytope, just as the triangles in 2D constitute a polygon.

Delaunay Triangulation, named after the mathematician Borís Nikolaevich Delaunay, is a special type of triangulation that generates a set of adjacent triangles that are as equilateral as possible. This condition is achieved by imposing the following rule: No point must exist inside the circumcircle of any of the tetrahedrons (or triangles) generated by the Triangulation [16].

The Convex Hulls of the 3D Delaunay Triangulations are widely used in computer graphics to recreate surfaces [17] [18]. Hence, the best option to generate or recreate a surface is always to divide into triangles. They are so good for this purpose because triangles are the simplest polygons and, more importantly, any arrangement of three vertices in 3D space will always be coplanar. Using higher-order shapes other than triangles to recreate a surface, might result in degenerated faces that aren't properly represented because its vertices aren't necessarily coplanar. Indeed, any 3D surface in the universe is able to be approximated by fitting together triangles.

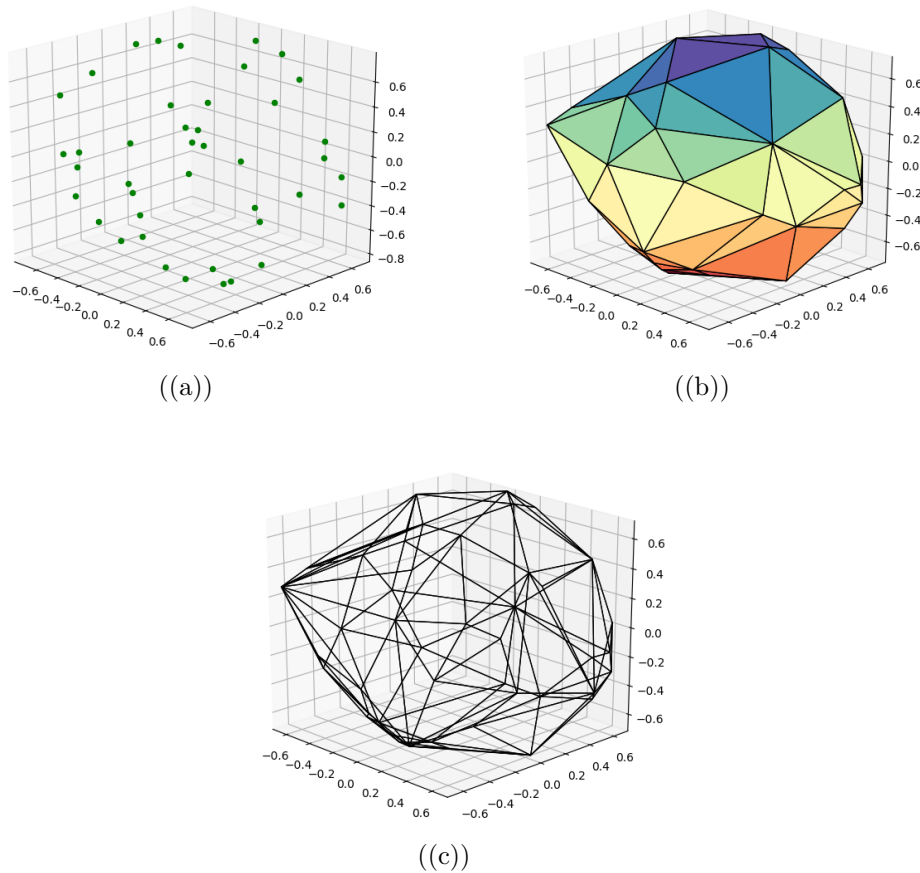


Figure 3.2: (a) Cloud of 46 points in 3D . (b) 3D Convex Hull of the triangulation in c (c)3D Delaunay triangulation of the cloud of points in a

Many algorithms have been developed to construct the Delaunay triangulation and Convex Hull of a 3D set of points [19] [20]. Among them, the *Incremental*

Algorithm [21] [22] has been chosen because its implementation is the least complicated. Its algorithm works iteratively and is indeed very simple. The process starts by choosing randomly three points of the given set; by definition they are coplanar and they are specifying the surface of two triangles, one on the front and one on the back. The way to determine if a triangle is facing in or facing out is carefully choosing the order in which the vertices are specified. By convention, if the orientation of the vertices is anti-clockwise, the face is pointing outwards; if not, the face is going inwards [16].

Once the double-faced triangle is defined, a fourth point is selected from the set; if it is not coplanar with the triangle, it is chosen to form the first tetrahedron of the 3D triangulation, i.e the initial convex hull H_0 . Then iteration begins:

1. For the i_{th} iteration consider $p = p_i$ a point from the set, and $Q = H_{i-1}$ the convex hull computed previous to the evaluation of p_i .
2. Determine if p is in the convex hull ($p \in Q$). If that is the case, discard p . Else, Q must be modified to include p . (See Figure 3.3)

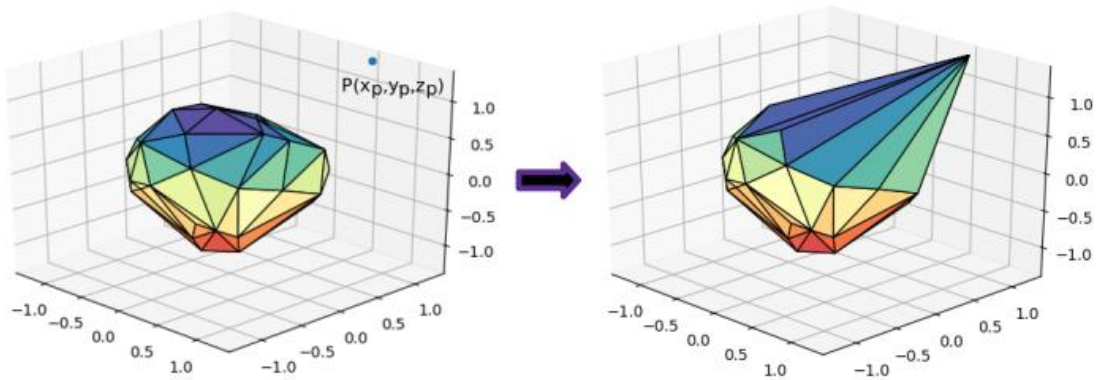


Figure 3.3: Convex Hull H before (H_{i-1}) and after (H_i) adding point p

The volumes of the tetrahedrons that p forms with the faces of Q are used to test whether p is outside or inside Q . The volume is a signed quantity that can be calculated with the determinantal form of the volume for a tetrahedron with vertices (a,b,c,d) [16]:

$$\frac{1}{6} \begin{vmatrix} a_x & a_y & a_z & 1 \\ b_x & b_y & b_z & 1 \\ c_x & c_y & c_z & 1 \\ d_x & d_y & d_z & 1 \end{vmatrix}$$

If p is inside the hull, all the tetrahedrons formed should present the same sign. By convention, it has been chosen to be positive. Else, If p is not in Q , the latter is

modified by adding tangent planes from p to Q . They delimit a cone with triangular faces, each of whose apex is p and whose base is an edge e of Q [16](See Figure 3.3). To determine the edges of the bases, first, the faces that are ‘visible’ from p must be identified. The ‘visible faces’ are those which tetrahedrons form with p have strictly negative-valued volumes. Then the edges e forming the bases are those that are adjacent to two faces, one which is visible from p , and one which is not. Therefore, they are on the border of the ‘visible’ region [16]. The Incremental Algorithm can be summarized in the following diagram:

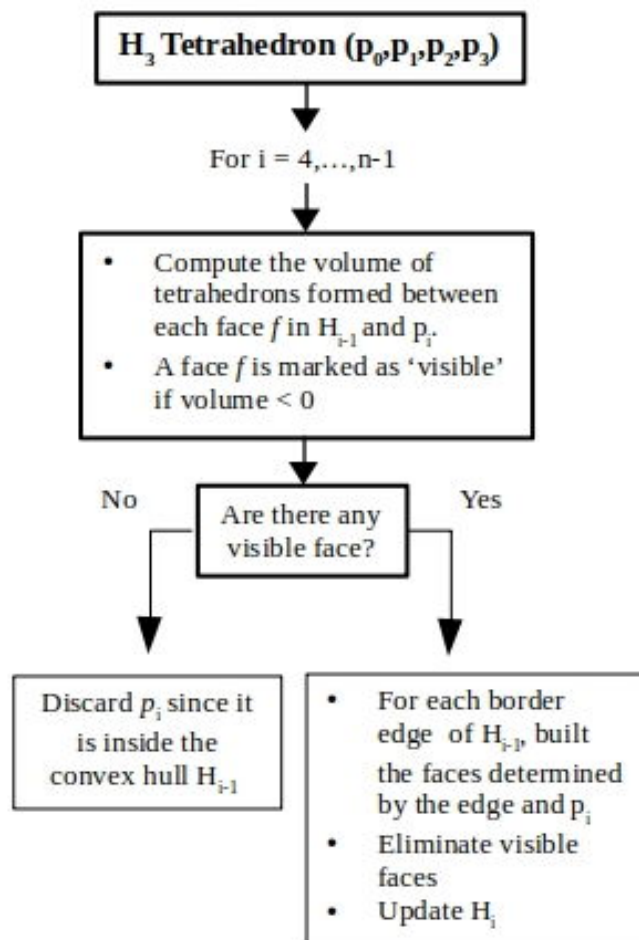


Figure 3.4: Incremental Algorithm for 3D Triangulation

3.1.3 Wythoff Construction: Spherical Trigonometry to make it Interesting

Uniform regular polyhedrons are highly symmetrical 3D objects which faces are regular polygons [16]. Their high symmetry provides them with an interesting characteristic: Through a method known as Wythoff construction, named after Willem

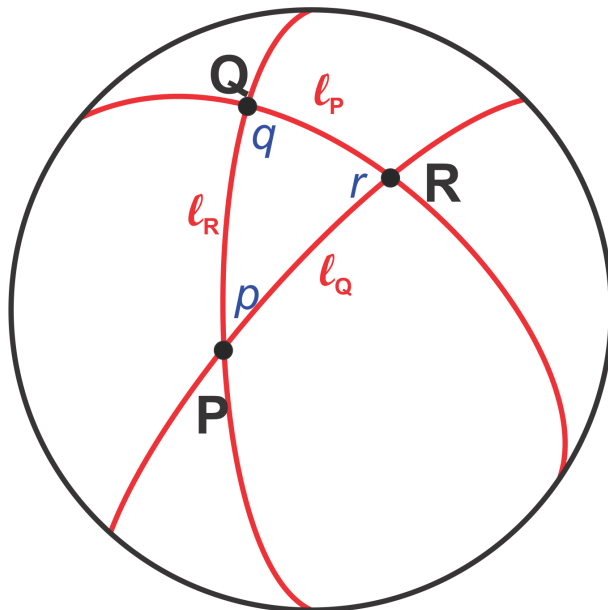


Figure 3.5: Spherical triangle PQR, surface defined by the intersection of the great circles of a sphere.

Abraham Wythoff, the surface of a regular polyhedron can be completely generated over the surface of any sphere, requiring only the information contained in a geometrical object called Schwarz triangle. This is a spherical triangle, i.e., a portion of the surface of a sphere delimited by the arcs of three sphere's great circles (See Figure 3.5). It is understood by large circles, those that cross the sphere exactly through the center [23]. Of course, since it is no longer on a plane, the sum of the internal angles of one of these triangles is necessarily greater than 180° or π radians. This also means that flat trigonometry or 'Euclidean' no longer applies. Spherical trigonometry has been in charge of providing the tools to study these geometric objects, and the relationships created between the internal angles and the arcs that make up the sides of these triangles are very useful for the elaboration of Wythoff constructions. Operations of rotation and reflection applied over the Schwarz triangle allow to obtain triangular partitions of the surface of the sphere with no gaps and no overlaps. This condition is achieved by carefully choosing the angles of the triangle. In effect, not every triangle meets this condition so not every spherical triangle can be a Schwarz triangle. Take the Schwarz triangle of vertices P, Q and R. Its angles can be expressed as $\frac{\pi}{p}, \frac{\pi}{q}, \frac{\pi}{r}$ radians, where p, q and r are integer numbers that defines the angles at the given vertices.

If p, q, and r are integers between two and five, at least one of them is equal to two and never two of them are five simultaneously, then the Schwarz triangle turns into a Möbius triangle. This special Schwarz triangle, hereinafter referred to as fundamental triangle, can be reflected through its edges to cover the surface

of its sphere exactly once. The Wythoff construction consist in set a point called the generator vertex, in the surface of the fundamental triangle and use the edges of the triangle as mirrors to reflect the generator vertex. This operation eventually generates all the vertices of a polyhedron. Which polyhedron will be created depends on the position of the generator vertex and the angles of its fundamental triangle. Together, the fundamental triangle and the generator vertex constitutes the **generator triangle**, which is characteristic of each polyhedron. For regular polyhedrons, there exist a few allowed positions for the generator vertex so there is a limited number of possible generator triangles.

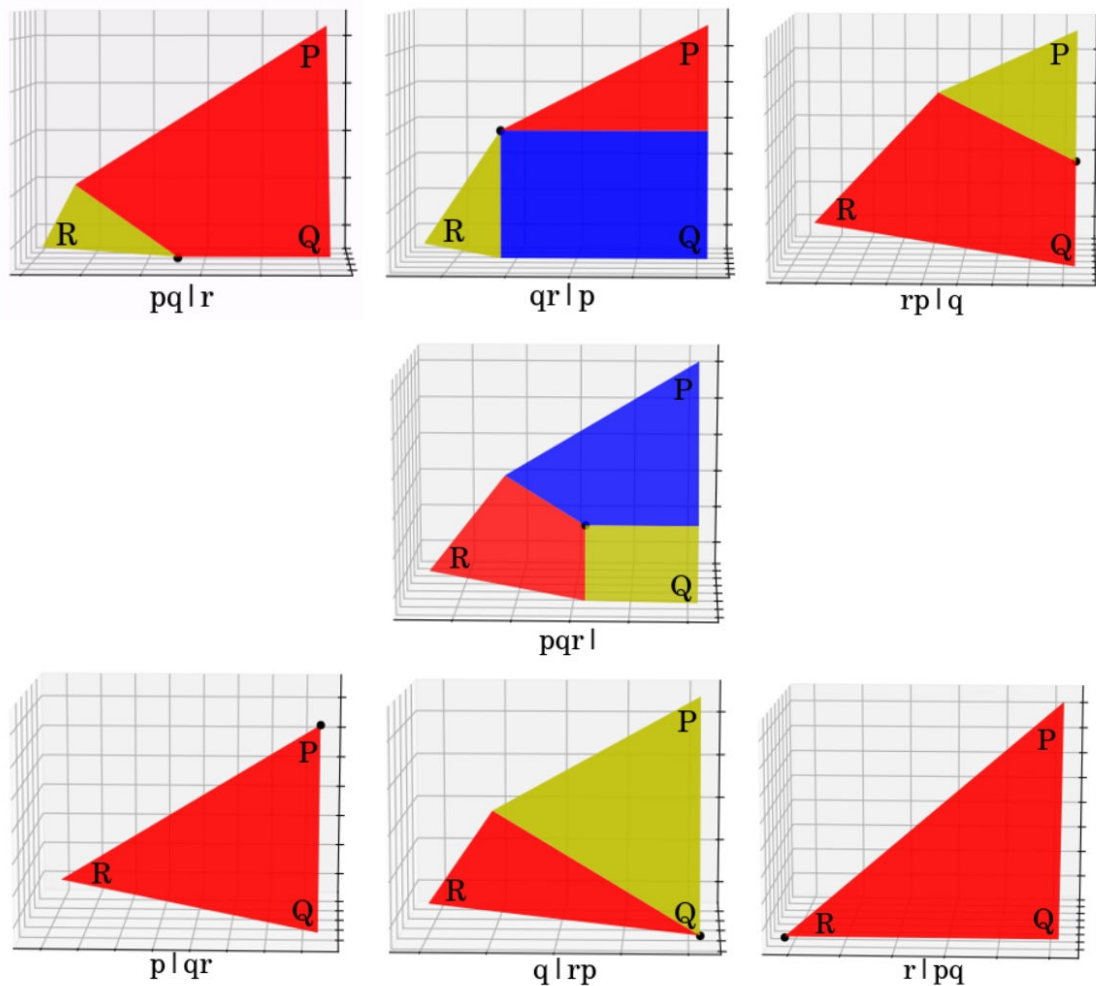


Figure 3.6: Wythoffian constructions for the elemental triangle (4, 2, 3)

The information regarding the angles and the position of the vertex in the generator triangle is compactly represented by a Wythoff symbol. This symbol contains three integers (p,q,r), and a straight bar | that represents the position of the generator vertex. In can be understood as follows:

- If the bar is at the end of the symbol $pqr|$, the generator vertex is placed in the incenter of the triangle.
- If the bar position is after the first number(counting from the left) $p|qr$, the generator lies on the corner represented by the first number(that one before the bar)
- Finally, if the bar is positioned between the second and third numbers $pq|r$, the generator lies in the line formed by the two vertices whose angles are represented by the numbers at both sides of the bar, at the point that bisects the angle of the remaining vertex.

The Figure 3.6 shows all the possible Wythoffian constructions for the triangle (4,2,3). The generator vertex is represented as a black dot.

3.1.4 A journey to the Center of a Porosity

The first step in the study of properties of practical interest in porous materials is to determine the most basic and representative aspects of its structure: the number of different porosities and their size. Computationally speaking, the usual method of structural characterization of porosities is carried out using DFT-based methods based on nitrogen or argon adsorption isotherms [9] [24]. However, these methods make use of a simplified model of the pore cavity that does not take into account several relevant structural factors such as internal cavity connectivity, material defects and tortuosity of the structure [1]. Therefore, in the development of DeltaChem, an alternative method has been chosen for the determination of porosity sizes, implementing the PSD_solve program created by Supriyo Bhattacharya [1]. In the paper entitled “Fast Method for Computing Pore Size Distributions of Model Materials”, the author defines porosity size distribution (PSD) as the statistical distribution of the radius of the largest sphere that can be placed within a porosity. The radius of this sphere must be such that it does not overlap with any of the Van der Waals spheres of the atoms belonging to the porosity. In this way the determination of PSD becomes a geometric optimization problem that consists in finding the largest possible sphere that is surrounded by a set of points.

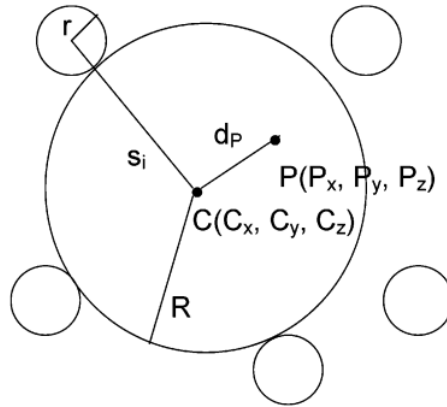


Figure 3.7: Graphic representation of the largest enclosing sphere optimization problem [1]

Figure 3.7 shows the 2D representation of the geometry optimization problem for maximum enclosed sphere. The radius R of the sphere is a function of the position of the center of the porosity C ; r is the radius of Van der Waals of the atoms that surround the sphere¹; S_i represents the distance between the centers of the sphere and the atom, i.e, the sum of the radii of the sphere and the corresponding atom:

$$R(C) = \text{MIN}(S_i) - r$$

The larger sphere that can be enclosed by the porosity atoms is obtained by maximizing the previous expression. The optimization problem can then be mathematically described as follows:

$$\text{MAXIMIZE}\{R(C) = \text{MIN}(S_i) - r\}$$

This maximization is subject to the constraint $d_P - R \leq 0$ where d_P is the distance between the center of the sphere and a point P whose position is different from that of the atoms that make up the porosity and is always within the structure to ensure that the sphere is found at all times inside the pore cavity and not outside it. Although the objective function to be maximized is linear, the constraint is an inequality, so there is a problem of non-linear optimization. For its resolution, Battacharya has implemented the SOLVOPT algorithm [25] in PSD_solve. In general, the PSD_solve algorithm consists of selecting random P points within the structure and applying the optimization process described above. The results for $R(C)$ are sampled at regular intervals over processing time to construct a cumulative histogram $H(D)$

¹For simplicity of the illustration, the radius is shown as a fixed value for all the atoms, although of course, it can vary from atom to atom

(that is function of the sphere diameter). Finally, the PSD is obtained as the negative derivative of the histogram function with respect to the diameter, that is:

$$PSD = -\frac{dH(D)}{dD}$$

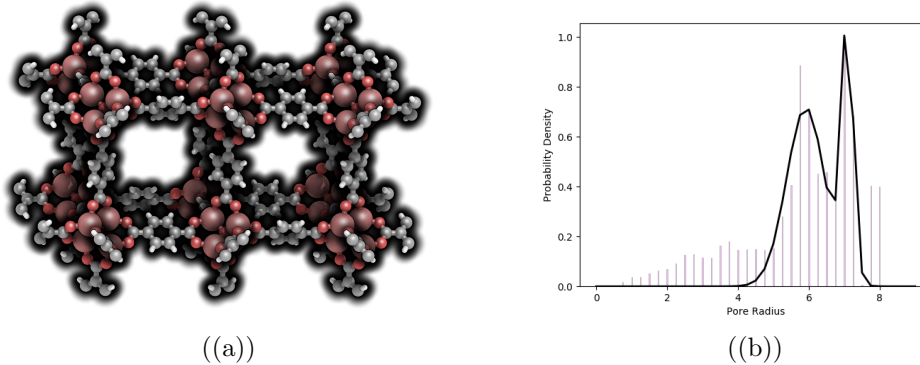


Figure 3.8: (a)Structure of MOF-5. (b)Pore size distribution obtained from PSD_solve for the structure given in (a)

The figure 3.8 shows the distribution of the porosity size obtained for the structure of the MOF-5. On it can be seen two peaks corresponding to the two types of porosity present in this material.

Once the porosity sizes are obtained, the positions of their centers are determined. This process is described in detail in the Methodology section and constitutes a fundamental link in the operation of the algorithm because it allows to determine which atoms of the structure belong to each porosity. Said atomic organization is used as input information for the Mozaiko subroutine to carry out the triangulation procedures.

3.2 Chemical Section:

3.2.1 About MOFs and zeolites: Why microporous materials are so cool?

Zeolites and metal-organic frameworks constitute wide and important categories in microporous materials. Both have been extensively studied due to their potential for important applications like catalysis [26], water treatment [27], drug delivery [28], and even micro-machinery [29] to mention a few. Due to their unparalleled capabilities and applications, zeolites and MOFs deserve an appropriate description.

Zeolites

Zeolites are three-dimensional inorganic crystalline networks of silicates and aluminosilicates linked through oxygen atoms. These networks contain well-defined channels and cavities [5]. Many types of Zeolites are naturally occurring so they are known at least since 1756 when Axel Fredrik Cronstedt coined the term ‘zeolite’, but some rudimentary applications maybe precede this date. It is only until the 40s of the last century that their properties as moisture adsorbents began to be investigated. The molecular structure of these materials provided them with high surface areas and molecule-sized pores [30]; properties that were used at first to separate long-chain hydrocarbons according to their size, taking advantage of the different channel and pore sizes in analcite and chabazite [30]. These capabilities were enough for the oil industry giants Exxon Mobile and Union Carbide to focus their attention on the studies of zeolites. In the late 70s, the chemical research group of Union Carbide lead by Jule Rabo discovered that the internal surface of these materials can act as a reaction channel whose activity and selectivity may be enhanced by the introduction of active acidic or basic sites inside the pore cavity [5]. These discoveries allowed Exxon to put on sale the first commercial catalyst for oil refining based on faujasites by 1964. Nowadays, 176 types of zeolite frameworks have been indexed in the 6th edition of the Atlas of Zeolite Framework Types [31], and 72 additional codes have since been added to give a total of 248 Framework Type Codes assigned to date according to the International Zeolite Association(IZA). And their applications go far beyond the oil industry but of course it still representing an important sector for industrial application of zeolites. Indeed, Zeolites constitute the most used industrial heterogeneous catalysts with large-scale applications in refining and petrochemistry [32]. However, the growing worldwide environmental pollution increased the interest in zeolites and their potential for environmental catalysis ² [32].

Metal-Organic Frameworks (MOFs)

The most representative and relevant category of microporous materials nowadays is that conformed by the metal-organic frameworks due to their wide range of applications, cutting-edge capabilities and their great diversity in structures and shapes. First MOFs were synthesized in the late 80s as results of zeolite-based experiments whose objective was to create crystalline extended structures, similar to those of zeolites, but based in coordination metal ions joined by organic linkers

²Catalytic elimination of gas, liquid, and solid-phase pollutants.

containing active acidic sites [33]. The length of these organic linkers was thought to provide the material with permanent, well-defined porosities. In 1995, gas adsorption studies were performed on the first MOFs, these studies suggested the presence of microporosities in those structures [34] [4] [33]. However, since the experiments were carried out at high pressure (30 atm), they didn't accomplish the gold standard for porosity determination: reversible gas adsorption isotherms using nitrogen at 77 K. [34] [33]. Ironically, the same year the term metal-organic framework was coined by Yaghi and Li to refer the structure with formula $\text{Cu}(\text{BIPY})1.5(\text{NO}_3)^3$ [35]. In absence of any definitive, proof of the existence of their porosities, most of MOFs were seen by 90s chemists as '*sculptures rather than useful materials*' [4]. It was not until 1998 that researchers from Arizona State University, through a comprehensive analysis that included synthesis, characterization with X-ray diffraction and Nitrogen adsorption isotherms at low pressures and temperatures, reported the creation of rigid frameworks that maintain their structural integrity and porosity during anion-exchange in MOF-2 [34]. These findings were fundamental for the ground-breaking synthesis of MOF-5 by the same research group at ASU one year later. Its simple three dimensional network with robust and well defined porosities, simple synthesis process through rational design principles, and a very high surface area, took it to be recognized as the most prominent example of a metal-organic framework by experts of a wide range of scientific disciplines [4], and its discovery boosted the popularity of MOFs to unsuspected levels. By end of 90s, MOFs had already captured the attention of the synthetic chemistry community in view of the possibility of designing materials with a large surface, unparalleled for conventional inorganic and organic porous materials [4]. During the first decade of this century more than 20,000 different MOFs were reported and studied [33]. This extensive range of reported model materials is due to flexibility with which the metal secondary building units (SBUs) and organic linkers can be varied to create open crystalline frameworks with permanent porosity [33]. Nowadays, MOFs' composition, chemical reactivity, pore opening and size can be designed to achieve unprecedented applications.

3.3 State-of-the-Art

This section is devoted to the description of the novel materials that are used along this project to illustrate, exemplify and test the job performed by Delta Chem. It is also an opportunity to take a look at how computational tools coming from

³Triangular Cu based building units connected through 4,4-bipyridine

disciplines other than chemistry are useful to accurately represent diverse chemical systems and bring a solution to chemical problems. The aim is to highlight the utility of the research in adsorption properties in these materials for the development of industrial-scale applications, and illustrate the importance of this project.

3.3.1 Analyzed Microporous Materials

The materials used along this project are framed in the previously described categories and they were selected to test the functioning of Delta Chem. The selection was based in the number of the porosities, the shape of the pore cavity and the importance of their applications. All of them present remarkable capabilities that have made them objects of extensive study, industrial-scale production, and application [33].

CuBTC or HKUST-1

This prototypal MOF was synthesized by researchers of Hong Kong University of Science and Technology (HKUST) in 1999 [36]. Coincidentally, the same year another iconic microporous material, the MOF-5 was synthesized for the first time. Cu-BTC or HKUST-1 is considered as ‘prototypal’ since a whole HKUST family of MOFs has been created from its particular structure (Figure 3.9d) [4]. This material presents the formula $\text{Cu}_3(\text{BTC})_2(\text{H}_2\text{O})_3$ [36] but can be dehydrated to obtain the anhydrous $\text{Cu}_3(\text{BTC})_2$. In this formula, BTC refers to the organic linker benzene-1,3,5-tricarboxylate (Figure 3.9b). It is a triangular linker that joins three $\text{Cu}_2(-\text{COO})_4$ SBUs (Figure 3.9a). Each of these metal-containing units can joint with four BTCs to form the paddlewheel core structure shown in Figure 3.9c. This ligand arrangement results in two coordinatively unsaturated Cu sites per paddlewheel which polar molecules can interact with [37]. This relatively big core structure allows the formation of large porosities. The disposition of the aromatic rings produces the formation of three different porosities on the HKUST-1 structure, two of comparable size (pore diameter $\approx 14\text{\AA}$) and a smaller pore (pore diameter $\approx 10\text{\AA}$) [37]. Nitrogen adsorption isotherms show that this MOF has approximately a BET surface area of $1055\text{m}^2\text{g}^{-1}$ [38]. This large surface area makes this material an attractive candidate for gas sensing and separation [37] [26] [38]. Of course, this value may seem a little bit short compared with the values obtained for other families of MOFs [26], however, it is several times higher than any naturally occurrent zeolite [39]. Its structure is also well suited for heterogeneous catalysis where the presence of metal centers for the stabilization of intermediates is convenient [37]. Their remarkable

adsorption capabilities [38] makes them very useful for trapping of air and water pollutants [40] [41]. Additionally, HKUST-1 has been proven to work as an antifungal and offers the controlled release of biologically active copper ions [42].

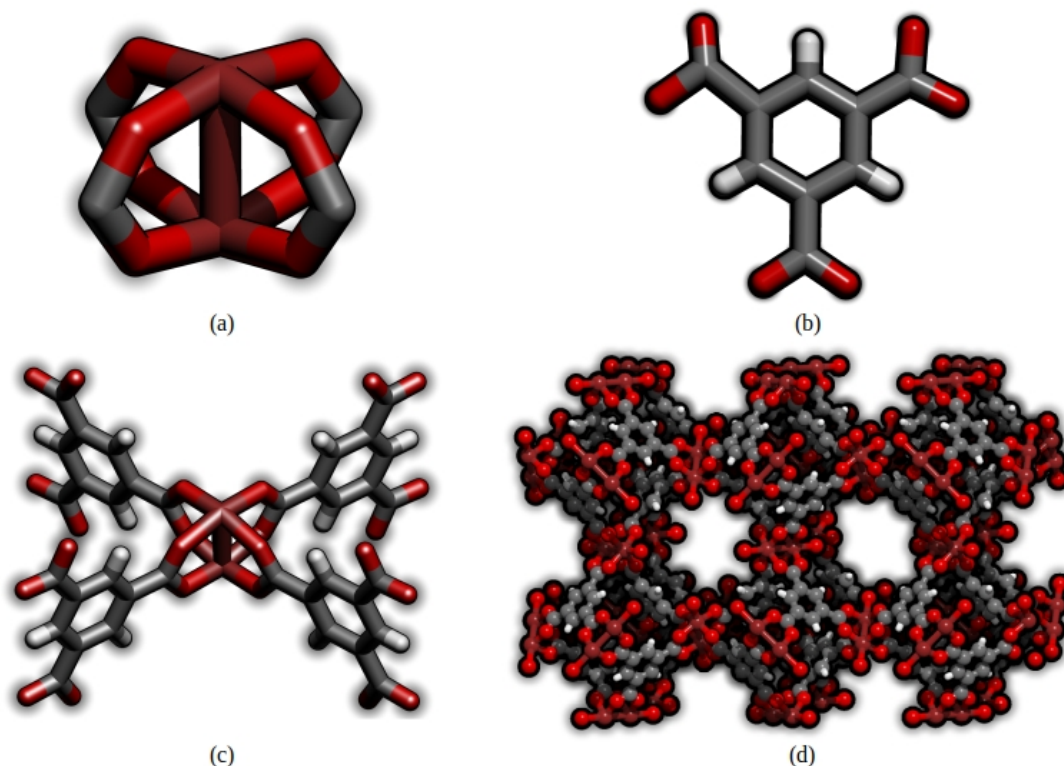


Figure 3.9: HKUST-1 Structure: (a) $\text{Cu}_2(-\text{COO})_4$ SBU, (b) $(\text{C}_9\text{H}_3\text{O}_6)^{-3}$ BTC organic linker, (c) Cu-containing core structure, (d) HKUST-1 unit cell used for Delta Chem analysis

. Color code: Cu-Brown, O-Red, C-Black, H-White

MOF-5 or IRMOF-1

With a paper titled “*Design and synthesis of an exceptionally stable and highly porous metal-organic framework*”, it is obvious that the creators of MOF-5, Li, Eddaoudi, Keffe, and Yaghi were pretty sure of how important their discovery was. Of course, the most iconic MOF couldn’t be excluded from this list. It was so ground-breaking because, before its creation, no other open framework had been capable of supporting permanent porosity and avoid collapsing in the absence of guest molecules, such as solvents [43]. It is constituted by $\text{Zn}_4\text{O}(-\text{COO})_6$ SBUs (Figure 3.10a), connected through BDC (benzene-1,4-dicarboxylate also known as terephthalate or TBA)(Figure 3.10b). On each SBU, a central oxide is surrounded by four Zn^{2+} ions. Every Zn^{2+} ion is tetrahedrally coordinated with the oxygens of the six bridging carboxylate group [4] as shown in Figure (Figure 3.10c).

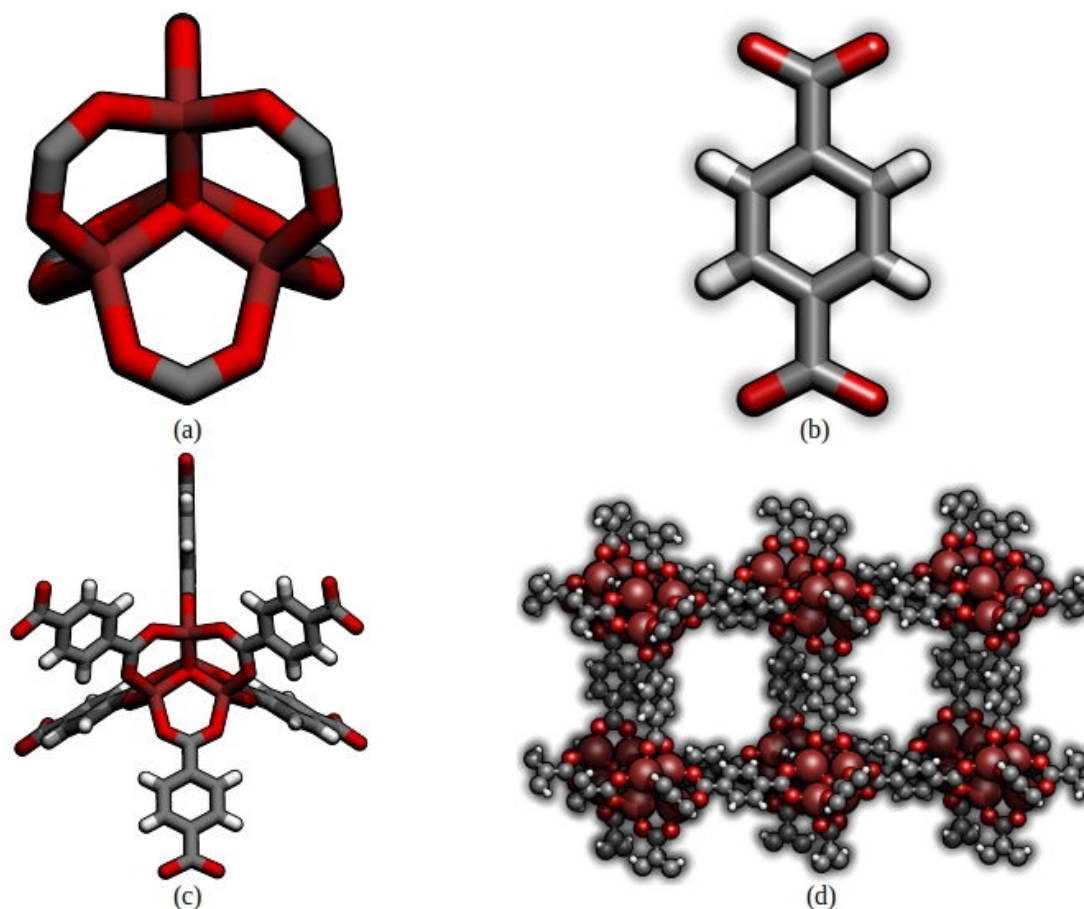


Figure 3.10: MOF-5 Structure: (a) $\text{Zn}_4\text{O}(-\text{COO})_6$ SBU, (b) $(\text{C}_8\text{H}_4\text{O}_4)^{-2}$ BDC organic linker, (c) Zn-containing core structure, (d) MOF-5 unit cell used for Delta Chem analysis . Color code: Zn-Brown, O-Red, C-Black, H-White

The structure shown in Figure 3.10d presents two types of porosities: a large cavity with a pore diameter of $\sim 15\text{\AA}$, and a small one of diameter $\sim 10\text{\AA}$ [43] [4]. MOF-5 presents a surface area of $3800\text{m}^2\text{g}^{-1}$ [26], the largest determined for a material by the date of its discovery [33]. Its comparatively high surface area and the large size of its pores made the MOF-5 quickly suggested for applications in gas storage and sequestration [44] [45]. Additionally, MOF-5 has been proven as a component of heterogeneous catalytic systems [46].

UiO-66

Potential applications of microporous materials like high gas storage requires dense packing of the material powder under mechanical compression without collapsing the pores [47]. Precisely the large pore cavities and surface areas of previously described MOFs are the reasons of their weak thermal and mechanical stability [48]. This constitute a drawback for their use in industry-scale applications for gas stor-

age. UiO-66 is a prototypical MOF with Zirconium based SBUs that combines an unprecedented mechanical stability with large pore sizes and surface areas. UiO-66 was synthesized for the first time at the University of Oslo in 2008.

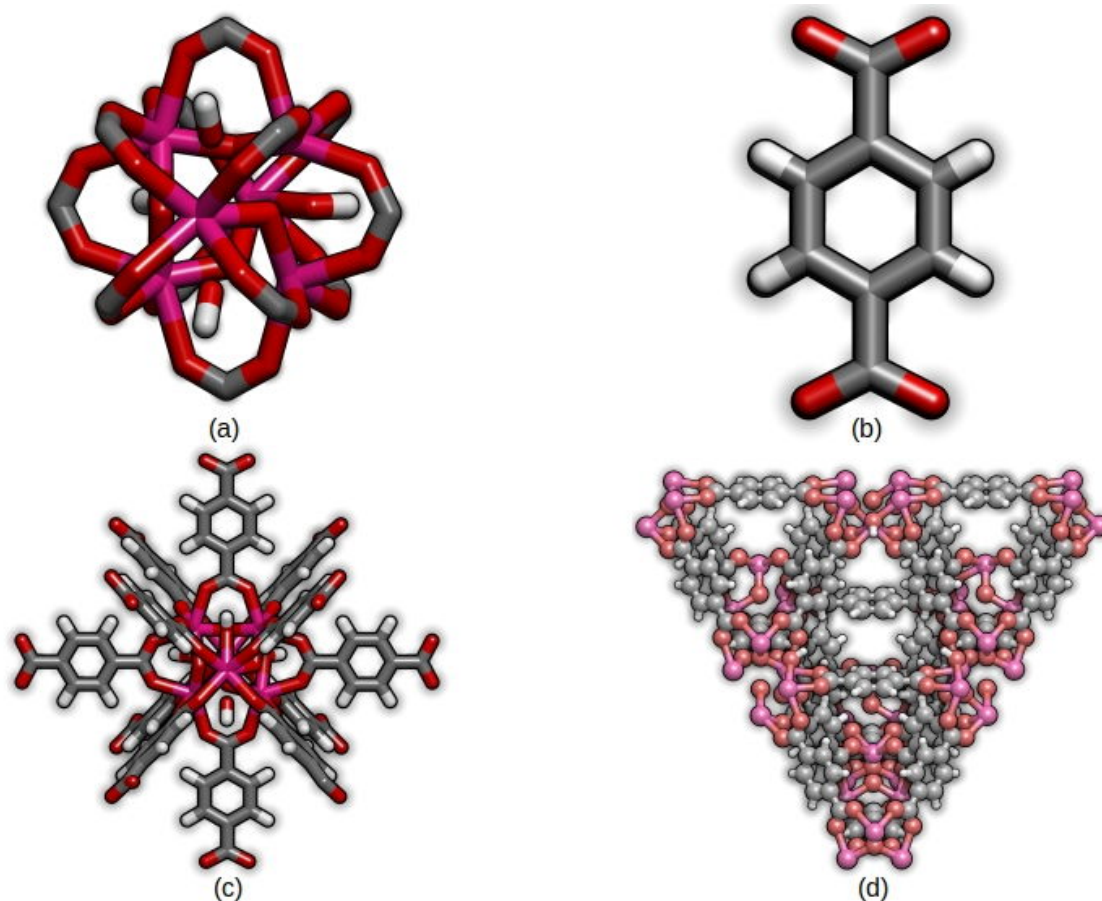


Figure 3.11: UiO-66 Structure: (a) $\text{Zr}_6\text{O}_4(\text{OH})_4$ SBU, (b) $(\text{C}_8\text{H}_4\text{O}_4)^{-2}$ BDC organic linker, (c) Zr-containing core structure, (d) UiO-66 unit cell used for Delta Chem analysis
. Color code: Zr-Purple, O-Red, C-Black, H-White

UiO-66 SBU has the chemical formula $\text{Zr}_6\text{O}_4(\text{OH})_4$ (Figure 3.11a) and is coordinated with 12 organic linkers (DBC for UiO-66) [49] (See Figure 3.11b and 3.11c). The high coordination of Zr allows the creation of a highly dense network whose increased number of connections provides high mechanical stability while the large size of the SBUs allows the presence of large porosities [47]. This material presents a BET surface area of $1180 - 1240 \text{ m}^2 \text{ g}^{-1}$, and two different porosities of similar size (pore diameter $\approx 14 \text{ \AA}$) [49].

ZIF-8

Zeolitic imidazolate frameworks, or simply called ZIFs, can be seen as MOFs with zeolitic architectures, consisting of metal ions of zinc or copper coordinatively

joined by four imidazolate rings ($C_3H_3N_2$)⁻ just like Si and Al atoms in zeolites are covalently joined by oxygens [17].

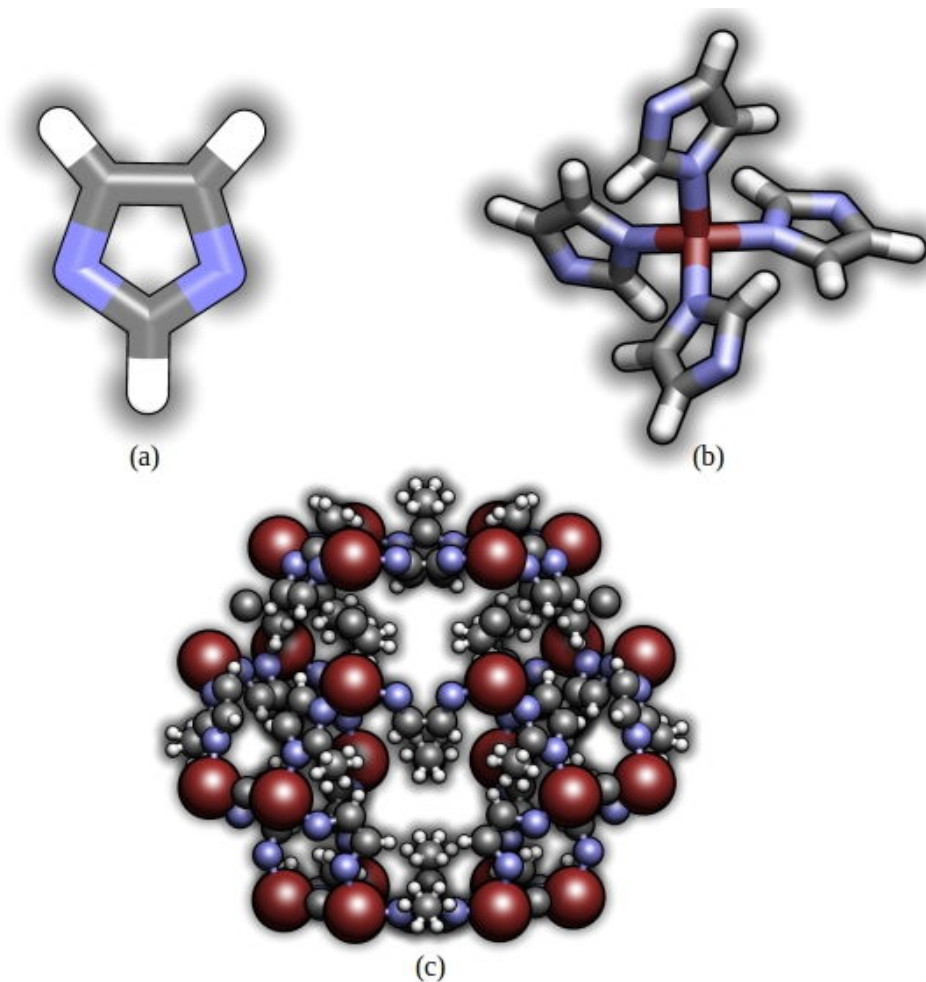


Figure 3.12: ZIF-8 Structure: (a) Imidazolate organic linker, (b) Zinc-coordinated core structure, (c) ZIF-8 unit cell used for Delta Chem analysis. *Color code: Zn-Brown, N-Blue, C-Black, H-White*

As could be expected, the hybrid structure of ZIFs provides these materials with advantages from both, MOFs and zeolites. These advantages include large surface areas, high crystallinities, abundant functionalities and remarkable thermal and chemical stabilities [17] [50].

Among these materials, ZIF-8 (Figure 3.12) is highlighted due to its large (compared with zeolites) pore diameter and surface area, $\sim 11.6\text{\AA}$ and $981.1\text{m}^2\text{g}^{-1}$, respectively [50] [51]. Due to its thermally and chemically stable properties and porous structure, ZIF-8 is well suited for the application of carbon dioxide adsorption/separation [17]. The organic reactivity provided by the linkers results in useful for catalysis applications. It has proven that ZIF-8 is an effective heterogeneous catalyst for a wide variety of organic chemical reactions and processes [17] such as

transesterification [52] and Friedel-Crafts acylation [53]. This material has been also tested for possible drug delivery applications due to its pH-sensitive structure [54]. Precisely this latter characteristic opens the door for cutting-edge applications for this material. A clear example is to use ZIF-8 as blocks to build metal-organic-framework-based biomedical microrobots. These MOFBOTs can be directed with magnetic fields and applied for controlled drug delivery [29].

3.3.2 About Geometry applied to Chemistry: Triangles and Pores

Geometric methods and operations have been applied for the study of chemical structures and systems at least since the 17th Century. Geometrical objects like polygons and polyhedrons have been used to represent and classify molecules and/or materials according to their structures or their symmetry. Indeed, important chemistry-related disciplines like crystallography have an important geometrical background. It is not surprising that computational geometry also presents applications for chemical purposes. Some of the geometrical processes and operations that were described in this chapter are already being used for the functioning and development of computational chemistry methods and models. Computational geometry provides molecular modelers with a powerful set of tools for solving a wide variety of conformational problems [55].

Triangulations (specially Delaunay triangulation) can be used to reconstruct curves and surfaces from sample points, resulting useful for analysis of surfaces of chemical interests like interaction sites of proteins [56] [57] or structural characterization of colloidal films [58]. Triangulations even have been applied in analytical chemistry as a local multivariate calibration method for analysis of near-infrared (NIR) data [59].

Of course, triangles are not everything in geometry; spheres also have relevant applications in computational chemistry to model solvent-accessible surface surrounding a solute in solvated systems [60]. This application is currently used to generate the molecule-containing cavities in COSMO and CPCM, two widely used computational solvent models. Spherical trigonometry has been mentioned briefly in studies regarding ‘flexocrystallography’, a proposal for a variant of crystallography to deal with ‘soft matter’ chemical and biological structures like vesicles.

The concept of ‘irreducible volume’ of uniform polyhedrons has been applied to analyze mechanical effects on symmetric materials, like uniaxial stress on band structure and electron mobility of silicon [61]. However, the irreducible volume used was obtained from the first Brillouin zone and it is calculated with programs for the

finite symmetry groups [62].

Particularly, for microporous materials, spheres are used to define their pore cavities. The generation of spheres can be coupled with statistical analysis and non-linear optimization to obtain the pore size distribution (PSD) function for these materials with reasonable accuracy, without requiring a DFT method [1]. Due to the high symmetry of many of these materials, uniform polyhedrons are used to model the geometry of cages, channels and building units. Indeed, some of them like MOFs and ZIFs adopt structures so symmetrical that their design and construction can be carried out schematically, entirely from a geometrical point of view, using SBUs as if they were LEGO bricks, joined by geometrical bridges [63].

It is very important to note that, until the delivery of this capstone project, no records have been found that establish the applications of triangulations in the study of microporous materials or the surface of their porosities. And neither was method for the direct determination of the positions of the centers of porosities in these materials. References to the construction of Wythoff in chemical applications could not be found. Interestingly, there is also no record of the use of this operation for the construction of irreducible volumes although geometrically they are equivalent to those obtained from the first Brillouin zone.

Finally, no previous studies of the use of irreducible volume in the determination of adsorption sites in micropores have been found.

Chapter 4

Methodology

Just like in the last chapter, the Methodology will be explained in two parts for a better description of the geometric and chemical components of the project. The first section of this chapter is dedicated to exploring the work performed by the program Delta Chem and describe the functioning of its routines. The second section describes the computational set used to test the program's performance in determination of the adsorption sites in the materials described in the introduction.

4.1 From vectors to MOFs: Exploring Delta Chem.

In a very general way, Delta Chem is a set of algebraic and geometric operations applied over a set of points distributed on a 3D space. These operations can be as simple as a dot product or as complex as a triangulation. The positions of the points are conveniently represented as vectors to allow their algebraic manipulation. For the functioning of Delta Chem, these operations were organized into four main routines. Each routine is a program itself and is in charge of performing one of the following tasks:

- To read an input *.xyz* file and transform the information from the string format of the text in the file to an adequate format for its processing in Delta Chem.
- To seek the existence of cavities within the cloud of points to determine their sizes, the position of their centers and the atoms that are closer to their surfaces.
- Computing the convex hull of a given set of 3D points and analyze the shape of the hull.
- To determine the regular polyhedron (platonic or archimedean) that best fits the shape of a given convex hull and compute the irreducible volume of the fittest polyhedron.

In Delta Chem, these tasks are executed sequentially so that the output of the former task is the input of the next. However, if an appropriate input is used, the

routines can be implemented individually. Each routine is constituted by a set of algorithms, some of them are proper of each routine but others are ‘external functions’ and can be used in more than one routine or independently. For all the algebraic operations the Python library Numpy is used, so the position vectors are represented as Numpy arrays. In the following subsections, each of the aftermentioned routines is described in the order in which they are executed by Delta Chem. For the purposes of the present project, the cloud of points analyzed corresponds to the atoms of a porous material. So that in some routines the cloud of points is treated like a *cloud of spheres* of radii given by the Van der Waals radius of each atom. The input of Delta Chem is a simple *.xyz* file containing the structure (atomic symbol and Cartesian coordinates) of a microporous material. To illustrate this section, the structures of the HKUST-1, UiO-66 and ZIF-8 were used.

4.1.1 Leganto: To understand Delta Chem is necessary to know how to read

Leganto¹ is the simplest and shortest of the four main routines, but its function is essential to put in motion the machinery of Delta Chem. It processes the structural information provided directly by the user with the *.xyz* file; organizes the data and convert it to a format adequate for the work of the subsequent routines. Regular expressions, RE, constitute a programming language by themselves with its own particular syntax. The RE constitute a very useful tool to find matches of groups of characters in a text; they are made available in Python by the module *re*. Leganto makes extensive use of these advanced search tools, so it can match alphanumeric expressions, numbers, letters, metacharacters, whole sentences, and even blank spaces according with the RE Python Manual².

Following the expected structure of the *.xyz* file, Leganto skips the first two lines of the file. Then matches all the lines that contain a letter at the beginning. Of course, this selection matches all the lines of the file bellow the third line since everyone begins with the atomic number. Each line is stored in a list as a string. Iterating over this list, the numeric characters of the coordinates are separated from the letters of the atomic symbol using the module *re* again. This process generates two lists to store the two different data. The list containing the strings of the coordinates is iterated to split the list into the blank spaces, generating arrays of three strings corresponding to the cartesian coordinates of the atoms in the analyzed

¹‘Leganto’ means ‘Reader’ in Esperanto

²Available at <https://docs.python.org/3/howto/regex.html>

material. Each string is converted to float and organized in a list of arrays of three elements. This information is conveniently organized in the form of a dictionary named **structure** which keys are the cartesian coordinates previously obtained, and which values are the corresponding atomic symbol.

The atoms in the the structure(and their coordinates) are then grouped according with the element type. The dictionary **grouped_atoms** is created using the information in the list of atomic symbols, using them as keys. For the values, lists with the coordinates of each atom belonging to a certain element are used. In this way a dictionary containing the position of all the atoms in the structure but organized in as many elements as are present in the material.

Another useful application of *re* is given to read the information regarding the Van der Waals radii and assign these values to the atoms in the structure. The information is obtained by reading the file 'radii_list.dat' included in the package of Delta Chem that is also used by PSD_solve. It is just a text file where each line contains the atomic symbol and the Van der Waals radii in Angstroms. The module *re* allows finding in the text the atomic symbols of the keys of **grouped_atoms**, stores each matching line, and separates the numerical information to use it as values of the dictionary **Vdw_radii**. This dictionary therefore contains the atomic symbols of the elements in the structure and their Van der Waals radii. This structural information is the base of the functioning of Delta Chem. The assignation of radii allows to treat the system as a set of spheres which size and surface is define by their corresponding Van der Waals radius instead of just a cloud of points. Therefore this small routine sets the frontier between the geometry and the chemistry in this project.

However, to analyze microporous materials the program also needs to know the size of the porosities that it should look for. The radii of the porosities are obtained by executing the program PSD_solve. This is a C-written program but it can be executed from a Python script through the module *subprocess* using the *.xyz* file and 'radii_list.dat' as inputs. The values for grid size and test particle size has been set in 0.25 Å as suggested by Battacharya and Gubbins, and 1.2 Å respectively.

The output file of PSD_solve, *.dat*, contains the Pore Size Distribution function calculated by the program with the method discussed in 3.1.4. The function *Porosity_Radius* reads the *.dat* file and separates the information regarding the PSD and the radii in different lists.

Once its job is done, Leganto returns the following information:

- The list **coordinates**. Contains the Cartesian coordinates of the analyzed structure.

- The list `lst`. This list contains other three list, each one corresponds to the X,Y or Z coordinates of the atoms but separated to be used for plotting in Matplotlib.
- The dictionaries `structure`, `Vdw_radii` and `grouped_atoms`.
- 1D array containing the PSD information
- List containing radii data provided by `Porosity_Radius`

Leganto contributes to the development of Delta Chem by making manipulable and graphically representable the structural information passed by the user. The atomic representations shown in Figure 4.1 constitute the framework within which all Delta Chem processes and operations are carried out.

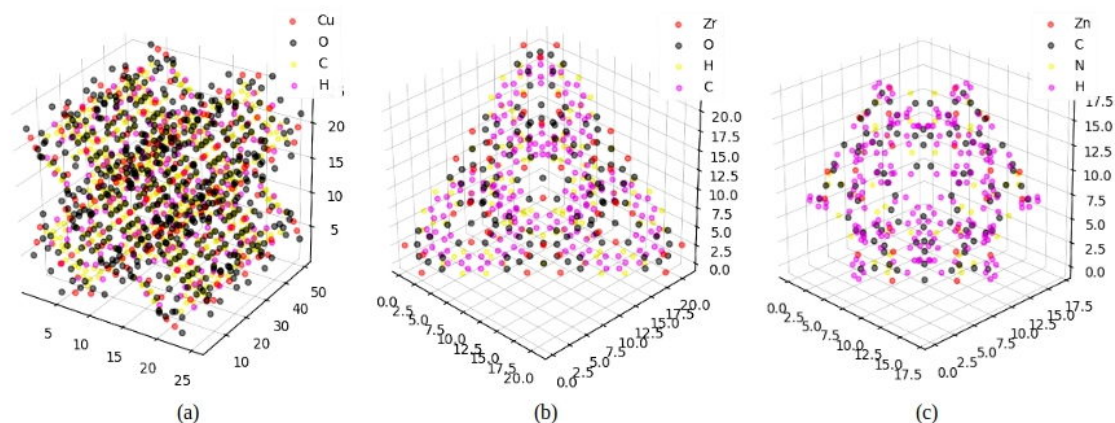


Figure 4.1: Structures of HKUST-1(a), UiO-66(b) and ZIF-8(c), read and represented by Leganto(and Matplotlib)

4.1.2 'Kerno': an unexpectedly (hard) journey to Find the Center of the Porosities

The routine `Kerno`³ is in charge of determining the existence of porosities and the position of their centers in a given material or a cloud of points. To perform this task, `Kerno` requires the information of atomic positions and pore sizes provided by Leganto.

With the function `find_peaks` taken from the SciPy module `signal`, `Kerno` analyzes the one-dimensional array that contains the information about the PSD to determine which peaks are relevant, so they could be considered as representative

³'Core' in Esperanto

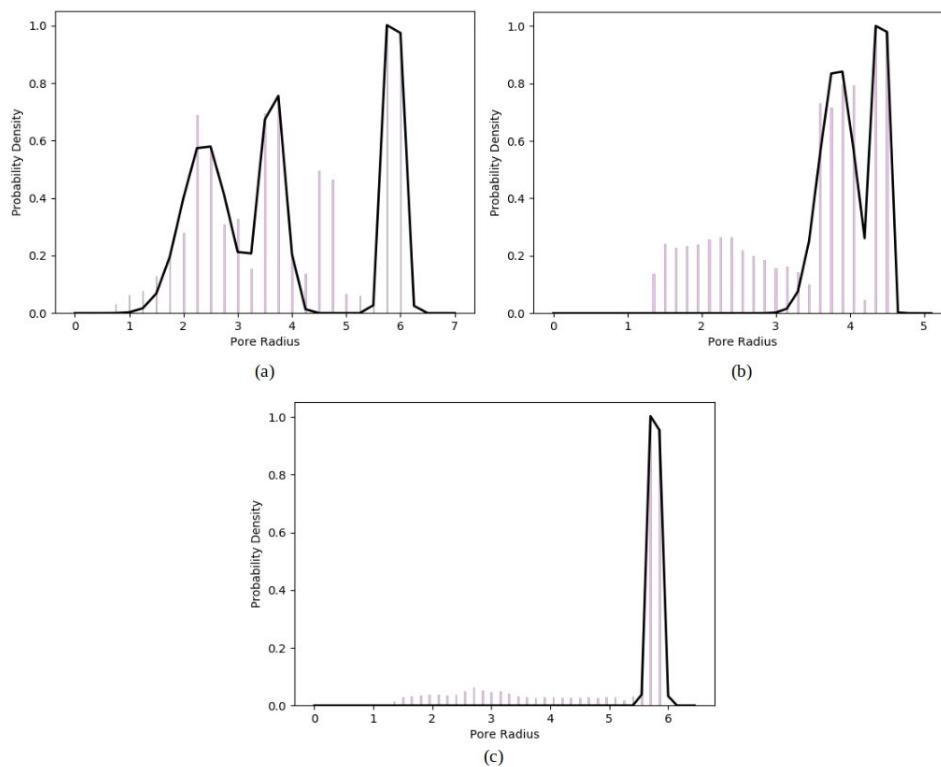


Figure 4.2: PSD vs pore radius plots for (a)HKUST-1, (b)UiO-66 and (c)ZIF-8. The different types of porosities present in a material coincide with the number of peaks in the plots

of the types of porosities in the material. According with SciPy online documentation⁴, by default *find_peaks* always finds all the peaks in the given data by simple comparison between neighbors. However, for this project, a more refined selection is required to separate the relevant peaks from this set of local maximums. The desired subset is obtained by specifying the height and the prominence of the peak. The former consider how strong is the signal generated by a possible type of porosity while the latter is a measure of the independence of a peak defined as the vertical distance between the peak and the lowest contour line [64].

These parameters have been set in 0.4 for both, height and prominence. These values work well for all the materials used during this project and shown in this chapter. The values of the probability density peaks in the selected subset are used to fit the PSD with Gaussians using the function *curve_fit* from SciPy module **optimize**. PSD vs Pore Radius plots for HKUST-1,UiO-66 and ZIF-8 are shown in Figure 4.2 with their corresponding gaussian fit. Delta Chem is suited to fit a maximum of four peaks with a tetramodal gaussian, i.e, the program can recognize

⁴Availble at: https://docs.scipy.org/doc/scipy/reference/generated/scipy.signal.find_peaks.html

up to four different types of porosity. This limit can be easily adapted to detect n porosities but it wasn't considered necessary for the materials analyzed in the present project. The pore diameters are chosen as the values corresponding to the maximums in the gaussian fit. The obtained values are just approximations so they can differ from experimental values up to 5Å [1]; however, they constitute good starting points for the following stages of the program. Provided with the structural information and the size of the porosities, Kernio is ready to begin an unexpectedly hard journey to achieve the main objective of the routine: To find the position of the centers of the porosities.

This task consists basically of finding the position of the center of a sphere of an arbitrary radius among a cloud of points so that no point of the cloud lies inside the surface of the sphere. The size of the pore is already known from the analysis of PDS_solve data, so the challenge is to detect the empty spaces in the given structure that match the radius of the spheres and find their centers. i.e, find a point that doesn't exist in a region where nothing exists.

For this reason, the first step in this process is to generate candidates to be the centers. A reasonable way to generate initial guests is to find the midpoints of the segments that can be formed between all the possible pairs of points in a given set. For a case where the points are treated as spheres(or atoms) the midpoint between two spheres of different sizes doesn't lie in the center of the segment their centers form and the calculation of the real position of the midpoint requires additional calculations that greatly increases the processing time required. Therefore, only the midpoints between spheres of the same radius (or atoms of the same element) are considered by Kernio to form pairs and obtain midpoints. As expected, systems with a considerable number of atoms present a huge number of initial candidates. To avoid the unnecessary calculation of midpoints, the distance between the points of each pair is taken into account. If this distance (taking into account the Van der Waals radii) is lower than a lower bound or higher than an upper bound, the pair is ignored from the subsequent calculations. For Delta Chem analysis, these values has been set as

$$lower_bound = smallest\ PSD\ radius - 1.2\text{\AA}$$

$$upper_bound = largest\ PSD\ radius + 1.2\text{\AA}$$

. The tolerance value $\pm 1.2\text{\AA}^5$, as many others in this routine, must be included to

⁵Hydrogen Van der Waals radius

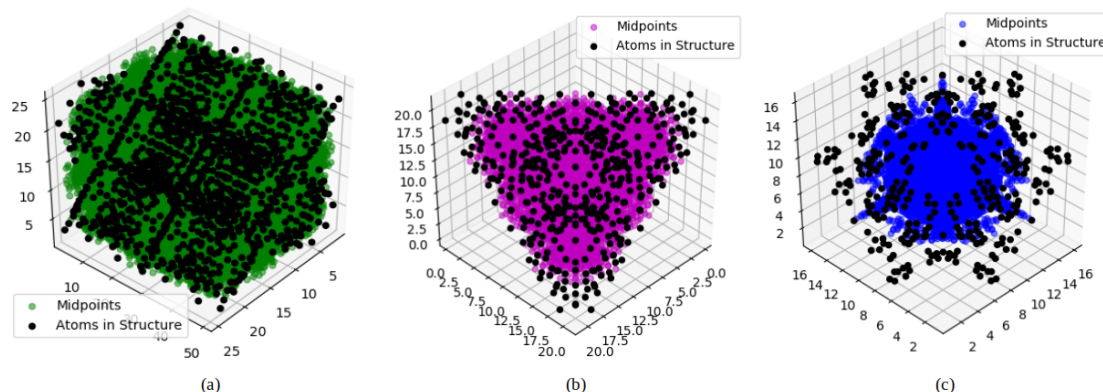


Figure 4.3: Initial candidates for porosities centers in: (a)HKUST-1, (b)UiO-66, (c)ZIF-8.

take into account deviations from the real values of the pore radius since PDS_solve results are just approximations. Distances between atoms outside these bounds are irrelevant since they obviously do not correspond nor are close to the position of the center of a porosity. Only if the distance is between this range the midpoints are calculated and stored in a list of candidates. Even with this restriction, the amount of candidates still too far to be realistic: 79950 candidates for HKUST-1, 7182 for UiO-66 and 5532 for ZIF-8. Kerno must be determine a single center per porosity type, so the quantities of initial candidates may seem absurd or even useless at first sight. However, the purpose of generating so many candidates is to populate the empty spaces in the analyzed structures, and as can be seen in Figure 4.3, it works very well.

A refinement process is necessary to eliminate the unlike candidates. Kerno applies a series of ‘filters’ and operations over these midpoints. The goal is to find the closest approximation to the real centers from the bulk of candidates.

Kerno’s First Filter: Pore Size

For this filter, Kerno first determines the closest atom for each candidate. The distance between them is used to classify the candidates as follows:

1. For each type of porosity, its pore radius lenght is compared against the ‘closest atom distance’(henceforth CAD) of each candidate.
2. If the CAD ranges between the bounds defined as

$$lower_bound = PSD\ radius - \frac{closest\ atom's\ VdW\ radius}{2}$$

$$upper_bound = PSD\ radius + \frac{closest\ atom's\ VdW\ radius}{2}$$

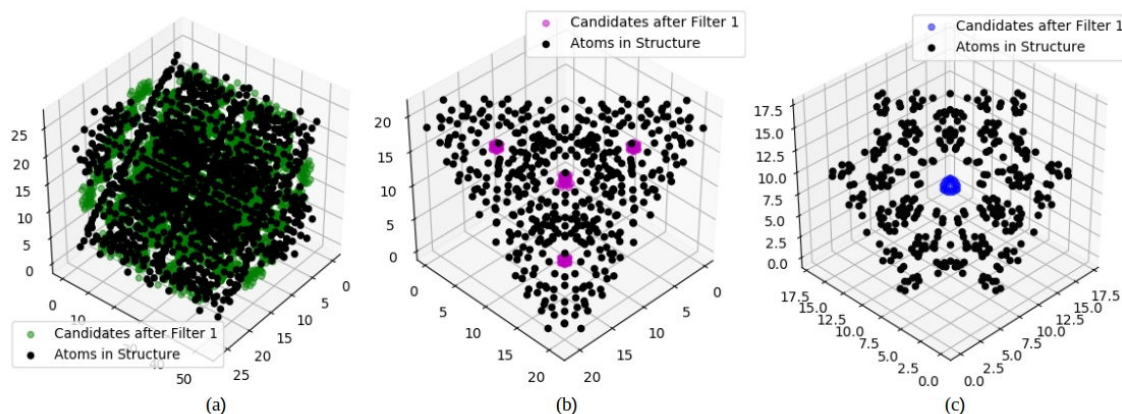


Figure 4.4: Candidates after Filter 1 for: (a)HKUST-1, (b)UiO-66, (c)ZIF-8.

i.e CDA of the candidate is really close to the length of a pore radius, the candidate represents a possible center for the given type of porosity and is allowed to pass this filter.

This filter drastically reduces the number of candidates at least to a 13% of the initial candidates: 11150 for HKUST-1, 198 for UiO-66 30 and for ZIF-8. Additionally, it allows the classification of candidates according to the porosity type. The great amount of data analyzed and classified makes this filter, the most time consuming process in Delta Chem execution. The effect of the first stage of refinement can be clearly appreciated in Figure 4.4. Even after this filter, the number of candidates remains too high to be useful, therefore further refinement is necessary.

Kerno's Second Filter: Neighbourhoods of Candidates

A way to reduce the amount and obtain more accurate candidates consist of form groups of 'closest neighbors' with the candidates. To perform this job Kerno calls the recursive function *grouping* which does exactly what its name suggests. The second filter process goes as follows:

1. Given a set of candidates to *grouping*, a random candidate is chosen to be the center of a sphere with the radius of the corresponding porosity.
2. The distance of the selected candidate with all the remaining candidates is calculated. Any other candidate lying inside the surface of the sphere is considered a neighbor of the former point.
3. A point belonging to a neighborhood cannot belong to any other so after a point is assigned to a neighborhood it is eliminated from the main list of points to won't be considered again in the assignation.

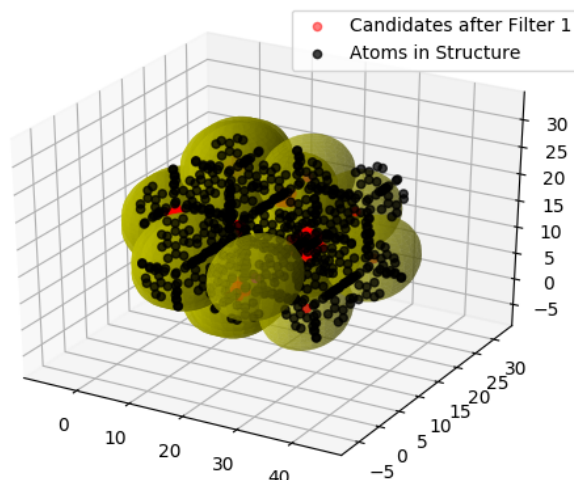


Figure 4.5: Neighbourhoods of Candidates created by Kerno through the function *grouping*. The structure used in the representation corresponds to the unit cell of MOF-5

4. Once all the possible neighborhoods are formed, their barycenters are calculated with the external function *Barycenter* which returns the position of the barycenter as an array of coordinates (x,y,z) .
5. The number of candidates per neighbourhood is determined.

Kerno makes use of *grouping* to repeat this operation with the new candidates until every neighborhood is formed by a single point. A graphical representation of this process is shown in Figure 4.5. This stage considerably reduces the number of candidates, passing from thousands to a few dozens. However, it is not good enough yet. A problem that arises from this process is that the candidates of a small porosity can be occupying positions of the candidates of bigger cavities since the smaller sphere can fit inside any of the others. To fix the problem of candidates of different porosities coexisting in the same pore cavity, the following sub-process is executed:

1. The distance between candidates of different porosities is measured.
2. If it results shorter than the pore radius of any of the pore cavities involved, then both candidates are marked for a further analysis to determine which of them actually belongs to the pore that both are occupying.
3. This analysis is straightforward: The distance to the closest atom for each candidate is compared against the radius of the porosity of which they are candidates. The selected candidate is the one that presents the minor difference.

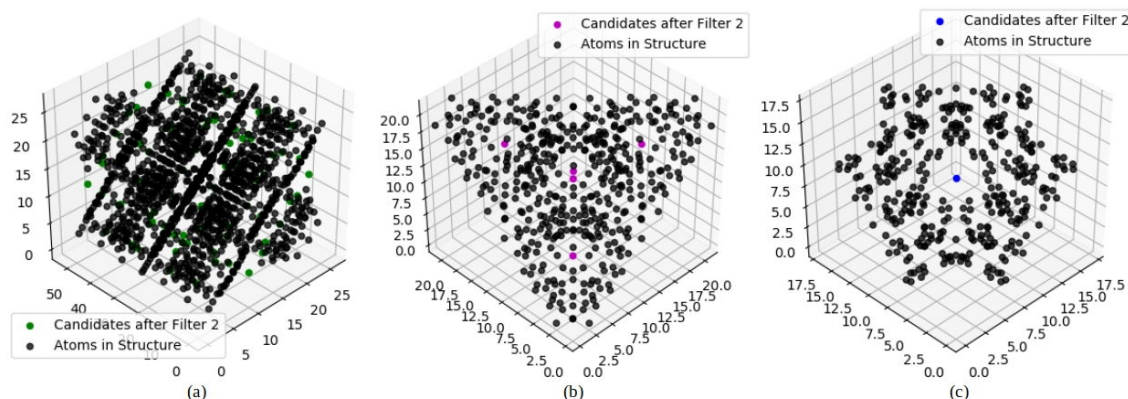


Figure 4.6: Candidates after Filter 2: (a)HKUST-1, (b)UiO-66, (c)ZIF-8

At the end of the second filter, the number of candidates has been reduced to 84 for HKUST-1, 5 for UiO-66 and 1 for ZIF-8. This can be appreciated in Figure. It is expected since the number of atoms in the unit cell HKUST-1 used for the calculation is much higher (1424) than that of UiO-66 and ZIF-8 unit cells (466 and 360 respectively). The effectiveness of both filters is undeniable, but the goal has been set to obtain one center per porosity type. A final refinement is imperative and as will be seen, the last candidates are the most difficult to eliminate.

Kerno's Third Filter: Pores in the Shell

By definition, the sphere representing the pore cavity shouldn't contain any point (or sphere) inside its surface. However, since the candidates and the pore sizes are just approximations based entirely on the geometry of the system, that condition is not fulfilled by any of the candidates. The best option to advance in the process is to find the candidate closest to the real center.

The logical step to continue the selection would be looking for the candidates in which spheres contain the least number of points or spheres inside. However, this strategy fails in structures like the MOF-5 in Figure 4.7a, that presents candidates outside the pore cavity. Since they are surrounded by fewer atoms, the count inside the surface of the yellow region will be lower than in the cyan sphere.

It shouldn't be a problem since, by symmetry, the points outside would be equivalent to those inside the pore cavities in the given structures. However, further calculation in Delta Chem requires the knowledge of all the atoms directly surrounding the center of the porosity; information that is incomplete if considering the candidates outside the pore cavities. One option is to use a bigger unit cell but the computational cost required to include more atoms is too much to pay, so another strategy is devised: to look instead for the candidates surrounded by the highest

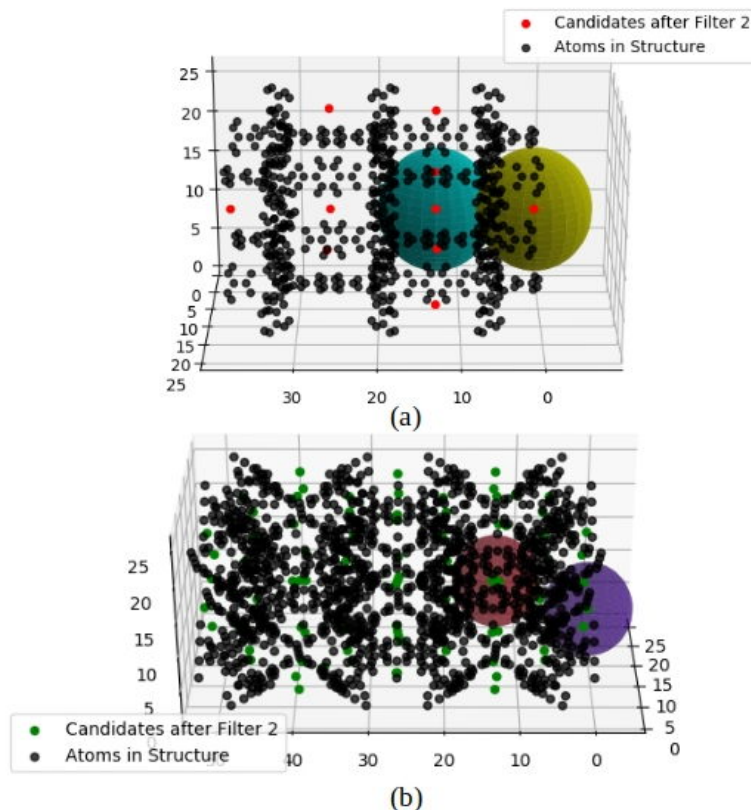


Figure 4.7: Special geometrical situations in the structures of (a)MOF-5 and (b)HKUST-1

number of spheres. This idea may seem a little bit countersensical but it works in the following way:

1. For each candidate define a spherical shell of thickness $\pm 1.2\text{\AA}$ (The Van der Waals radius of the Hydrogen atom) and a radius equal to that of the corresponding porosity.
2. The candidates with more atoms inside this shell are considered for the next stage.

The application of this strategy effectively eliminates false positives as expected. The ‘shell technique’ is used instead of just counting atoms inside the surface of a sphere to avoid the problem depicted in the Figure 4.7b, where the candidates in the indigo region also have a lot of atoms inside its sphere, but they are not evenly distributed around the shell as for the candidate in the crimson region. The candidates that have advanced at this point of the selection process constituted less than one percent of the original candidates. However, Delta Chem requires a single center per porosity type, so a final cut is necessary.

For each candidate, if the difference between its CAD and the length of the radius of the porosity results less than 1\AA , the candidate passes this stage, else

it is not considered for further stages. At the end of this filter, just a few atoms (or maybe just one) are left. The winner is finally determined as the one which CAD differs the less from the pore radius length. The atoms that contribute to the shell of the winner candidate are selected to be the input data for the next routine. These are the atoms that directly contribute to the internal surface of the cavity. In this laborious, countersense but effective way, Kerno determines the position of the centers of the pore cavities in a porous material and defines which atoms belong to each porosity.

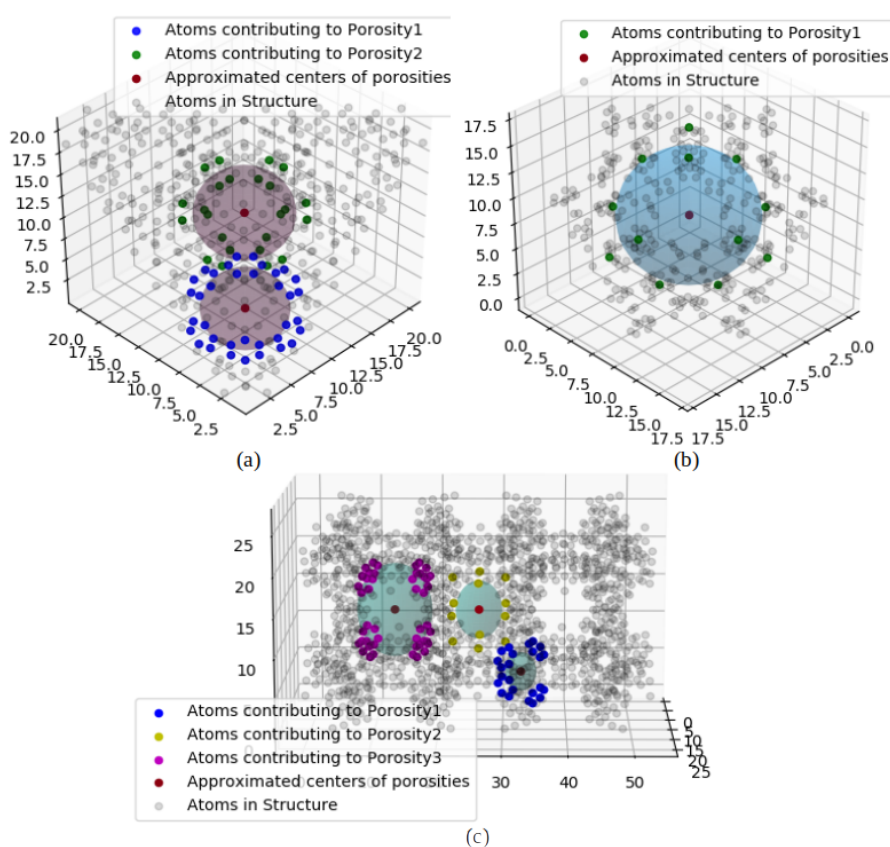


Figure 4.8: Final results provided by Kerno, includes centers of porosities, pore cavities' spheres, and contributing atoms of each porosity for (a)UiO-66, (b)ZIF-8, (c)HKUST-1

The final work performed by Kerno can be visualized in Figure 4.8 The returned information of this routine includes:

- A list containing the pore radii values
- A dictionary with the Cartesian coordinates of the centers as keys and the coordinates of the atoms contributing to each porosity as values.

4.1.3 Mozaiko: Modelling everything with Triangles

Mozaiko⁶ is the routine in charge of computing the `Convex_Hull` of any set of 3D points, and perform an analysis of the shape of the triangulated surface of the `Convex_Hull`. To accomplish the first task, Mozaiko creates a ‘convex hull object’ with the class `Convex_Hull`. This class is a translation to Python of the C-written code of Joseph O’Rourke [16] that implements the incremental algorithm discussed in Chapter 3. Using the cartesian coordinates of a given set of points, the function `Convex_Hull` computes a 3D Delaunay triangulation and makes easily accessible and modifiable information regarding connectivity between vertices to form edges and faces. The ‘class’ format allows treating the triangulation as an object whose elements can be easily accessed and manipulated. The method `Export_faces` makes available the organization of the faces of the created convex hull, i.e. the coordinates of each vertex in every triangle of the hull. Similar information can be obtained with the method `Export_triangles` that contains the indices of each vertex of every triangle; these indices are assigned in the order that data is received in the `.xyz` file. The coordinates in the faces correspond to the points used as input since no transformation is applied during the triangulation process.

The implementation of this algorithm is not as straightforward as it may appear by its description, and a relatively complex data structure is required to represent vertices, edges, and faces. The function `Convex_Hull` only deals with points, so in their calculations, the information regarding the type of atoms or Van der Waals radii is not required nor considered. In Delta Chem, Mozaiko controls the execution of `Convex_Hull`. It makes use of the information regarding the atoms contributing to the porosity shape to use them as vertices for a triangulation. This generates a ‘limiting mesh’ for the internal surface of the porosities in the studied materials. The triangulations of the pore cavities for HKUST-1, UiO-66 and ZIF-8 are shown in Figure 4.9, there their symmetrical conformation is highlighted. Only the convex hull and not the whole triangulation is calculated here because only the surface of the polytope generated is required to model the shape of the internal surface of a pore cavity and because the convex hull is easier to handle than the whole triangulation since the former only deals with triangles instead of tetrahedrons. The triangles (indices) and faces (coordinates) are used in the next stage of Mozaiko’s execution.

The triangulation is analyzed with the function `Convex_Hull_Analysis` which determines the polygonal planes that can be formed with the triangles. This informa-

⁶‘Mosaic’ in Esperanto

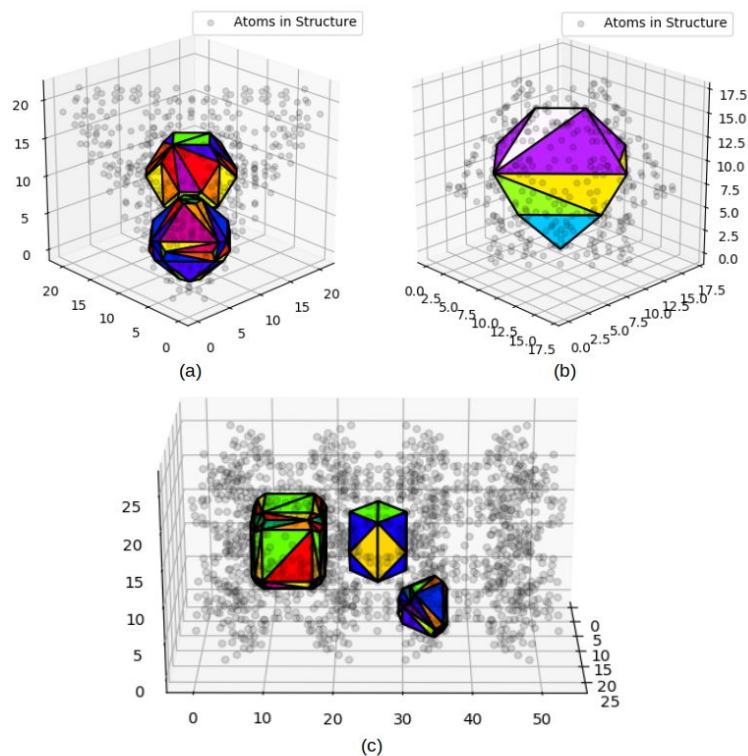


Figure 4.9: Convex Hulls of pore cavities for the structures of (a)UiO-66, (b)ZIF-8, (c)HKUST-1. Note the high symmetry of the resulting convex hulls.

tion is essential for further fitting with uniform polyhedrons. The strategy is simple: to chose an arbitrary triangle of the hull and determine which other points lie in the plane defined by the triangle; then determine the convex hull of the polygonal plane and its area, store this information and continue to other triangle until all the possible polygonal planes of the convex hull have been determined.

The work performed by *Convex_Hull_Analysis* goes as follows:

- A copy of the list *triangles*, obtained with **Export_ triangles**, is created.
- An iteration over this list takes one triangle and then a copy of triangles is made again but the selected triangle is removed from this new list.
- The indices of the triangle are used to obtain its coordinates and are added to a list called *tetrahedron*. Therefore, this list contains three elements initially. The fourth point is added iteratively over a list containing the coordinates of all the vertices of the triangulation except for those corresponding to the triangle's vertices. Once the fourth coordinate is added to it, the list is turned into a numpy matrix to obtain the volume.
- To determine if a given point is coplanar to the points of the triangle, the

fourth point passed to *tetrahedron* is used to generate a tetrahedron which volume is calculated with the determinantal form of the tetrahedron volume. If the volume is equal or is very close to zero, the tetrahedron results to be a flat body with its four vertices lying on the same plane.

If the tetrahedron meets the after-mentioned requirements the vertex index is added to the list of vertices of the plane defined by the triangle whose vertices are already included in the *in_plane_indices* list. Once the iteration is over, all the vertices belonging to the plane are used to determine which other triangle belongs to the same plane by a simple comparison of indices. If all the indices of a triangle are in the list of plane indices, that triangle is included in the *in_plane_triangles* list and is removed from the main list so that it won't be part of the calculation more than once. The final list contains the indices and triangles of a plane, it is passed to another list outside the main iteration. As consequences of this selection-deletion process, the list formed has as many elements as polygonal planes can be formed from the analyzed convex hull, and the smallest polygonal face that can be obtained is a triangle.

For this project, the term 'polygonalization' is used henceforth to refer to the process of classifying the surface of a triangulated polytope according with the largest polygons that can be formed by coplanar triangles. The polygonalization process consists in determining the convex hull of the points belonging to each of the previously determined planes, i.e, the vertices that define the perimeter of each polygonal face of the polytope. It is not necessary to create a 'convex hull object' again since all the triangles that conform to the polygonal face are already known from the triangulation. According to O'Rourke [16], in the case of the plane triangulation, a point is a vertex of the polygonal convex hull if it belongs to an edge that also belongs to the hull. An edge belongs to the convex hull if and only if it belongs to a single triangle in the triangulation. The list *in_plane_triangles* is used for this task. It contains k lists of triangles, with k being the total number of polygonal faces of the polytope. So, for each triangle in *in_plane_triangle* all the possible combinations between the vertices of the triangle are computed. Of course, only three combinations are possible, but this sub-process allows us to manipulate the triangle edge by edge, represented by each pair in the combination. Each edge of the triangle is evaluated looking for its presence in other triangles of the plane.

For each edge in the triangle, its both indices are compared against the indices of each triangle in *in_plane_triangles* list. A counter is set in zero before the iteration this list begins. If both indices are found in a given triangle the counter adds one. At the end of the loop, if the counter is equal to one, that edge of the triangle

belongs to the convex hull of the plane. The process finalizes when every edge of each triangle has been analyzed and the polygonal convex hull is totally conformed. During the iteration over this list, the area of each triangle is calculated and summed to determine the total area of each polygonal face. The area of one of these triangles is calculated based on the rule of the parallelograms: The cross product of any pair of vectors formed by the vertices of the triangle is calculated, then the norm of the resultant vector is divided by two.

The planes obtained as result of the polygonalization *Convex_Hull_Analysis* are shown in Figure 4.10, for the three types of pores in HKUST-1, in Figure 4.11 for both types present in UiO-66, and in Figure 4.12 for the single porosity in ZIF-8. The symmetry of the limiting mesh is obvious at first sight. They are indeed regular polyhedrons, but not all of them are uniform (platonic or archimedean). This differentiation is performed in the final stage of Mozaiko's execution, and is based on the relation of the sides of the polygons that constitute the faces of the polytope.

The indices of the polygonal convex hull are used as keys for different dictionaries. Since each list of indices represents a single face in the polytope, this is a good way to relate the information of the faces of the polytope with other useful structure information like the area of each plane.

Additionally the dictionary *Hull_polygons* is created. It contains the faces of the polytope as keys, but the values are strings that identify each polygonal face as 'regular', 'semi-regular', or 'irregular'. Once the polygons of the polytope have been identified, each one is evaluated to find its largest and shortest edges and obtain the ratio min_edge/max_edge . If a face is a regular polygon this relation should be close to 1. Mozaiko considers that a value bigger than 0.9 is also valid as has been demonstrated by the analysis of the structures used for the illustration of this chapter. If the ratio value lies between 0.4 and 0.9, the face is semi-regular and if the value is lower than 0.4 the face is irregular.

This information is used to classify the polytope's general shape. For a given 3D convex hull, it is considered 'Regular_a' if all its faces are regular polygons or semi-regular polygons with an area of at least 80% of the maximum area found in a plane of the hull. If regular and semi-regular polygons are present but the area of the latter is less than the aftermentioned area percentage, the polytope is marked as 'Regular_b' type. Consider cases like the octagonal face in the convex hull of the big cavity of HKUST-1 (Figure 4.10c). It seems regular but the value of 0.76 marks it as 'semi-regular'. The relaxation in the selection is included to take into account this imprecision associated with the structure of the material. However, always taking into consideration finding the best possible fit of the polytope shape, a 'semi-regular'

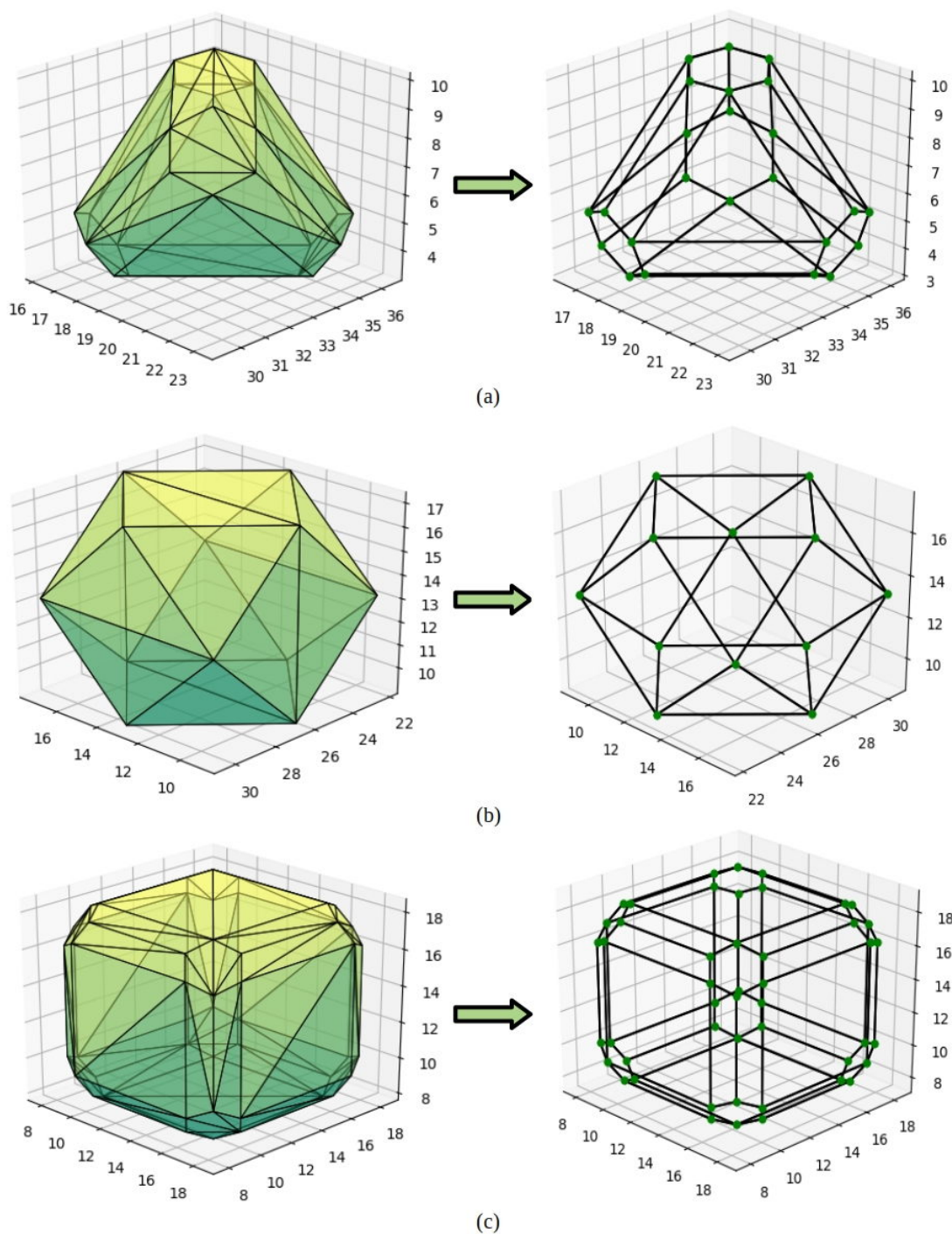


Figure 4.10: Polygonalizations of the convex hull of (a) Small porosity (radius $\sim 2.382\text{\AA}$), (b) Medium porosity (radius $\sim 3.649\text{\AA}$), (c) Large porosity (radius $\sim 5.873\text{\AA}$) in HKUST-1 structure

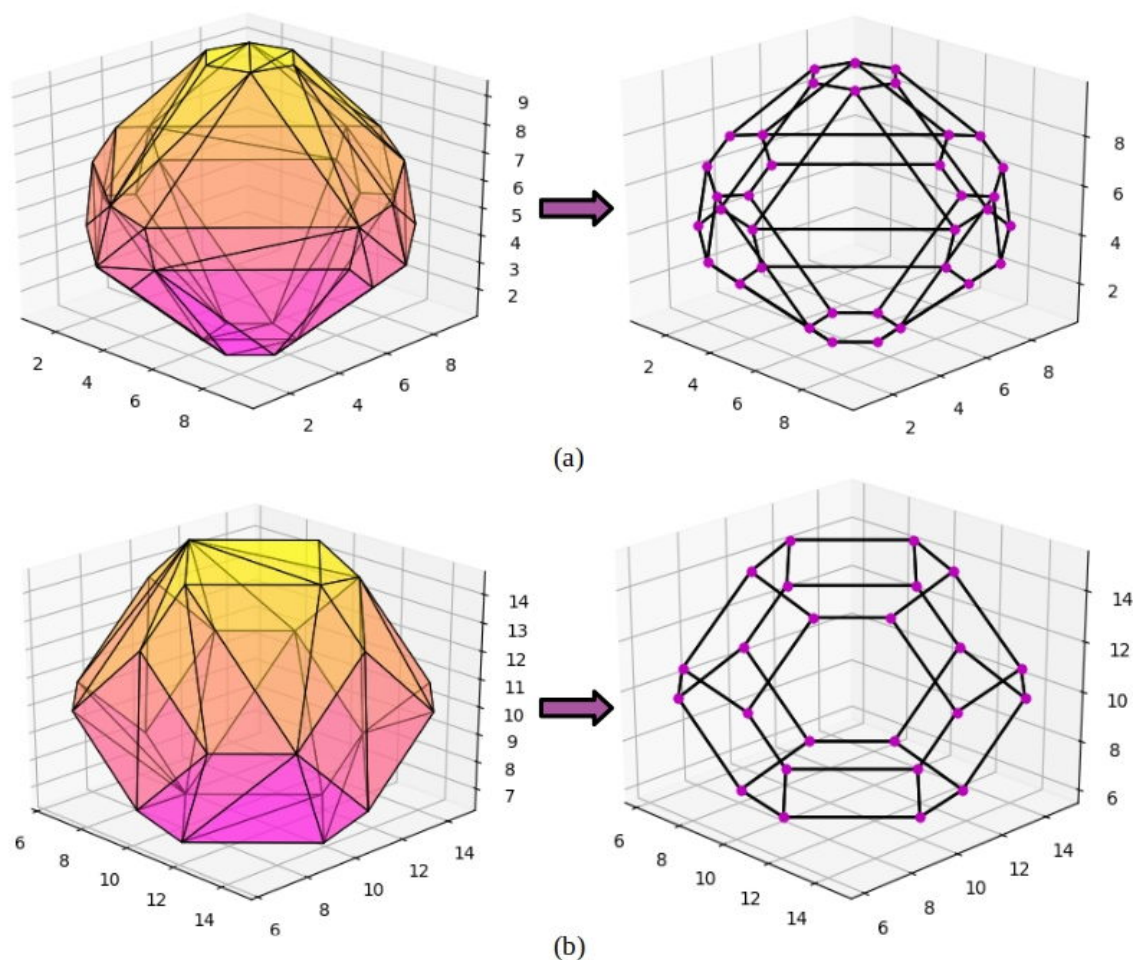


Figure 4.11: Polygonalizations of the convex hull of (a) Small porosity (radius $\sim 3.828\text{\AA}$) (b) Large porosity (radius $\sim 4.425\text{\AA}$) in UiO-66 structure

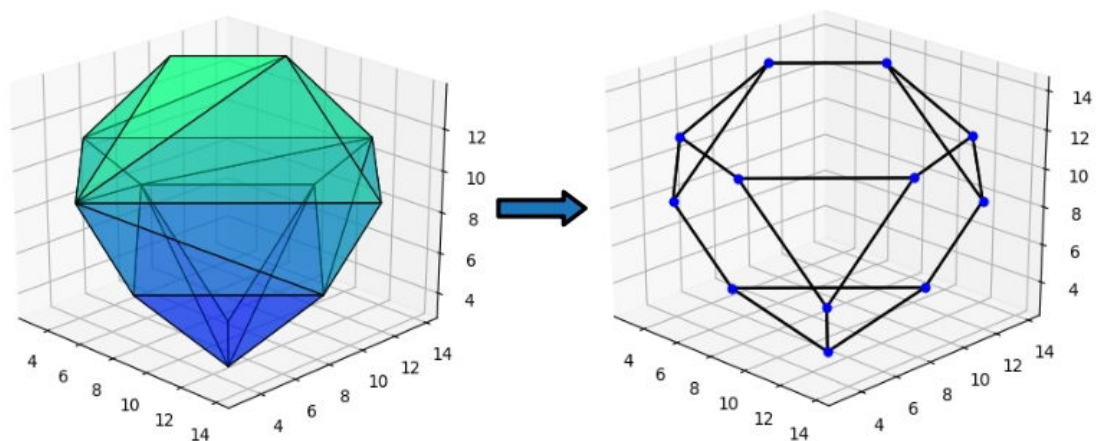


Figure 4.12: Polygonalization of the convex hull of the single porosity (radius $\sim 5.773\text{\AA}$) in ZIF-8 structure

face is accepted only if it is the surface area of the polytope. This selection avoids the detection of false positives with faces that could be characteristic of some other type of polytope.

If *Convex_hull_analysis* detects that the polytope of a cavity meets the requirements to be considered regular, it stops the calculations over the convex hull and returns the following elements:

- **C_hull_v_area**, a dictionary containing arrays with the coordinates of each vertex of the polygonal faces as keys, and the corresponding areas as values.
- **C_hull_i_area**, a dictionary similar to the last one, but with the indices of the vertices as keys instead of the coordinates.
- *suggestions*, a list of integers corresponding to the number of vertices of the faces that Mozaiko considers must be present in the fittest polyhedron to procure the best fitting of polytope shape.
- The number of faces of the polytope.
- The area of the largest polygonal face.
- The indices of this polygon, and the polytope type as a string.

This output is generic for every type of polytope. The difference lies in the suggestions, the number of faces and areas returned. For the ‘regular’ case, the suggestion corresponds to all the polygons present in the polytope. The number of faces returned also corresponds to the total number of planes found in the triangulation.

However, the situation is not always that simple and the convex hull cannot always be considered ‘regular’. The presence of ‘irregular’ polygons is indicative of two operations that may be present in the polytope and define the real shape of the pore cavity. These operations may be Truncation and Expansion.

Truncation is the removal of partitions of solids talking outside a set of symmetrically placed planes [65]. This operation is easy to identify in the smallest polytope of the MOF-5 shown in Figure 4.13. There, the irregular octahedron can be seen as originated by removal of the triangular section from the corner of a square. In 3D, this sectioning is applied over a cube. Depending on the volume removed, this process can generate solids as the truncated cube and the cuboctahedron.

Expansion, also known as Cantellation, is an operation where faces are separated and moved radially apart. It is characterized by the formation of new facets at separated elements [65]. The presence of irregular quadrilaterals and triangles may

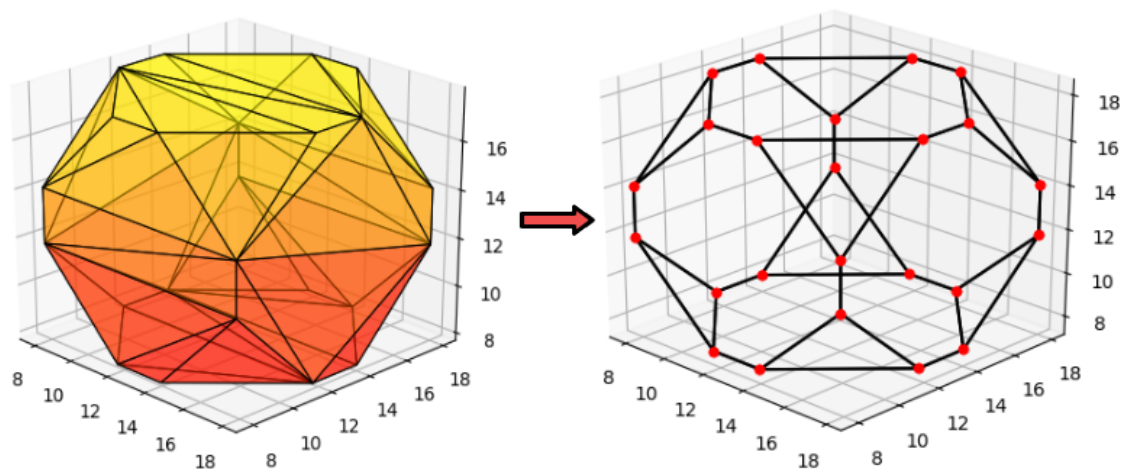


Figure 4.13: Example of Truncation in the small porosity (radius $\sim 5.911\text{\AA}$) in MOF-5 structure

indicate the cantellation of the polytope. The small porosity of UiO-66 (Figure 4.11a), the biggest and the smallest porosities of HKUST-1 (Figure 4.10a and 4.10b).

The treatment given by Mozaiko is different for a ‘Truncated’ or ‘Cantellated’ polytope. The difference is based in the presence of irregular ⁷ quadrilaterals and triangles. If they are present Mozaiko marks the polytope as ‘Cantellated’ else, it is marked as ‘Truncated’. The suggestion list for the truncated case is composed by:

- The integer corresponding to the number of vertices in the convex hull of the biggest regular polyhedron, passed always as the first element by *Convex_hull_analysis*.
- The integer corresponding to the number of vertices in the biggest irregular polygon.
- The same integer of the previous index but divided by two.

In this way the possible solids and faces that can be generated in the truncation are taken in consideration to determine the fittest polyhedron. The number of faces returned is the same of the polytope.

If a cantellation process is identified, the number of faces to be returned must follow certain constraints:

- All the polygons that have the area of the biggest regular polygon of the polytope contribute to the count of faces.

⁷‘Irregular’ refers to that the polygon doesn’t have all their sides equal, but they are still being symmetrical.

- The irregular quadrilaterals and triangles contribute if their area is meaningful, i.e., it represents at least 80% of the area of the largest regular polyhedron.
- Other irregular polygons contribute to the count if their area corresponds to that of the biggest irregular polyhedron.

Another characteristic that allows the identification of cantellations is the presence of small regular polyhedrons with more than four vertices like the hexagons in the small polytope in the HKUST-1. These polygons always contribute to the number of faces. In a cantellation, two numbers of faces returned the first one accounts for all the regular polyhedrons. The second one also accounts for the contributions of irregular faces. In this way, an increased number of faces due to the cantellation can also be considered to fit the polygon.

The suggestions for a cantellation also must obey some rules:

- The biggest regular polygon is always included as the first element.
- Quadrilaterals are included if they contribute to the number of faces.
- The biggest irregular polygon is included only if it corresponds to that of the largest polygonal face in the hull.

Mozaiko offers a complete analysis of the surface delimited by a 3D convex hull and provides the information necessary to reach the main goal of the project: Find the irreducible volume of the pore cavities. Just like *ConvexHull*, *Convex_hull_analysis* only requires the coordinates of the points. If a ‘convex hull object’ is passed as an argument, it can work independently.

4.1.4 Fragmento: Let’s find that Irreducible Volume

The last routine of Delta Chem pursues the main objective of the program: To calculate the irreducible volumes of the porosities in the studied material. Mozaiko analyzed the polytope obtained from the triangulation and provided hints about the shape of the internal surface of the pore. Fragmento⁸ makes use of this information to orient the election of the polyhedron that best resembles the shape of the pore cavity. The dictionary ‘polyhedron’ is used to access the information of the polyhedra that will be tested to find the fittest. The keys of this dictionary are strings with the name of the polyhedrons and the values are functions with the same name. For each polyhedron, the function named after it contains the information necessary to

⁸‘Fragment’ in Esperanto

build the polyhedron on the surface of a unitary sphere. This function is called with the name of the polyhedron, passing arbitrary radius and center as an argument. The former argument is used to scale the vertices of the polyhedron to be in the sphere's surface of an arbitrary radius, while the latter is used to translate them to be centered about this point.

The volume and surface area of the polyhedron is also calculated inside each function. The faces of the polyhedron are grouped by areas. The return values of each of these functions is the following:

- Vertices and indices of the polyhedron
- Number of faces
- Volume and surface area
- Area of the largest face of the polyhedron
- A dictionary with the faces of the polyhedron, grouped by the areas of the polygons that conforms it.

For a given porosity, the dictionary 'polyhedron' is iterated. For each solid selected, the after mentioned parameters are obtained using the radius and center of porosity as arguments. The process that follows each polyhedron to be selected or rejected, differs if the polytope that is being analyzed was marked by Mozaiko as 'Regular_a', 'Regular_b', 'Truncation' or 'Cantellation'.

If the analyzed polytope turns out to be going through a process of Cantellation, the elimination process of the non-adequate polyhedrons is the following:

1. The selected polyhedron passes this filter if the number is equal to any of the two possibilities passed by Mozaiko.
2. In the next filter, the selected polyhedron must present faces with the same number of vertices of the biggest regular polygon of the polytope. This information (the number of vertices) is always passed by Mozaiko as the first value in the list 'suggestions'. For the cantellation, the test polyhedron must also present (if exist) the remaining suggestions too.
3. If a polyhedron fulfills these requirements it is added to the list of possible candidates.
4. The fittest polyhedron is selected from this list by choosing that one in which the biggest face area differs the least from the area of the biggest regular polygon of the polytope.

If the polytope is going through a truncation process only one number of faces is passed by Mozaico. The selection rules are similar to those of the cantellation and go as follows:

1. A test polyhedron passes the first filter only if it presents the same number of faces specified by Mozaico.
2. To advance this stage the polyhedron must present faces with the same number of vertices as the biggest regular polygon just like in the cantellation . The difference is that the presence of faces corresponding to the other suggestions (if exist) is optional.
3. The fittest polyhedron is finally defined in the same way as the cantellation.

If the polytope is Regular_a or Regular_b, the selection process is simplified. The fittest polygon will have the same number of faces. The shape will be preserved and no suggestions are necessary. The fittest polyhedron is the one that presents the volume closest to that of the polytope. The results of the selection process gives a single fittest polyhedron per porosity in a material and they are shown in Figure 4.14 for the HKUST-1 porosities, in Figure 4.15 for UiO-66 and in Figure 4.16 for ZIF-8 pore cavity.

Alignment of the Fittest Polyhedrons

After being selected, the fittest polyhedron must be aligned so that it accurately represents the shape of the pore cavity. The examples in the Figure 4.17 shows that a misaligned polyhedron is not an appropriate representation of the cavity, and if the fittest polyhedron is not aligned, neither will be its irreducible volume. The alignment must be as general as possible and entirely based on the system. The faces of the polyhedron must be oriented so that their disposition resembles those of the faces of the polytope.

The first step in the alignment process is to orientate the biggest face of the polyhedron parallel to the biggest face of the polytope. Both polyhedron and polytope have many faces whose areas equals the maximum one found in them. Since they are equivalent in uniform polyhedrons, one of them is chosen randomly.

Algebraically, the objective is to rotate the vector perpendicular to the face of the polyhedron so that it points to the same direction of the vector perpendicular to the face of the polytope. It implies a transformation, therefore a rotation matrix is used for this alignment. The matrix is built to rotate an object an angle defined by the dot product of these vectors, around an axis defined by their cross product.

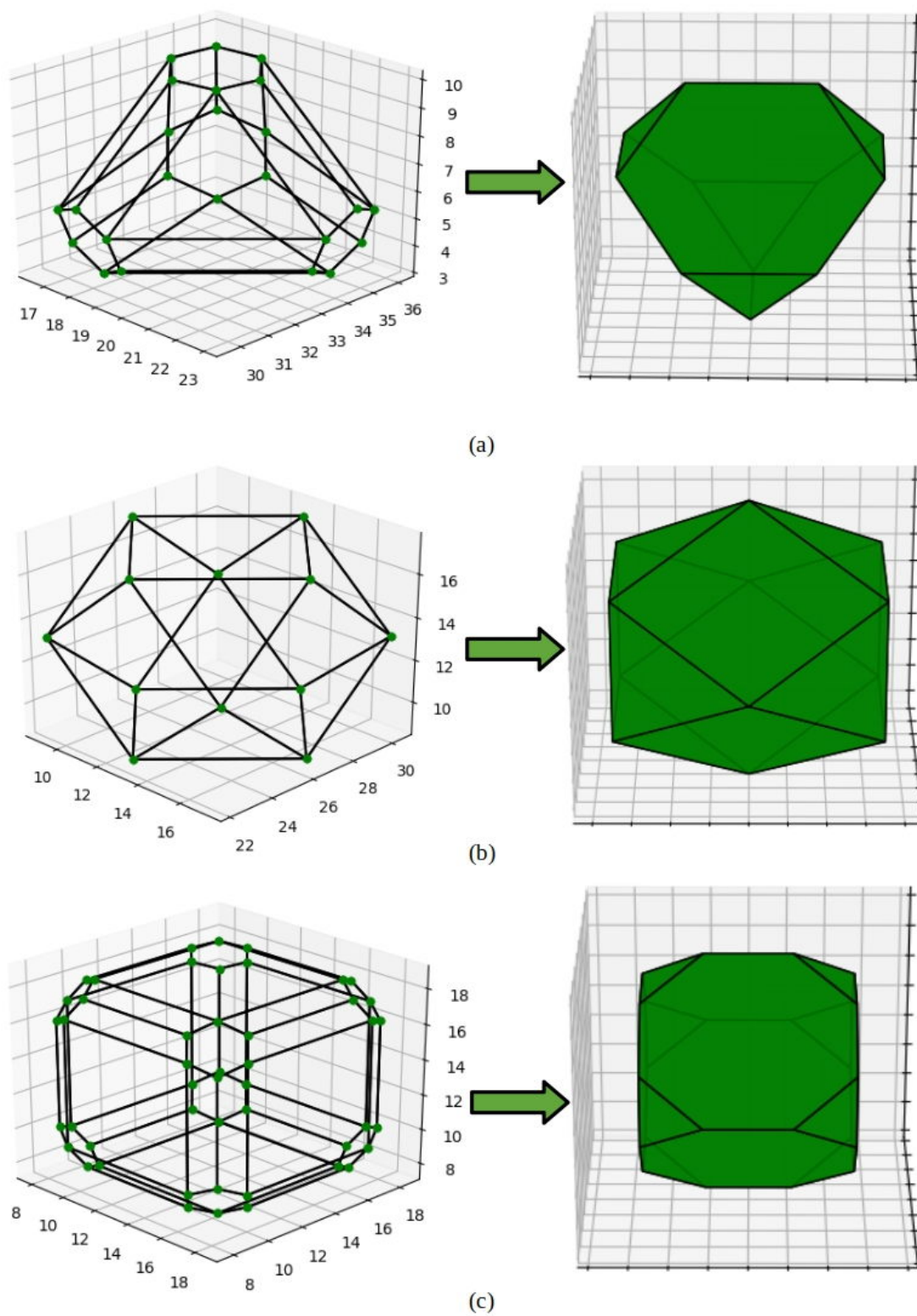


Figure 4.14: Fitting with regular uniform polyhedrons for (a) Small porosity (radius $\sim 2.382\text{\AA}$), (b) Medium porosity (radius $\sim 3.649\text{\AA}$), (c) Large porosity (radius $\sim 5.873\text{\AA}$) in HKUST-1 structure

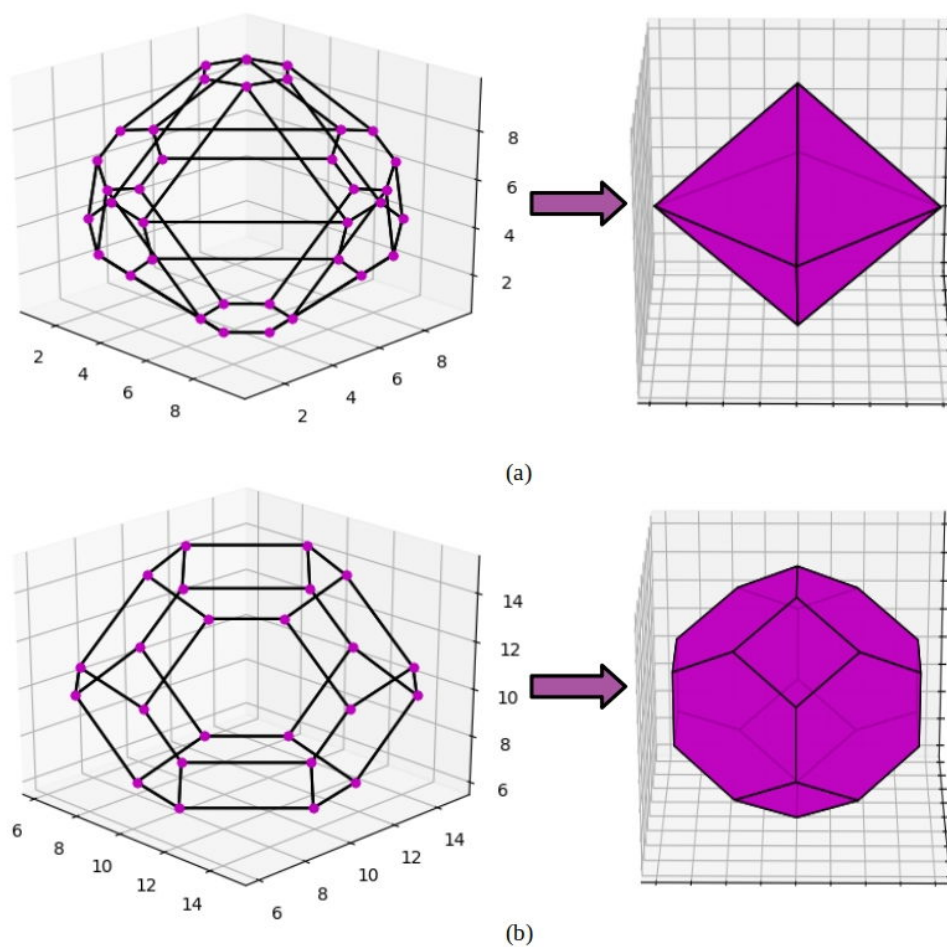


Figure 4.15: Fitting with regular uniform polyhedrons for (a) Small porosity(radius $\sim 3.828\text{\AA}$), (b) Large porosity(radius $\sim 4.425\text{\AA}$)

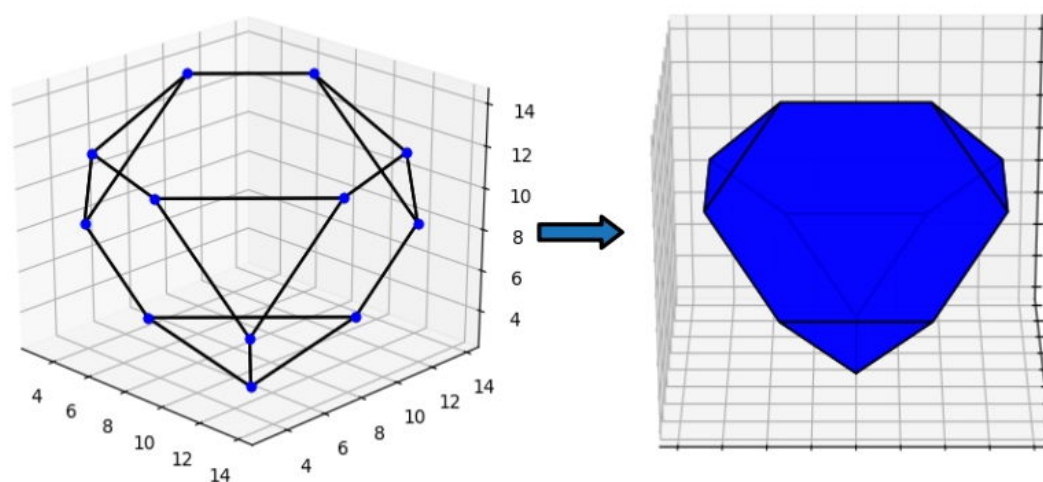


Figure 4.16: Fitting with regular uniform polyhedrons for the single porosity(radius $\sim 5.773\text{\AA}$) in ZIF-8 structure

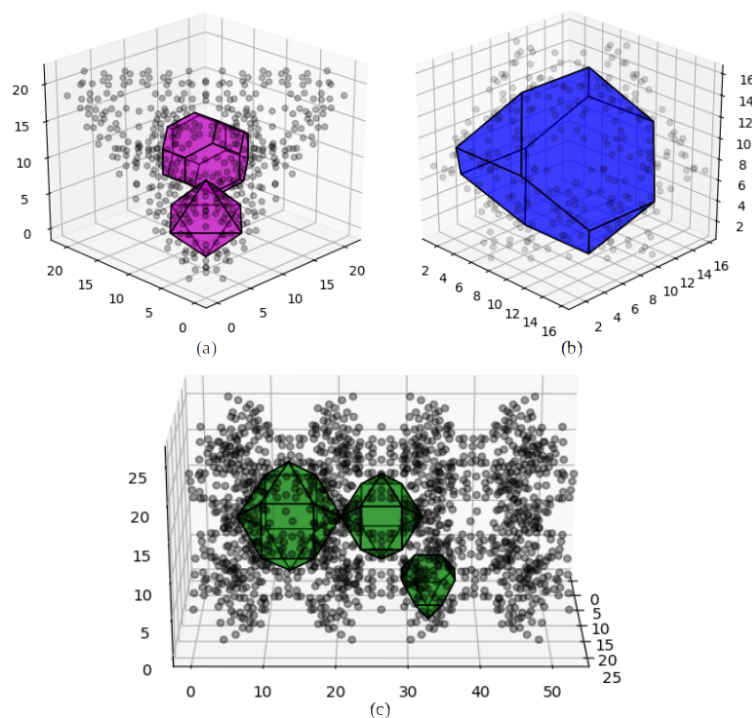


Figure 4.17: Fitting with regular uniform polyhedrons for the structures of (a) UiO-66,(b) ZIF-8,(c) HKUST-1.Note the misalignment of some the polyhedrons.

Once the matrix is built, every position vector corresponding to the vertices of the polyhedron is transformed with the matrix. It is called with the function *rotation_matrix* using the vector to be aligned as the first argument and the target vector as the second.

As can be appreciated in the large pore cavity of UiO-66 in Figure 4.18a, the small porosity of HKUST-1 (Figure 4.18c) and the pore cavity of ZIF-8 (Figure 4.18b), even after the application of the latter transformation some polyhedra are still misaligned and often a second rotation is necessary to ensure the correct rotation of the edges and the faces of the fittest polyhedrons. This new process requires the construction of a second alignment matrix. However, depending on the type of polytope, the second matrix building may requires different processes.

If the polytope is going through truncation or cantellation, the second rotation matrix is built as follows :

1. The target vector is defined between the barycenter of the biggest irregular polygon of the polytope and the midpoint of its largest edge .
2. The polyhedron direction vector (to be aligned) is defined from the barycenter of the biggest face of the polyhedron to the midpoint of a side that connects with a face with the same largest area. The aim is to orientate correctly the

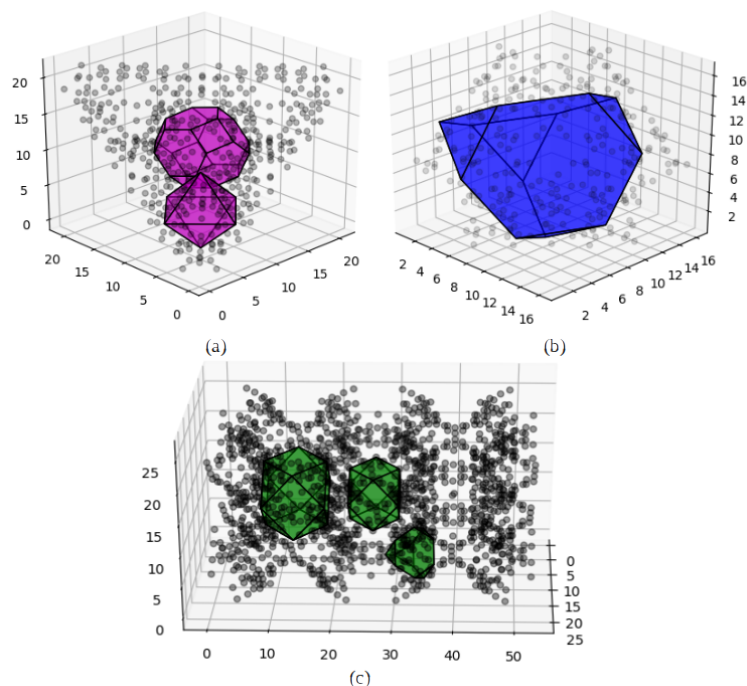


Figure 4.18: Fittest polyhedron after first alignment transformation for structures of (a) UiO-66,(b) ZIF-8,(c) HKUST-1.

edges and model appropriately the “windows” of the structure. As before, the rotation matrix is a structure with these two vectors.

This transformation works perfectly for the cantellation and truncation types of polytopes. However, the regular polytopes present an unexpected problem for the alignment and its symmetry turns into an inconvenience. A representative case is the truncated cube in the small porosity of MOF-5 shown in Figure 4.19, whose biggest face is an octagon. In this particular polyhedron, the octagonal face connects with two types of polygons, triangles and other similar octagons. The last strategy fails because depending on the number of distinct polygons in the polyhedron surrounding the big ‘reference’ face, more than one midpoint may be associated with nonequivalent rotations. In the case of the octahedron, two midpoints or two different vectors may be formed pointing to the triangular and octahedral faces. One of them leads to the optimal alignment of the polyhedron and the other doesn’t produce any change. The edge that should be aligned must be chosen in a way applicable to different systems other than the MOF-5. Therefore, the election of the correct polyhedron direction vector must depend on the structure of the pore cavity and cannot be arbitrarily determined. This problem is not present in polyhedrons like the cuboctahedron since the biggest polygonal face is surrounded by a single type of polygon, all the midpoints are equivalent and the matrix for truncation and

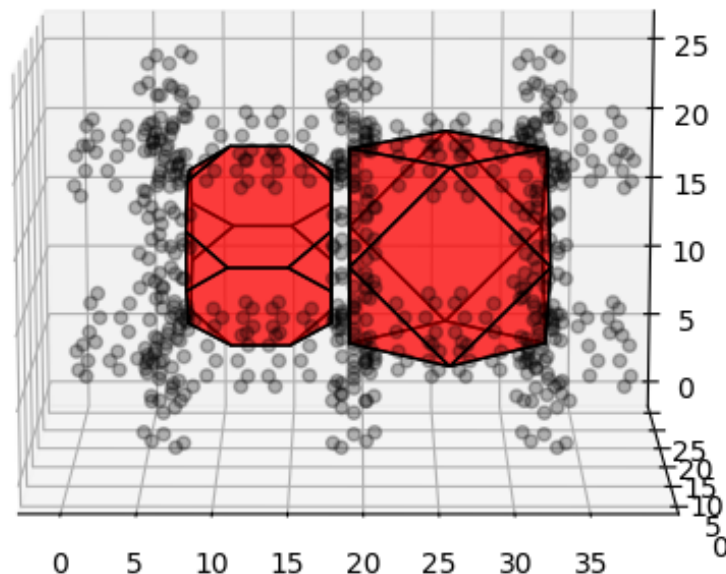


Figure 4.19: Example of alignment problem in regular polyhedrons: The cuboctahedron in the small porosity of MOF-5 structure.

cantellation also works for it. For regular solids like the truncated cube, a generic strategy to find the adequate direction vector was devised. The aim is to align all the biggest faces of the polyhedron with those of the polygon. This is possible because the number of faces is the same and they have the same shape, so if the biggest faces are aligned, the whole polyhedron will also be.⁹

Multiple ‘targets’ are created to align the polyhedron. These targets are vectors perpendicular to the biggest faces of the polytope. ‘Test’ vectors are created from the vertices that conform to the edges of the polygon that connects with the faces whose area is the closest to that of the biggest regular polygon of the polytope. The strategy is to create multiple polyhedron direction vectors from the barycenter of the biggest face of the polyhedron to each midpoint of the edges. One by one, they are used to create a rotation matrix that is used to transform the test vectors. Then, the direction of these vectors is compared against that of the targets. Multiple targets, tests, and directions are handled by Fragmento as follows:

1. A previous test must be executed. For each of the test vectors, its cross product is calculated with each target vector. The dot product between these vectors should be zero if effectively the faces are oriented parallelly.
2. If every vector of the test group presents at least one dot product equal to

⁹It Applies only for Regular polytopes

zero with the target vectors, the polyhedron is considered to be aligned and the rotation matrix is only the identity matrix.

3. If it is not the case the polyhedron is not aligned. The list of directions vectors of the polyhedron is iterated. For each vector in this list, a rotation matrix is created to align the selected vector with the direction vector of the polytope. The latter is defined from the barycenter of polytope's biggest face to the midpoint of any of its edges. The rotation transformation is then applied to the test vectors.
4. Once again, the orientations of the test vectors are compared with those of the targets. Only if all of them have dot products equal to zero is the alignment considered appropriate, the iteration stops and the rotation matrix that provides this alignment is selected to align the fittest polyhedron.

Due to the symmetry of the regular polyhedrons this alignment is guaranteed to occur. Of course not all directions need to be tested since many of them will lead to equivalent rotations. This strategy works well for any regular polytope, independently of the shape of the faces surrounding the largest polygon of the polyhedron. It also makes the election of the midpoint to define the direction of the polytope vector irrelevant, its only purpose is to provide a second vector to align with.

As designed, this process of alignment takes into account the particularities of the internal surface of the porosity in varied chemical structures. It provides an aligned fittest polyhedron that successfully resembles the shape of the cavities represented by the polytope. At this point in the execution of Delta Chem, the data provided by the user with the *.xyz* file has been completely analyzed. Important geometrical and structural parameters (the number of porosities, their sizes, centers, and atoms contributing to their surfaces) were determined by Kern. Mozaik has made good use of this information to define a 'limiting mesh' for the surface of each porosity using their contributing atoms as the vertices of a 3D Delaunay Triangulation. The shape of the 'mesh' polytope has been analyzed by the same routine to provide Fragmento with the information necessary to determine and align the fittest polyhedron. Only one task left, and Fragmento is ready to begin the last ride to find the Irreducible Volume.

Reversed Wythoff Construction

As was mentioned in the Theoretical Framework, the information necessary to construct the generator triangle of a convex, uniform polyhedron is contained in its

Wythoff symbol. `Fragmento` uses a codification based in this symbol to call the function `Irreducible_Volume` and built the generator element of the fittest polyhedron (or any other uniform convex polyhedron since this function can work independently). The dictionary ‘`elemental_triangles`’ helps with this task. Its keys are strings with the name of each platonic and archimedean polyhedron, while the values are functions `Irreducible_Volume` with lists that are characteristic for each polyhedron as their arguments. These lists are conformed by:

- The three Wythoff numbers, p, q, r , of the elemental triangle as integers.
- A string ‘c’, ‘i’, or ‘s’ indicating the position of the generator vertex in a corner, the incenter or a side of the elemental triangle respectively.
- The center and the radius of the circumscribed sphere (for Delta Chem purposes, the center and radius of the analyzed porosity are used).
- If the generator is on a position other than the incenter, an integer 0,1 or 2 are also included in the list to specify the corner or the side where the generator lies.

`Irreducible_Volume` is really just a wrapper of the real constructors. Its function is to receive and analyze the information in the argument list to call the adequate constructor. Depending on the position of the generator, three different constructor functions can be called to create the generator triangle of the analyzed polyhedron.

A first good step is positioning one of the vertices on an arbitrary point of the surface of the unitary sphere. For simplicity, the vertex P is located on (1,0,0). This reference vertex also requires a reference side, so the side l_R that passes through P is conveniently positioned to be perpendicular to the x-axis, i.e the normal vector defining the great circle that forms the side l_R is (0,0,1). The trigonometric problem is now to solve a spherical triangle with three angles and one known side. According with the method shown by Zucker¹⁰, to find the remaining vectors, they must satisfy certain requirements:

- The edge l_Q contains P
- The dihedral angle formed by the planes with normals l_Q and l_R is ϕ
- Q is a unit vector.

¹⁰Notes taken for the GitHub repository <https://mzucker.github.io/2018/04/06/why-every-gfx-cv-robotics-programmer-should-love-sympy.html#fn:2>

The vertices Q and R can be represented as unitary vectors located at the intersection of the planes. If the vectors of the sides are known, they can be used to solve:

$$Q = \frac{l_P X l_R}{|l_P X l_R|} \quad \text{and} \quad R = \frac{l_Q X l_P}{|l_Q X l_P|}$$

This strategy has been implemented by Mathew Zucker to program his amazing Wythoff Explorer ¹¹ and his solutions obtained with SymPy are used by Fragment to determine the x,y,z values for the side vectors. This process is common for all the constructors. The Figure 4.20 shows the elemental triangle (4,2,3) created with this method.

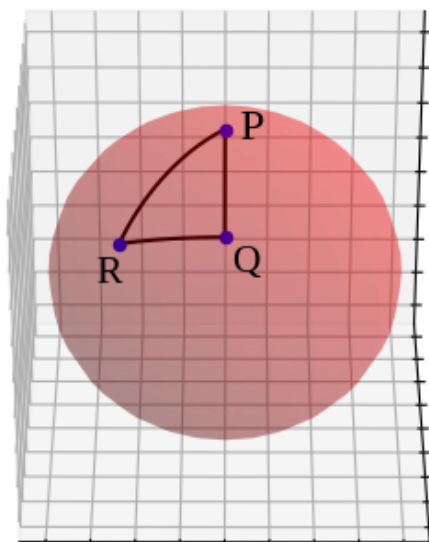


Figure 4.20: Elemental Triangle (4,2,3)

Generator Vertex at the Incenter

If the generator is located at the incenter of the elemental triangle, the constructor function *Elemental_Triangle_Incentered* is called. To obtain the generator vertex, the incenter of the just created spherical triangle must be found. The Figure 4.21a shows a graphical representation of the problem on a generalized triangle ABC. As can be seen, the arcs OD, OE, and OF are all equal in length since all of them are indeed radii of the incircle. They are also perpendicular to the incenter O.

¹¹Wythoff explorer by Zucker can be found at <https://www.shadertoy.com/view/Md3yRB>

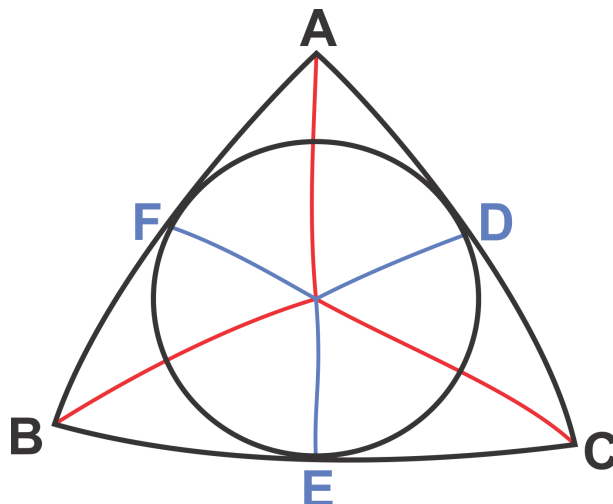


Figure 4.21: Finding the incenter of a spherical triangle: Graphic Depiction

The task of finding the incenter is simplified considerably taking into account that all the generator triangles in the Wythoff constructions are right triangles. Since the triangle is a right one, the arcs AF and AE are also equal by construction. The strategy is to move by rotation the vertex A to the positions F and E and then move these new two points in the directions of OF and OE respectively. Both points must coincide in the position of the incenter. To accomplish this task, the external function *general_rotation* is called. This function allows rotating any object on a given angle, around an arbitrary axis centered at any point. The process performed by *general_rotation* consists of successive translations and rotations around the coordinates axes as it has been discussed in the Theoretical Framework. The operation to find the incenter goes as follows:

1. Take the spherical triangle from Figure 4.21, and set on it the vertices A,B,C so that A lies on the right angled corner of this triangle.
2. Calculate the angular radius of the incircle with the formula:

$$\tan(r) = \sqrt{\frac{\sin(s-a)\sin(s-b)\sin(s-c)}{\sin(s)}} = \frac{n}{\sin(s)} \quad (4.1.1)$$

Where s is the half sum of the arcs $s = \frac{(a+b+c)}{2}$. This formula has been taken from the textbook *A treatise in spherical trigonometry* by John Casey [66].

3. Determine the angle associated with the radial angle through the formula [66]:

$$d = r\Delta\Phi \quad (4.1.2)$$

Where ‘d’ stand for the angular length of an arc of a sphere with radius ‘r’ that defines an angle $\Delta\Phi$.

4. Rotate the vertex A to reach the positions F and E by applying *general_rotation* with an angle $\Delta\Phi$, around the axis defined by the cross product \mathbf{AXB} (or \mathbf{AXC}) centered at the origin of coordinates. (Figure 4.22a)
5. The new points located in the legs of the triangle (Shown as purple dots in Figure 4.22b) are rotated again in the same angle but around the axis defined by the opposite leg \mathbf{AXC} (\mathbf{AXB}), so that their intersect at the position of the incenter.

Once the incenter is localized (Shown as a black spot in Figure 4.22b), the partitions of the triangle must be generated. To form the small square shown in Figure 4.22c it is just necessary to join the incenter with the two points of the legs. To generate the last point for the partition, the vertex B is rotated along the plane that defines the hypotenuse on an angle given by the arc BF.

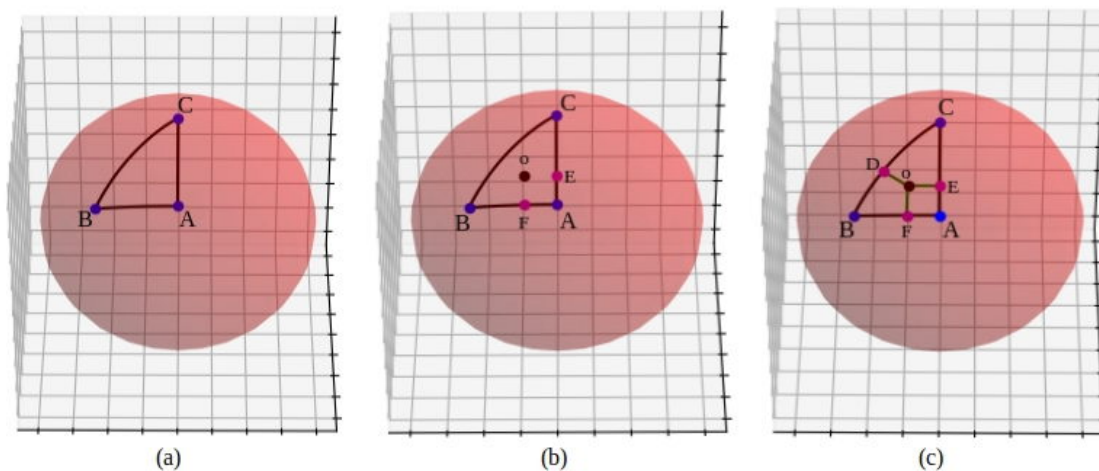


Figure 4.22: Wythoff construction of the triangle (4,2,3), with the generator vertex localized at the incenter (Part I)

The generator triangle that has been created doesn't present the flat planes typical of a polyhedron. Additionally, at the end of the construction the only point of this triangle that should remain in the surface of the sphere is the generator, as can be seen in the Wythoff Explorer of Zucker.

6. To create the planes, the generator vertex is rotated along the direction of each partition in an angle of $2\Delta\Phi$. That is equivalent to reflect the generator using the edges of the elemental triangle as mirror planes (Figure 4.23a). The generator and its rotated counterparts define three different planes.

7. The partitions of the triangle in the planes defined by the generators can be obtained as the midpoints between the original generator vertex and its rotated versions. They are shown as green dots in Figure 4.23b and 4.23c)
8. Once the new partitions are obtained, the vertices A, B, and C of the triangle are orthogonally projected over the surface of the planes. (Purple dots Figure 4.23b and 4.23c)
9. The rotated counterparts of the generator vertex, and all the other points in the surface of the sphere are deleted since they are not necessary anymore.
10. The planes corresponding to the faces of the polyhedron are created and represented in the generator triangle of Figure 4.23d.

The function *Elemental_Triangle_Incentered* returns a list with the cartesian coordinates of all the relevant points calculated: the generator vertex, the projected triangle vertices and the vertices of the partitions.

Generator Vertex on a Side

If the generator is located in one of the sides of the elemental triangle, its exact position corresponds to the intersection of the side where it lies and the bisector of the angle it opposes [67]. The general trigonometrical problem that this type of triangles require to be solved is depicted in the Figure 4.24. There, a generic spherical triangle ABC is partitioned by the arc BE cutting the angle at B. For this specific situation this arc is the bisector of the angle, then the value ϕ is the half of the angle at B, and the generator vertex lies at the position E. It is only necessary to determine the length and angle of the arc $b - \theta$. Since all the angles and arcs are known, the value of $b - \theta$ can be calculated from the relation: [66]

$$\tan(b - \theta) = \tan(a) \cos(C) \quad (4.1.3)$$

The values for a and b in the last relation can be found by solving the Napier's Analogies as a simple system of two equations with two unknowns [23]:

$$\tan\left(\frac{a+b}{2}\right) = \frac{\cos\left(\frac{A-B}{2}\right)}{\cos\left(\frac{A+B}{2}\right)} \tan\left(\frac{c}{2}\right) \quad (4.1.4)$$

$$\tan\left(\frac{a-b}{2}\right) = \frac{\sin\left(\frac{A-B}{2}\right)}{\sin\left(\frac{A+B}{2}\right)} \tan\left(\frac{c}{2}\right) \quad (4.1.5)$$

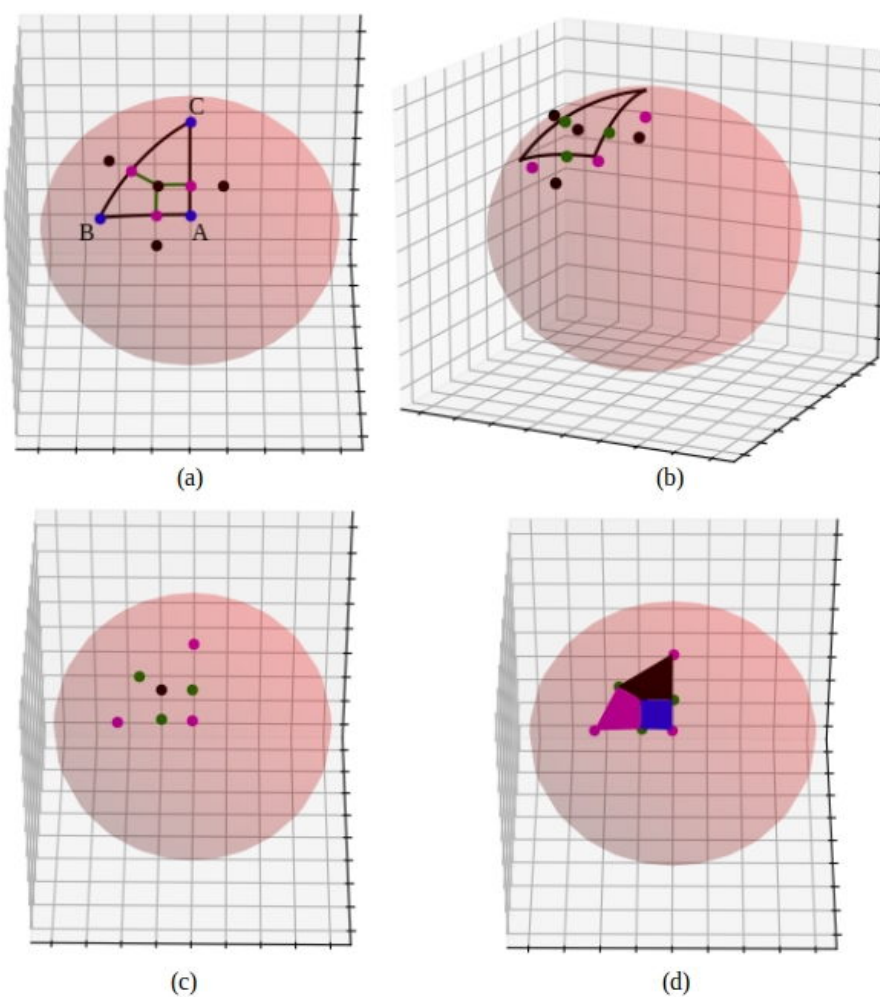


Figure 4.23: Whythoff construction of the triangle (4,2,3), with the generator vertex localized at the incenter (Part II)

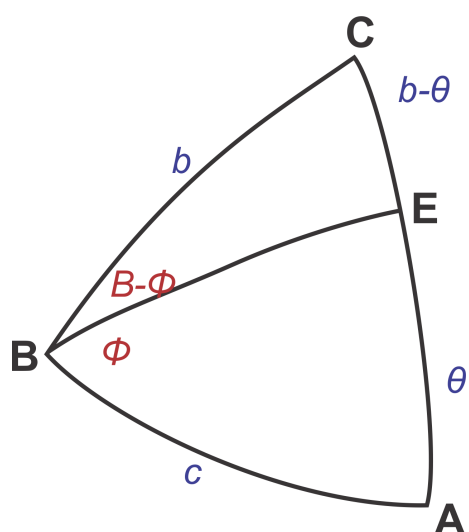


Figure 4.24: Finding the generator vertex on a side: Graphic depiction

In this way, the generator vertex in any of the sides can be easily localized. For these kind of triangles two situations may present. If the generator lies in one of the legs, the partition will follow the perpendicular projection of the generator over the hypotenuse and two planes are generated. On the other hand, if the generator lies on the hypotenuse the partitions follow the directions of the perpendicular projections of the generator over the two legs defining three planes. For this reason, the information about the position of the generator is also passed by the argument list. To obtain the coordinates of the generator, the vertex specified as **C** in figure 4.24 is rotated with *general_rotation* along the corresponding side (leg or hypotenuse) on an angle defined by the just calculated $b - \theta$ (See Figure 4.25)

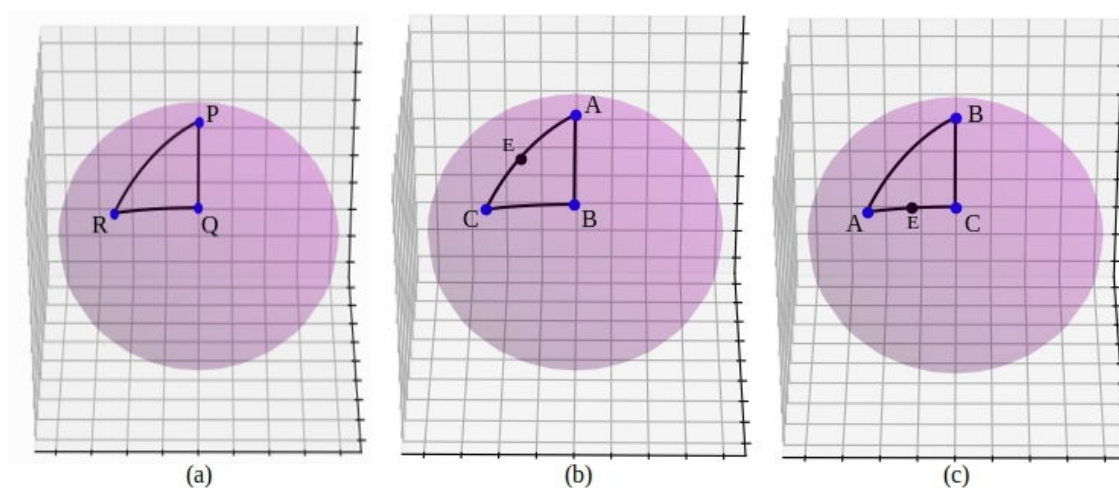


Figure 4.25: (a) The elemental triangle (4,2,3). (b) Generator vertex (black dot) positioned on the hypotenuse (c) Generator vertex positioned in one of the legs of the elemental triangle. Note that the configuration A,B,C of the triangles in (b) and (c) is adapted so that the angle at B is bisected.

The partitions for this type of triangle are not obtained as straightforward as in the ‘incentered’ case and each of the aftermentioned situations has its own process for partitions’ construction.

The situation is a little bit less complex if the generator is on the hypotenuse. The process followed to construct this triangles goes as follows:

1. The triangle in Figure 4.25b is ‘duplicated’ by moving the vertex B across the generator like in Figure 4.26a. This can be done for this triangle since the angle at B is cut exactly in the half. Therefore, this moving with *general_rotation* is equivalent to reflect the vertex B across the mirror lane defined by the arc containing the generator vertex.
2. The arc between the generator and the vertex it opposes cuts the triangle in

two smaller spherical right triangles. The problem of finding the projections over the legs is reduced to repeat the same operation to find the generator vertex but over the two smaller triangles. The projections for both triangles are shown in Figure 4.26b as green or yellow dots for the original triangle and the duplicated one respectively.

3. To define the planes of the generator triangle, the generator vertex is rotated along the direction defined by itself and the points of the projections with an angle of twice that of the arc between the generator vertex and the projections. The rotated generator vertices are shown as black dots in Figure 4.26c.

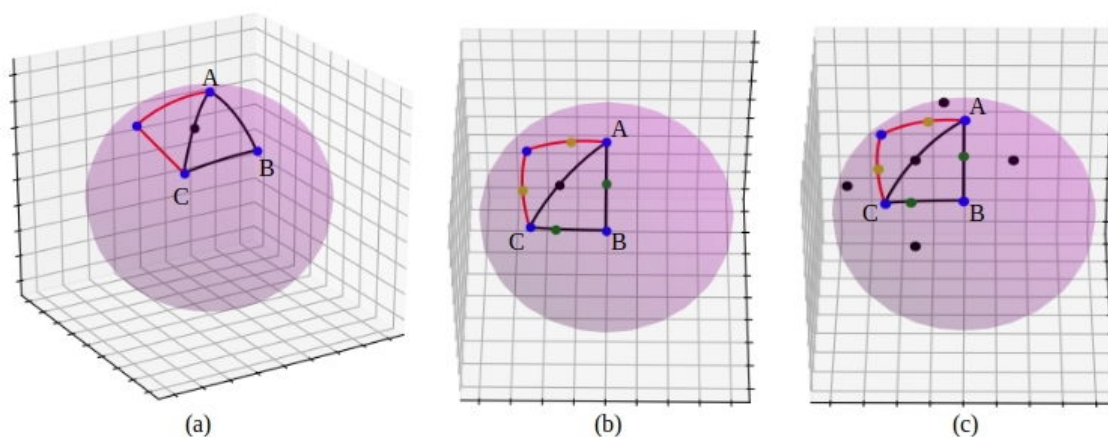


Figure 4.26: Wythoff Construction of the triangle (4,2,3), with the generator vertex localized at the Hypotenuse (Part I)

4. The partitions of the generator triangle are obtained as the midpoints of the segments defined between generator vertices (See purple dots in Figure 4.27a)
5. The vertices of the elemental triangle are projected orthogonally over the surface of the plane defined by the generator vertices (green dots Figure 4.27b). Rotated generators are deleted since they are not necessary anymore.
6. The planes are constructed and the generator triangle is done (Figure 4.27c)

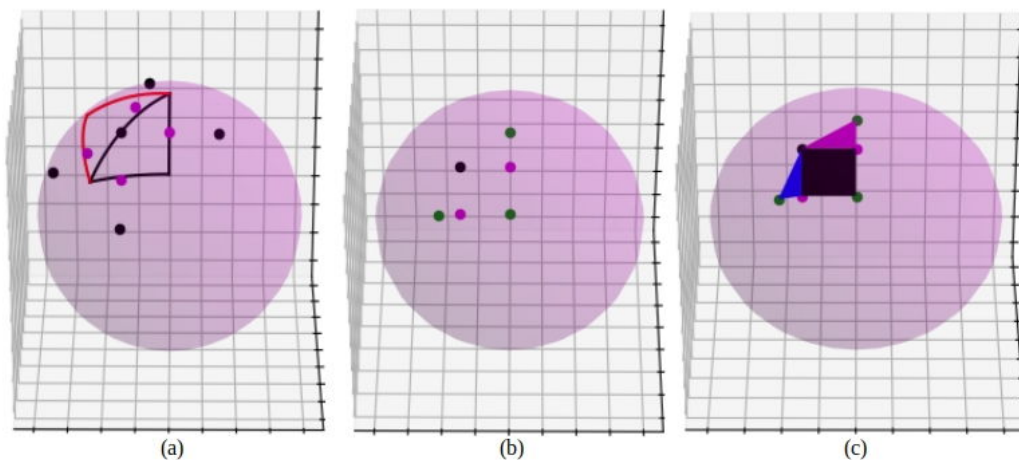


Figure 4.27: Wythoff construction of the triangle (4,2,3), with the generator vertex localized at the hypotenuse (Part II)

If the generator is on a leg, the process of construction is the following:

1. The triangle shown in Figure 4.25c is ‘duplicated’ just like in the previous case. The difference is that the duplicated triangle shares a leg with the original one, instead of the hypotenuse. (Figure 4.28a).
2. The arc BE is used to generate two smaller triangles ABE and BEC. The obtuse triangle (ABE) contains the hypotenuse, so the problem of finding the projection over the hypotenuse is reduced to repeating the process followed to obtain the generator vertex originally, but in the small obtuse triangle aforementioned. The projections are shown as green dots in Figure 4.28b.

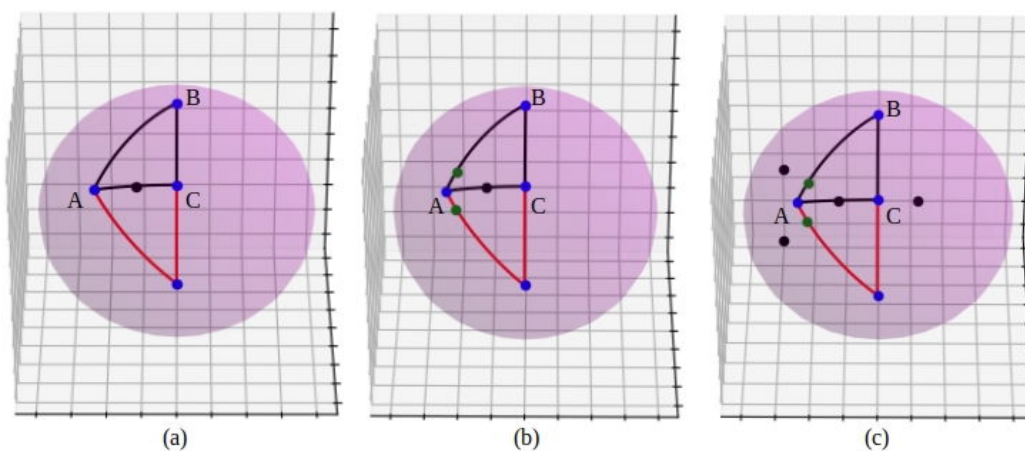


Figure 4.28: Wythoff construction of the triangle (4,2,3), with the generator vertex localized at one of the sides (Part I)

3. Three vertices are needed to define each plane of the generator triangle. For

this purpose, the generator vertex is rotated along the arc it forms with the projections. This process generates two rotated generator vertices. The third one is generated by rotation of the generator vertex along the arc it forms with the vertex C. (See Figure 4.28c)

4. Just like before, the partitions of the generator triangle are obtained as the midpoints of each pair of generator vertices. (Purple dots in Figure 4.29a)
5. The vertices of the elemental triangle are projected over the surfaces of the planes defined by the generator vertex and the partitions. The rotated generators are deleted (Figure 4.29b) and the generator triangle is done (Figure 4.29c)

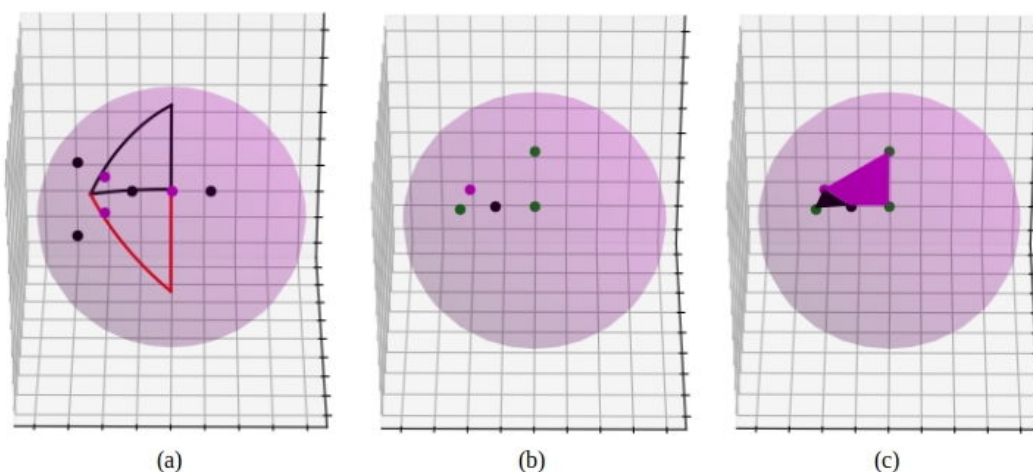


Figure 4.29: Wythoff construction of the triangle (4,2,3), with the generator vertex localized at one of the sides (Part II)

The number of points returned by *Elemental_Triangle_Sided* varies depending on which side the generator vertex is positioned: if it is on the hypotenuse, six points are returned corresponding to the generator, the two points of the partitions and the three projected vertices. On the other hand, if the generator is on a leg, only five points (the generator, the vertices and the partition) are returned.

Generator Vertex on a Corner

The last triangle is that whose generator is positioned in one of the corners. This also may derive in two different constructions depending if the generator vertex is at the reference¹² corner (Figure 4.30b) or at any remaining corner (Figure 4.30c).

¹²Recall that the 'reference' is that whose angle is equal to $\frac{\pi}{2}$

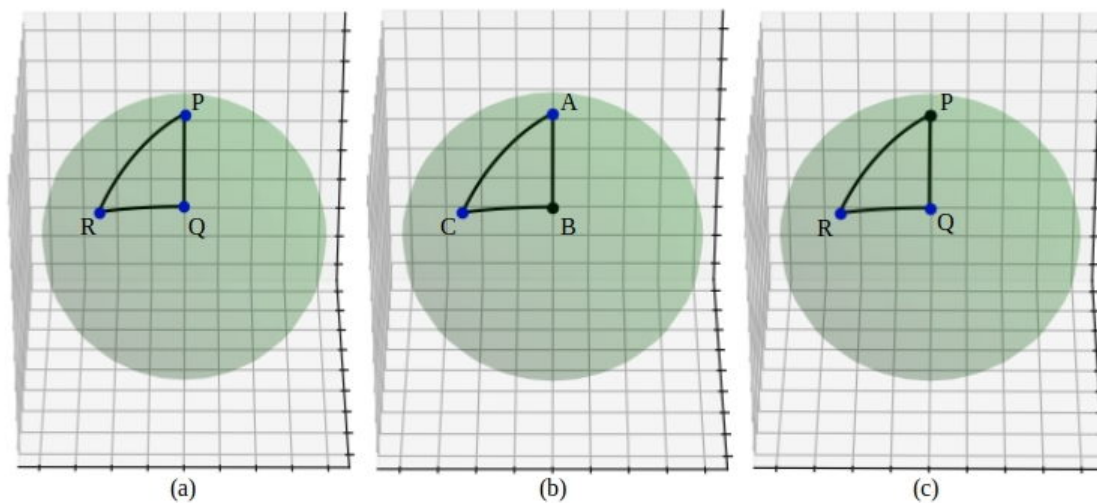


Figure 4.30: (a) The elemental triangle (4,2,3). (b) Generator vertex (black dot) positioned on the reference corner. (c) Generator vertex positioned in a corner other than the reference. Note that the configuration A,B,C of the triangle in (b) is adapted so that the angle at B is bisected just like in the previous generator triangles.

If the corner of the generator also corresponds to the reference corner, then a partition exists along the perpendicular projection of the generator over the hypotenuse. To built this triangle, the following process is necessary:

1. The projection is created straightforward using Napier's Analogies (Equations 4.1.4 and 4.1.5) and the relations presented by Casey (Equations 4.1.2 and 4.1.3) just like in the 'sided' case. (Purple dot in Figure 4.31a)
2. The vertex P is moved through the generator vertex to create a 'duplicated' triangle in which the projection of the vertex is also found (Figure 4.31b).
3. The generator vertex is rotated along the arc it forms with the projections. This process generates two rotated generator vertices. The third one is generated by rotation of the generator vertex along the arc with the projection in the duplicated triangle, but in the opposite direction. (Look for the black dots in Figure 4.31c)

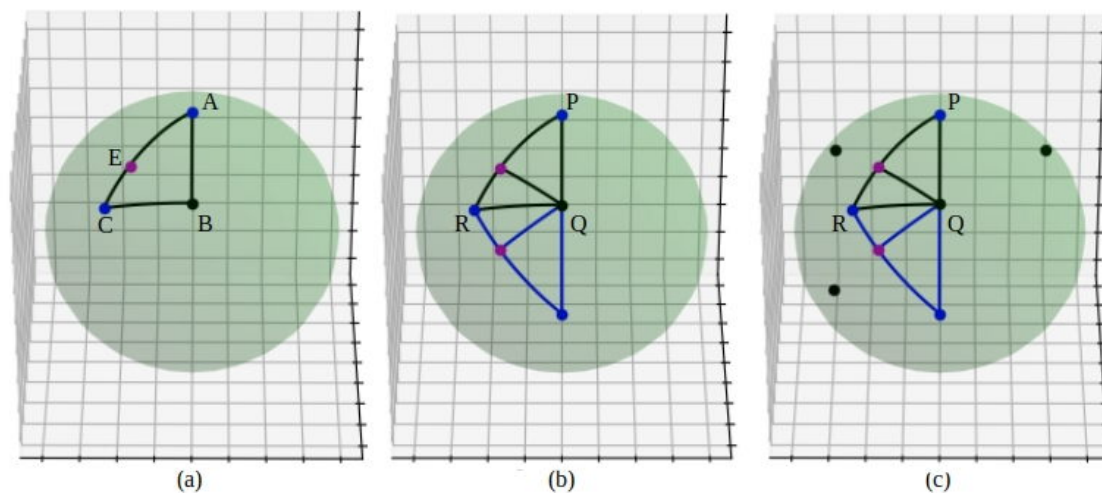


Figure 4.31: Wythoff Construction of the triangle $(4,2,3)$, with the generator vertex localized at reference corner (Part I)

4. As always, the partitions of the generator triangle are obtained as the mid-points of the segments formed between the original generator vertex and its rotated counterparts. They are represented as green dots in Figure 4.32a.
5. The vertices of the elemental triangle are projected over the surface of the planes defined by the generator vertices. They can be seen as purple dots in Figure 4.32a.
6. Rotated generators, duplicated projections and original vertices are deleted (Figure 4.32b), the planes are created, and finally this generator triangle is built (Figure 4.32c).

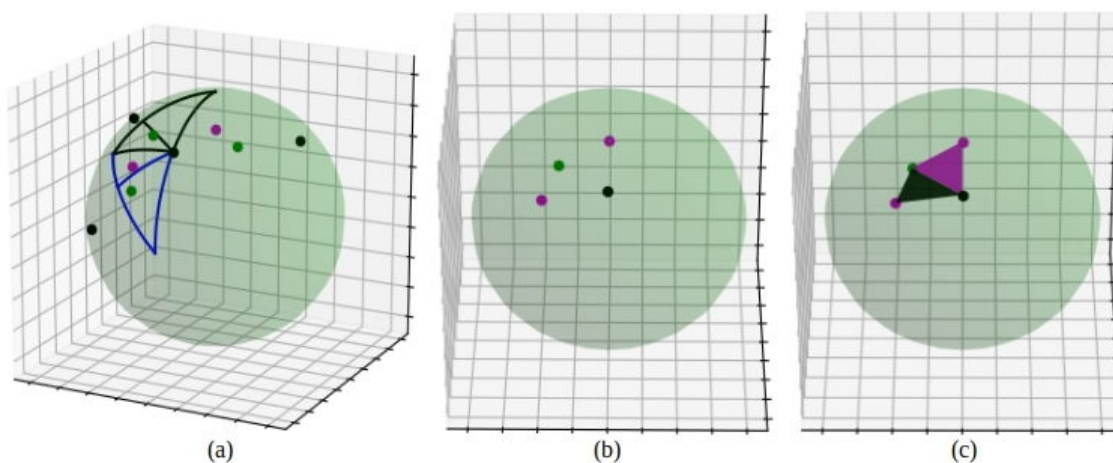


Figure 4.32: Wythoff Construction of the triangle $(4,2,3)$, with the generator vertex localized at reference corner (Part II)

On the other hand, if the generator vertex is in any of the remaining corners there are no partitions, just a whole triangle. The plane of this triangle requires the presence of another two generators to be defined. The process of construction goes as follows:

1. The triangle is duplicated by rotating the vertex Q (The reference corner) along the bisector (Figure 4.33a).
2. To create the necessary generator vertices, the original one is rotated along the arc defined by the generator and the reference corner, twice the angle defined by this arc. The process is repeated using the duplicated reference corner (Figure 4.33b).
3. The projections in the plane of the vertex Q and its duplicated are obtained as the midpoints of the segments formed by the generator vertices (green dots in Figure 4.33c).

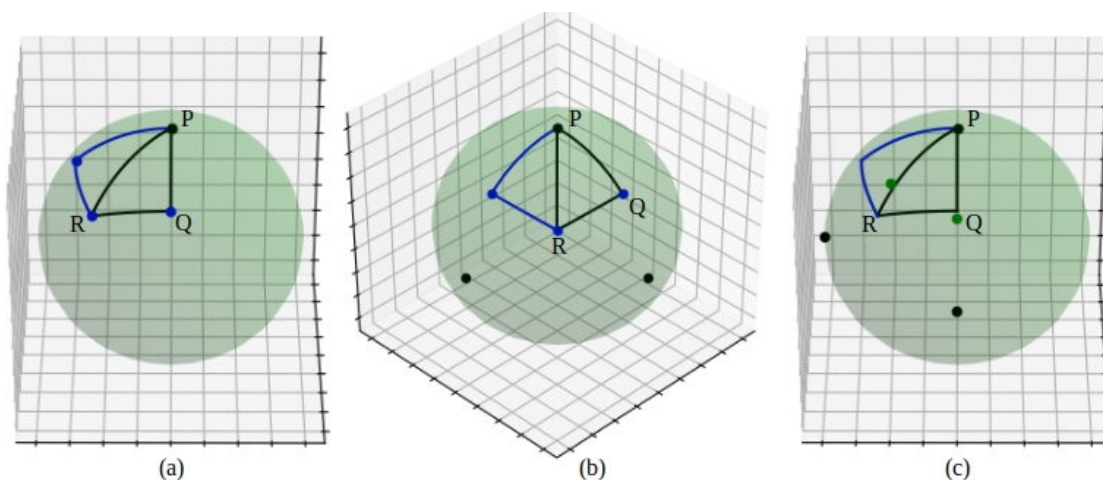


Figure 4.33: Construction of the triangle (4,2,3), with the generator vertex localized at a corner other than the reference (Part I)

4. The remaining vertex of the elemental triangle is projected over the plane defined by the generator vertices and can be seen as the purple dot in Figure 4.34a
5. Duplicated points, original vertices and rotated generators are not necessary anymore so they are deleted (Figure 4.34b). Finally the generator triangle is created (Figure 4.33c).

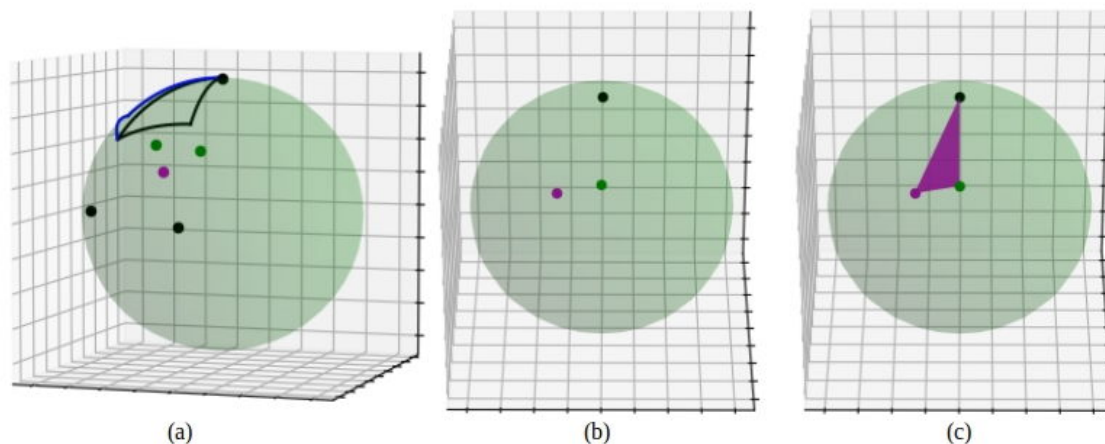


Figure 4.34: Construction of the triangle (4,2,3), with the generator vertex localized at a corner other than the reference (Part II)

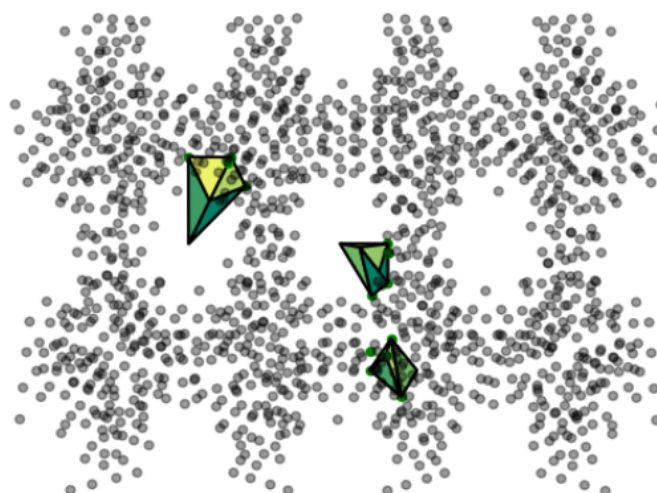
Like in the ‘sided’ case, a different quantity of points is returned depending on the location of the generator vertex. Four points are returned if the generator is on the corner of the reference vertex: the generator vertex, the point of the partition, and the projected remaining two vertices. If it is on any other corner, only three points are returned because there are no partitions.

The generator triangle created by any of the constructors has been designed over the sphere of radius one centered at the origin of coordinates. With scaling and translation, these vertices are adapted to a sphere of arbitrary radius and center. The return values of any of the constructors is organized by *Irreducible_Volume*. This function returns a list of coordinates to Fragmento containing the relevant points of the generator triangle adapted to the size of the porosity. The points provided to Fragmento are aligned with the non-transformed version of the fittest polyhedron. Therefore they must pass by the same transformations of the polyhedron in order to be aligned with the polytope representing the porosity. Fortunately, since all the rotation matrices used to align the fittest polyhedron are already known, the transformation of the points to align the generator triangle is straightforward and only requires to multiply each position vector by the matrix obtained as the product of the rotation matrices used before.

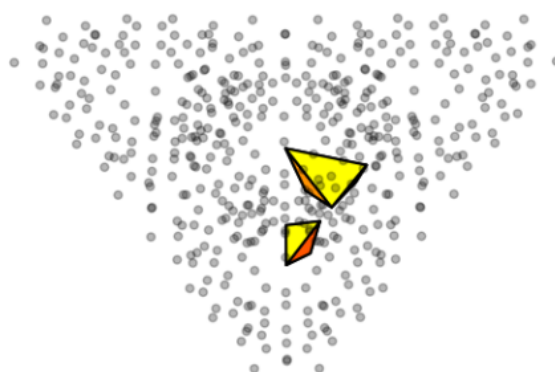
Once these points are correctly aligned, the center of the porosity is added to the set. Then, this set of points is used for the last triangulation with *Convex_Hull*. The polytope generated by this triangulation is the irreducible volume of the fittest polyhedron (Figure 4.35).

The final output is a *.xyz* file, with identical structural information of the input file but with the coordinates of the points of the irreducible volume added as helium atoms.

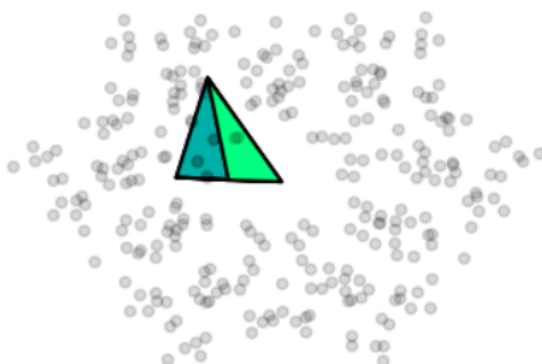
It has been a long trip full of transformations, literally, but the main objective of Delta Chem has been finally achieved with success.



(a)



(b)



(c)

Figure 4.35: Irreducible volumes obtained by Delta Chem for (a) HKUST-1, (b) UiO-66 and (c) ZIF-8

4.2 Preliminary test of Delta Chem.

In this part, a preliminary calculation test is done using Density Functional Theory in the material MOF-5, which is a prototypical MOF for numerous studies. The goal of this example is to encounter the possible adsorption sites for Helium inside the porosity of MOF-5. The calculation were done using the Quantum Espresso software with periodic DFT. The main idea is to compare the positions generated by Delta Chem with the positions obtained at the end of the optimization process. Due to the size of the systems (typically few hundred atoms for MOFs), a suitable computational facility should be used. For these project, DFT calculations were run in the supercomputer Quinde 1. Operational in Urcuquí, Quinde 1 operates with Linux operating system Red Hat Enterprise Linux Server release 7.2 (Maipo) little endian. It has 1640 CPU cores, 84 computing nodes, 4992 GPU(cuda) cores per node and 10.5 TB of RAM [68]. For periodic DFT calculations some considerations should be made:

Method consideration:

DFT comes in different flavors with different levels of approximations of the exchange-correlation term: LDA, GGA, meta-GGA and hybrid. The size of the systems obtained in modeling microporous materials limits the usage of the best DFT methods (meta-GGA or hybrid). Historically, the local density approximation was the method of choice for making DFT calculations of materials. However, with increasing calculating power, the GGA methods are now generally used. Among the GGA methods, PBE functional has proven numerous times to be very efficient. Another point to consider in that example is that it concerns the adsorption of helium atoms which are expected to interact with the framework only through VdW forces. One well-known shortcoming of DFT is the non-representation of dispersion interactions, crucial when considering apolar adsorbents. Fortunately, this problem was solved by Grimme which include dispersion interactions in an ad-hoc manner [69]. The dispersion forces are included through a Lennard-Jones potential, similar to the approach used in molecular mechanics inside the forcefields. The keyword `vdw_corr = 'DFT-D3'` is used in these calculations.

Size consideration:

The Cubic unit cell of MOF-5 used for Delta Chem analysis consists of 424 atoms(See Figure3.10d). As expected, this size of system is not suitable for using the PBE functional in a practical manner. Fortunately, it is possible to reduce

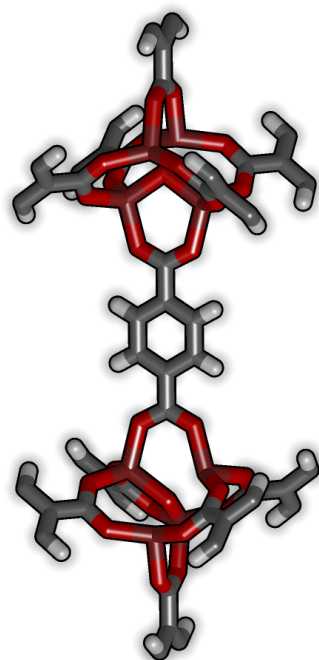


Figure 4.36: MOF-5 cluster used for DFT calculations with Quantum Espresso. *Color code: Zn-Brown, O-Red, C-Black, H-white*

the size of the cell using symmetry to 106 atoms in the rhombohedral cell shown in Figure 4.36. The replication of the primitive cell gives the same structure as the cubic cell and can therefore be used to represent the total material. The only important point is to exactly orient the structure used in Delta Chem based on the smaller primitive cell.

Basis-set completeness consideration:

In molecular DFT calculation gaussian functions are used as basis-sets for representing the orbitals. In periodic calculations the plane waves are usually used. In a structured material the potential is periodic and makes it natural to use plane waves which are inherently periodic. Theoretically an infinite number of plane waves can represent all little variation of the electronic structure. In order to limit the number of plane waves taken into account a kinetic energy cut-off could be applied. Typically, the total energy is calculated for different cut-offs, then, the cut-off value is taken when the total energy is constant. As only a preliminary test, we took a fairly small value of 25 Ry controlled by the keyword `ecutwfc`.

Structure consideration:

One question which always rise when doing this type of calculation is which structure should be taken: a structure determined by XRD or a structure optimized by the same DFT method. The two approaches can be used:

1. When using the XRD structure the coordinates of the porous structures should be frozen (constrained optimization) or would otherwise move and cause a displacement of the possible sites.
2. When using the DFT pre-optimized structure, the atoms constituting the MOF could be let free of frozen.

The advantage of letting the atoms free during optimization is that structural information can be obtained about the deformation of the MOF due to the presence of the adsorbent molecules. For this calculation we used the first approach constraining the positions of the framework atoms.

Convergence consideration:

During the optimization process reaching the minimum is verified by two criteria, the energy and the forces. At each step of the optimization these two values are compared to the previous step and should be inferior to a criteria defined in the input defined through the keywords `etot_conv_thr = 0.000001` and `forc_conv_thr = 0.00001`. In each optimization step, there are several SCF cycles done in order to find the minimal electronic distribution corresponding to the new atom positions.

K-points consideration:

The K-points are sampling points in the Brillouin zone in order to evaluate electronic properties. The number of kpoints should be tested usually in increasing grids in form $2*2*2$, $3*3*3$. . . When there are no more changes in the electronic structure the number of K-points is considered accurate. In the particular case of the MOF-5, the number of K-points influence was tested several times and concluded that one K-point (at coordinates 0,0,0) is sufficient for evaluating properties accurately.

Chapter 5

Results and Discussion

Prior to Quantum Espresso calculations, Delta Chem was used to find the porosities shapes and the possible adsorption sites. Delta Chem, through the use of PSD_solve and Kerno correctly detected the presence of two type of porosities (Figure 5.1a): the largest one with *pore radius* $\sim 9.574\text{\AA}$ centered at the position (25.832, 12.916, 12.916), and the smallest with *pore radius* $\sim 7.221\text{\AA}$ centered at (12.916, 12.916, 12.916). The routine Kerno also determined that a total of 96 atoms contribute to the internal surface of the first porosity while 24 contribute to the second one. These results are graphically represented in Figure 5.1. Only one minute of running PSD_solve was necessary to obtain good first approximations of the pore radii. Kerno is the most time consuming routine in Delta Chem, however only took five minutes to complete their task and return the information necessary to continue Delta Chem processes.

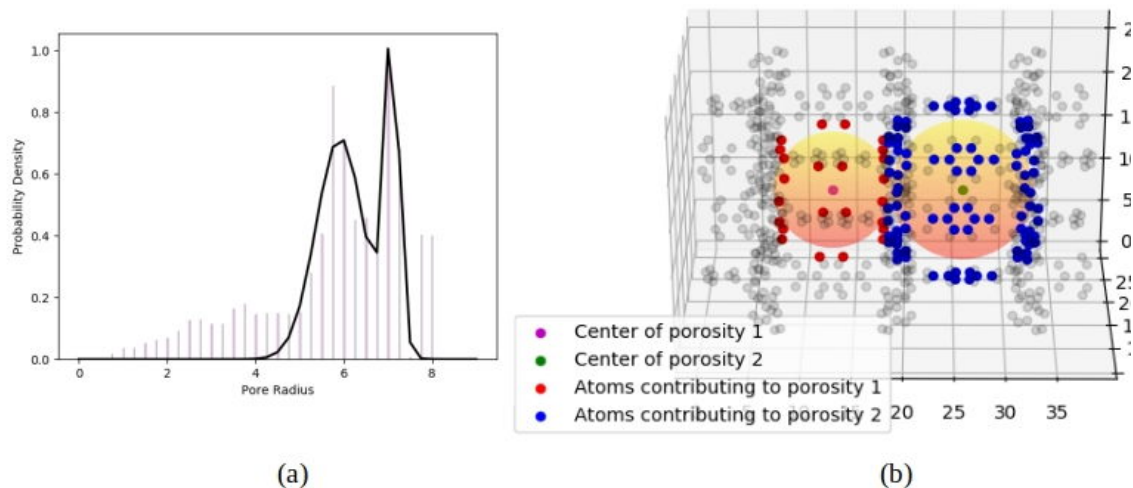


Figure 5.1: Kerno's process results for MOF-5 structure, they include: Position of the centers of porosities, atoms contributing to the internal surface of each pore cavity, and sphere representing the pore cavities.

The work performed by Mozaiko can be appreciated in Figure 5.2; there, the triangulations and polygonizations of both porosities are shown. After these processes, Mozaiko determined that the large polytope went by a cantellation process while the small polytope experimented truncation. This information was used by

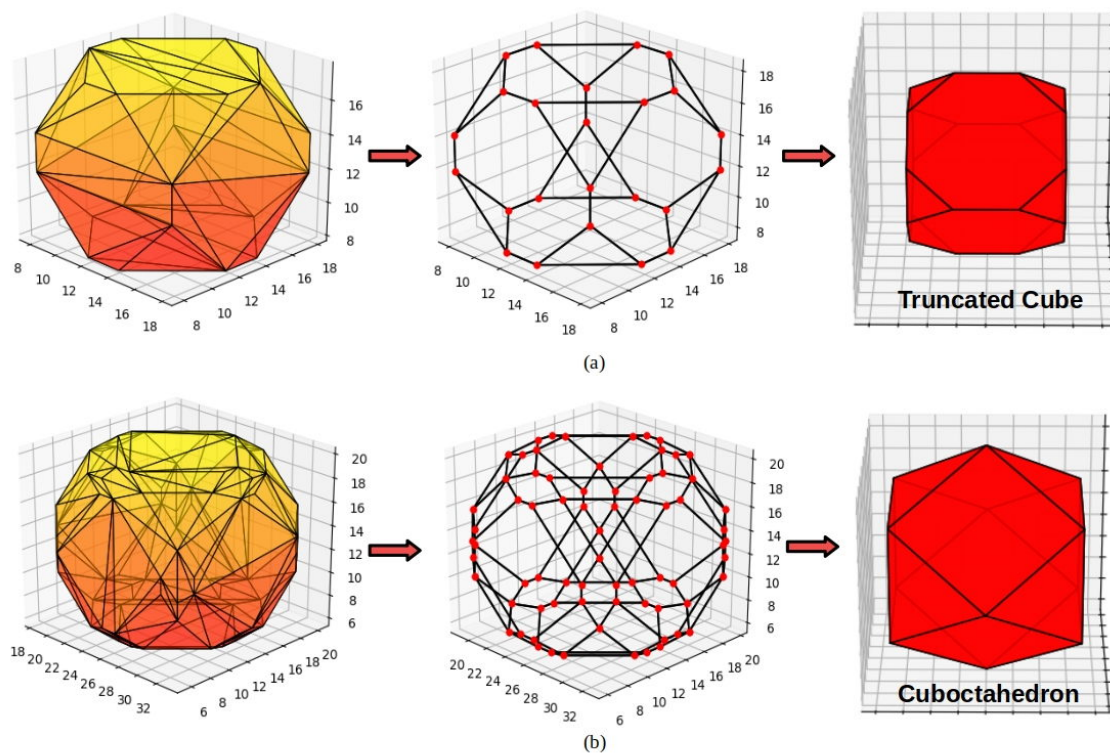


Figure 5.2: Triangulation, Polygonalization and Fitting processes results for MOF-5 structure: (a) Small porosity, (b) Big porosity.

Fragmento to determine that the truncated cube is the polyhedron that best fits the shape of the small porosity, while the cuboctahedron is the fittest polyhedron for the large polytope. These polyhedrons were aligned and analyzed in order to obtain the irreducible volume of the porosities. The results of this job, driven by Fragmento, are shown in Figure 5.3.

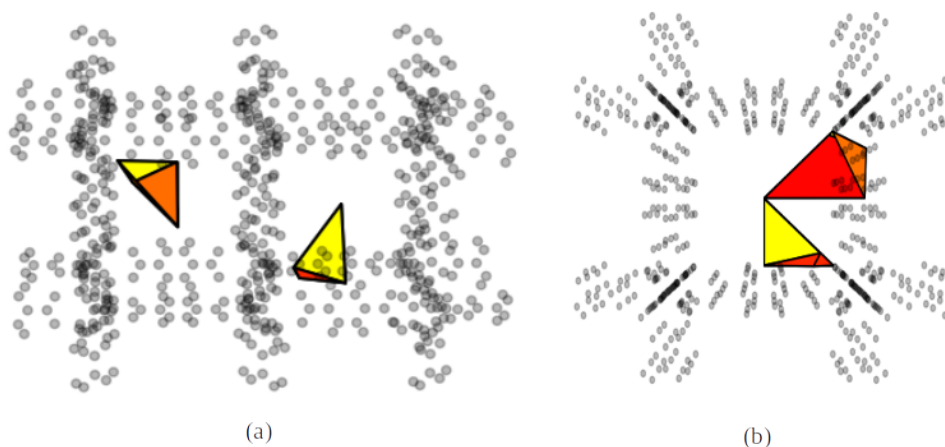


Figure 5.3: Irreducible volumes of the porosities in MOF-5: (a) Side view,(b) Front view.

The whole process of Delta Chem took seven minutes to be completed for MOF-5 structure, conformed by 424 atoms. Seven points (corresponding to the relevant points of the irreducible form), and also two points (corresponding the porosities centers) were generated. For each possible site one different calculation should be made. This points can be visualized in Figure 5.4.

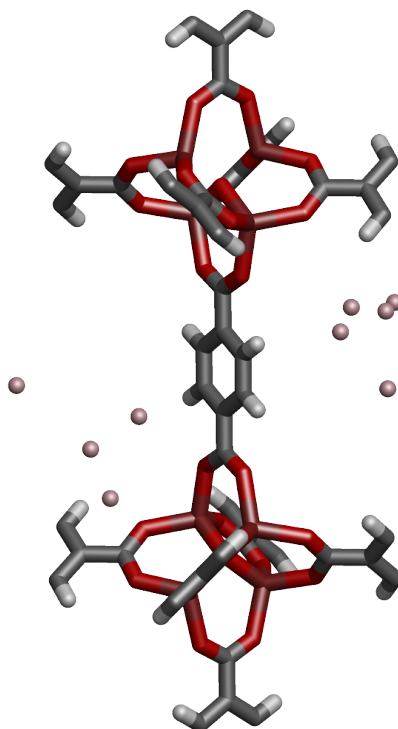


Figure 5.4: Position of the relevant point provided by Delta Chem, around the cluster model used for DFT calculations

Preliminary geometry optimization calculations using the convergence criteria discussed in the previous section show that, for the system analyzed represented in the Figure 5.4, six out of nine helium atoms used to represent the possible positions of the adsorption sites did not move during optimization. This is an indication that their positions were effectively close to minimum energy. The points corresponding to the centers of the porosities move as expected. Only one point failed to reach convergence for reasons that are not clear after the calculation (probably a small discontinuity). The observed displacements are very small for all cases. This effect could be due to the weak interaction forces generated by the small size of the helium atoms. The opposite case can be observed in the work of Thibault Terencio [11] in which instead of using helium atoms, much larger acetone molecules have been used; these generate greater interactions that make them move forcefully towards the adsorption sites.

Chapter 6

Conclusions and Perspectives

The main objective of the present Capstone Project has been achieved: A new approach for the geometric modeling of pore cavities in microporous materials has been proposed. Unlike the traditional model that only considers the atoms at the joints of the frameworks, this new approach has been constructed using the atoms that directly contribute to form the internal surface of the porosities. In this way, a more realistic representation of the particularities at the interior of the porosities is provided. This model is useful for surface processes like adsorption in which the proper modeling of the surface area of these materials is especially relevant. The program Delta Chem has been created to implement this approach in highly symmetric microporous materials including MOFs, ZIFs, COFs, and Zeolites. A total of 3016 Python's code line has been necessary to successfully perform the following tasks: Read the input file provided by the user to make the structural information accessible for its processing in Delta Chem; determine the positions of the center of each type of porosity and the atoms in the structure of the studied material that contributes to them; use Delaunay Triangulation to create a limiting mesh for the internal surface of the porosities; determine the regular uniform polyhedron that best fits the shape of these surfaces; align the fittest polyhedrons and use a reversed Wythoff Construction to build the irreducible volumes of the porosities.

This Irreducible Volume-based approach was successfully tested in MOF-5. The geometrical optimization of the critical points provided by Delta Chem results in positions that are very close to the energy minima. It shows that the implementation of this method greatly simplifies the process of determining the position of adsorption sites in microporous materials. Of course, a reduced number of adsorbate molecules implies a decrease in the computational cost and processing time. At the moment this approach has only been implemented for MOF-5 so further studies in different materials are required, but it is promising. It is a local order method, it can be applied for materials that are locally ordered but works as well for crystalline matter. It could be used as the geometrical base for new methods like DFT using local geometry and similar geometric approaches could be created to model the adsorbate molecules.

Delta Chem is fast, indeed 20 minutes are necessary to wholly process the 1440

atoms in HKUST-1 unit cell. It is generic since it is based entirely on the geometry of the materials and not in the nature of the atoms, therefore the process can be generalized for a wide variety of microporous materials. Additionally, the program can be switched to generate the traditional geometrical model based in the atoms at the joints of the framework, i.e Delta Chem is capable of generate two different geometric approaches of porosity and perform similar further processes, like determine the irreducible volumes, for both of them.

In general terms, Delta Chem works well... but it could be improved. The polyhedron fitting is now limited to only eighteen polyhedrons, six platonic and twelve archimedean. It works perfectly for regular pore cavities, but Truncations and Cantellations could be better approximated analyzing the displacement of the generator vertex in any of these processes. In this way the shape of the porosity could be fitted exactly and the appropriate Irreducible Volume could be generated instead of doing only an approximation of their shapes. The Wythoff construction also allows generation of prisms, so the irreducible volume of channels could also be obtained.

The diverse algorithms implemented and created to build up Delta Chem are as interesting as the program itself. The final organization of Delta Chem allows making use of almost any of these algorithms for purposes that are not necessarily related to the objectives of this Project, but that requires the implementation of some of the Delta Chem methods like Delaunay Triangulation, determination of centers of porosities, Convex Hull analysis and polygonalization, General Rotation, Alignment Rotation, Scaling and Translation transformations and Determination of irreducible volumes of regular polyhedrons. Delta Chem and the Irreducible Volume approach are the result of a highly interdisciplinary project work at the interface of geometry, linear algebra and chemistry. They are a sample of how mathematics can be used as a cure for chemical diseases.

Bibliography

- [1] S. Bhattacharya and K. E. Gubbins, “Fast method for computing pore size distributions of model materials,” *Langmuir*, vol. 22, no. 18, pp. 7726–7731, 2006.
- [2] J. S. Beck, J. C. Vartuli, W. J. Roth, M. E. Leonowicz, C. T. Kresge, K. D. Schmitt, C. T. Chu, D. H. Olson, E. W. Sheppard, S. B. McCullen, J. B. Higgins, and J. L. Schlenker, “A New Family of Mesoporous Molecular Sieves Prepared with Liquid Crystal Templates,” *J. Am. Chem. Soc.*, vol. 114, no. 27, pp. 10834–10843, 1992.
- [3] M. J. Rosseinsky, “Recent developments in metal-organic framework chemistry: Design, discovery, permanent porosity and flexibility,” *Microporous Mesoporous Materials*, vol. 73, pp. 15–30, aug 2004.
- [4] A. Schoedel and O. M. Yaghi, “Porosity in metal-organic compounds,” in *Macrocyclic and Supramolecular Chemistry: How Izatt–Christensen Award Winners Shaped Field* (R. Izatt, ed.), ch. 9, John Wiley & Sons, first ed., 2016.
- [5] A. Corma, “State of the art and future challenges of zeolites as catalysts,” *Journal of Catalysis*, vol. 216, no. 1-2, pp. 298–312, 2003.
- [6] K. V. Kumar, S. Gadipelli, B. Wood, K. A. Ramisetty, A. A. Stewart, C. A. Howard, D. J. Brett, and F. Rodriguez-Reinoso, “Characterization of the adsorption site energies and heterogeneous surfaces of porous materials,” *J. Mater. Chem. A*, vol. 7, no. 17, pp. 10104–10137, 2019.
- [7] Y. Artioli, “Adsorption,” in *Encycl. Ecol. Five-Volume Set*, pp. 60–65, Elsevier Inc., jan 2008.
- [8] S. Gadipelli, W. Travis, W. Zhou, and Z. Guo, “A thermally derived and optimized structure from ZIF-8 with giant enhancement in CO₂ uptake,” *Energy Environ. Sci.*, vol. 7, no. 7, pp. 2232–2238, 2014.
- [9] J. Landers, G. Y. Gor, and A. V. Neimark, “Density functional theory methods for characterization of porous materials,” *Colloids Surfaces A Physicochem. Eng. Asp.*, vol. 437, pp. 3–32, 2013.
- [10] M. Fischer, J. Gomes, and M. Jorge, *Computational approaches to study adsorption in MOFs with unsaturated metal sites*. PhD thesis, University College London, 2000.

-
- [11] T. Terencio, *Etude de l'adsorption des COVs dans les MOFs par une approche complémentaire théorie-expérience*. PhD thesis, 2013. Thèse de doctorat dirigée par Trens, Philippe Chimie-Physique Théorique Montpellier, Ecole nationale supérieure de chimie 2013.
- [12] T. Düren, L. Sarkisov, O. M. Yaghi, and R. Q. Snurr, "Design of new materials for methane storage," *Langmuir*, vol. 20, no. 7, pp. 2683–2689, 2004.
- [13] E. V. Ludeña, M. Cornejo, H. Baykara, P. Iza, D. Arroyo, and J. Corregidor, "Nanotechnology and the Oil Industry : Potential Applications in Ecuador Nanotecnología Y La Industria Petrolera : Aplicaciones Potenciales En El Ecuador," *Momento, Rev. Física*, no. 56, pp. 54–64, 2018.
- [14] M. Bailey and S. Cunningham, *Introduction to computer graphics*, vol. 2015. 2008.
- [15] K. I. Joy, "General rotation about an axis," tech. rep., Computer Science Department, University of California, Davis.
- [16] J. O'Rourke, *Computational Geometry in C*. USA: Cambridge University Press, 1994.
- [17] K. Chen, S. M. Anthony, and S. Granick, "Extending Particle Tracking Capability with Delaunay Triangulation," *Langmuir*, vol. 30, pp. 4760–4766, apr 2014.
- [18] Q. Yang and C. Zhong, "Molecular simulation of adsorption and diffusion of hydrogen in metal-organic frameworks," *J. Phys. Chem. B*, vol. 109, no. 24, pp. 11862–11864, 2005.
- [19] E. O. Nwachukwu, B. O. Eke, O. Deh, and P. Harcourt, "An efficient 3d triangulation algorithm and data structure for computer-aided-design," pp. 117–123, 2006.
- [20] D. A. Sinclair, "A 3d sweep hull algorithm for computing convex hulls and delaunay triangulation." Unpublished manuscript, Imense Ltd.
- [21] M. Kallay, "Convex hull algorithms in higher dimensions." Unpublished manuscript, Dept. of Mathematics, Univ. of Oklahoma, Norman, OK, 1981.
- [22] R. Seidel, "Constructing higher-dimensional convex hulls at logarithmic cost per face," in *Proceedings of the Eighteenth Annual ACM Symposium on Theory of Computing*, p. 404–413, Association for Computing Machinery, 1986.

- [23] I. Todhunter, *Spherical trigonometry, for the use of colleges and schools*. London: Macmillan and Co, fifth ed., 1886.
- [24] T. Mueller and G. Ceder, “A Density Functional Theory Study of Hydrogen Adsorption in MOF-5,” *J. Phys. Chem. B*, vol. 109, no. 38, pp. 17974–17983, 2005.
- [25] A. Kuntsevich and F. Kappel, “Solvopt: The solver for local nonlinear optimization problems,” *University of Graz, Graz*, <http://imsc.uni-graz.at/kuntsevich/solvopt/index.html>, 05 1997.
- [26] Y. He, W. Zhou, G. Qian, and B. Chen, “Methane storage in metal-organic frameworks,” *Chem. Soc. Rev.*, vol. 43, no. 16, pp. 5657–5678, 2014.
- [27] R. Malik and A. Baruah, *Nanotechnology Based Solutions for Wastewater Treatment*, pp. 337–368. 2019.
- [28] W. J. Rieter, K. M. Pott, K. M. Taylor, and W. Lin, “Nanoscale coordination polymers for platinum-based anticancer drug delivery,” *J. Am. Chem. Soc.*, vol. 130, no. 35, pp. 11584–11585, 2008.
- [29] X. Wang, X. Chen, C. C. J. Alcântara, S. Sevim, M. Hoop, A. Terzopoulou, C. de Marco, C. Hu, A. J. de Mello, P. Falcaro, S. Furukawa, B. J. Nelson, J. Puigmartí-Luis, and S. Pané, “MOFBOTS: Metal–Organic–Framework–Based Biomedical Microrobots,” *Adv. Mater.*, vol. 31, p. 1901592, jul 2019.
- [30] R. M. Barrer and D. A. Ibbitson, “Occlusion of hydrocarbons by chabazite and analcite,” *Trans. Faraday Soc.*, vol. 40, pp. 195–206, jan 1944.
- [31] C. Baerlocher, L. B. McCusker, and D. H. Olson, “Introduction and explanatory notes,” in *Atlas of Zeolite Framework Types (Sixth Edition)*, pp. 3 – 11, Amsterdam: Elsevier Science B.V., sixth ed., 2007.
- [32] J. Čejka, G. Centi, J. Perez-Pariente, and W. J. Roth, “Zeolite-based materials for novel catalytic applications: Opportunities, perspectives and open problems,” *Catal. Today*, vol. 179, no. 1, pp. 2–15, 2012.
- [33] H. Furukawa, K. E. Cordova, M. O’Keeffe, and O. M. Yaghi, “The chemistry and applications of metal-organic frameworks,” *Science*, vol. 341, no. 6149, 2013.

- [34] H. Li, M. Eddaoudi, T. L. Groy, and O. M. Yaghi, "Establishing microporosity in open metalorganic frameworks," *Journal of the American Chemical Society*, vol. 120, no. 33, pp. 8571–8572, 1998.
- [35] O. M. Yaghi, H. Li, C. Davis, D. Richardson, and T. L. Groy, "Synthetic Strategies, Structure Patterns, and Emerging Properties in the Chemistry of Modular Porous Solids," *Acc. Chem. Res.*, vol. 31, no. 8, pp. 474–484, 1998.
- [36] S. S. Chui, S. M. Lo, J. P. H. Charmant, A. G. Orpen, and I. D. Williams, "A chemically functionalizable nanoporous material $[\text{Cu}_3(\text{TMA})_2(\text{H}_2\text{O})_3]_n$," *Science*, vol. 283, no. 5405, pp. 1148–1150, 1999.
- [37] C. H. Hendon and A. Walsh, "Chemical principles underpinning the performance of the metal-organic framework HKUST-1," jul 2015.
- [38] K. S. Lin, A. K. Adhikari, C. N. Ku, C. L. Chiang, and H. Kuo, "Synthesis and characterization of porous HKUST-1 metal organic frameworks for hydrogen storage," in *Int. J. Hydrogen Energy*, vol. 37, pp. 13865–13871, sep 2012.
- [39] H. Furukawa and O. M. Yaghi, "Storage of hydrogen, methane, and carbon dioxide in highly porous covalent organic frameworks for clean energy applications," *J. Am. Chem. Soc.*, vol. 131, no. 25, pp. 8875–8883, 2009.
- [40] J. B. DeCoste and G. W. Peterson, "Metal-organic frameworks for air purification of toxic chemicals," *Chemical Reviews*, vol. 114, no. 11, pp. 5695–5727, 2014.
- [41] K. Y. Andrew Lin and Y. T. Hsieh, "Copper-based metal organic framework (MOF), HKUST-1, as an efficient adsorbent to remove p-nitrophenol from water," *J. Taiwan Inst. Chem. Eng.*, vol. 50, pp. 223–228, 2015.
- [42] C. Chiericatti, J. C. Basilico, M. L. Zapata Basilico, and J. M. Zamaro, "Novel application of HKUST-1 metal-organic framework as antifungal: Biological tests and physicochemical characterizations," *Microporous Mesoporous Mater.*, vol. 162, pp. 60–63, nov 2012.
- [43] L. Hailian, E. Mohamed, M. O'Keeffe, and O. Yaghi, "Design and synthesis of an exceptionally stable and highly," vol. 402, no. November, pp. 276–279, 1999.
- [44] J. Li, S. Cheng, Q. Zhao, P. Long, and J. Dong, "Synthesis and hydrogen-storage behavior of metal-organic framework MOF-5," *Int. J. Hydrogen Energy*, vol. 34, pp. 1377–1382, feb 2009.

- [45] D. Saha, Z. Bao, F. Jia, and S. Deng, "Adsorption of CO₂, CH₄, N₂O, and N₂ on MOF-5, MOF-177, and zeolite 5A," *Environ. Sci. Technol.*, vol. 44, no. 5, pp. 1820–1826, 2010.
- [46] V. I. Isaeva, O. P. Tkachenko, I. V. Mishin, G. I. Kapustin, A. A. Kostin, K. V. Klementiev, and L. M. Kustov, "Application of MOF-5 as a component of heterogeneous catalytic systems for the liquid phase hydrogenation," *Stud. Surf. Sci. Catal.*, vol. 174, pp. 463–466, 2008.
- [47] H. Wu, T. Yildirim, and W. Zhou, "Exceptional mechanical stability of highly porous zirconium metal-organic framework UiO-66 and its important implications," *J. Phys. Chem. Lett.*, vol. 4, no. 6, pp. 925–930, 2013.
- [48] J. C. Tan and A. K. Cheetham, "Mechanical properties of hybrid inorganic–organic framework materials: establishing fundamental structure–property relationships," *Chem. Soc. Rev.*, vol. 40, pp. 1059–1080, 2011.
- [49] J. H. Cavka, S. Jakobsen, U. Olsbye, N. Guillou, C. Lamberti, S. Bordiga, and K. P. Lillerud, "A new zirconium inorganic building brick forming metal organic frameworks with exceptional stability," *J. Am. Chem. Soc.*, vol. 130, no. 42, pp. 13850–13851, 2008.
- [50] C. Avci, "*Zeolitic Imidazolate Framework-8: Control of Particle Size and Shape and Its Self-assembly*". Universitat Autònoma de Barcelona, 2018.
- [51] N. A. Nordin, A. F. Ismail, A. Mustafa, R. S. Murali, and T. Matsuura, "The impact of ZIF-8 particle size and heat treatment on CO₂/CH₄ separation using asymmetric mixed matrix membrane," *RSC Adv.*, vol. 4, pp. 52530–52541, sep 2014.
- [52] C. Chizallet, S. Lazare, D. Bazer-Bachi, F. Bonnier, V. Lecocq, E. Soyer, A.-A. Quoineaud, and N. Bats, "Catalysis of Transesterification by a Nonfunctionalized MetalOrganic Framework: Acido-Basicity at the External Surface of ZIF-8 Probed by FTIR and ab Initio Calculations," *J. Am. Chem. Soc.*, vol. 132, pp. 12365–12377, sep 2010.
- [53] L. T. Nguyen, K. K. Le, and N. T. Phan, "A zeolite imidazolate framework ZIF-8 catalyst for Friedel-Crafts acylation," *Cuihua Xuebao/Chinese J. Catal.*, vol. 33, pp. 688–696, apr 2012.
- [54] C. Y. Sun, C. Qin, X. L. Wang, G. S. Yang, K. Z. Shao, Y. Q. Lan, Z. M. Su, P. Huang, C. G. Wang, and E. B. Wang, "Zeolitic imidazolate framework-8

- as efficient pH-sensitive drug delivery vehicle,” *Dalt. Trans.*, vol. 41, pp. 6906–6909, jun 2012.
- [55] T. F. Havel, “Distance Geometry: Theory, Algorithms, and Chemical Applications,” *Encycl. Comput. Chem.*, 2002.
- [56] Z. Wen, M. Li, Y. Li, Y. Guo, and K. Wang, “Delaunay triangulation with partial least squares projection to latent structures: A model for G-protein coupled receptors classification and fast structure recognition,” *Amino Acids*, vol. 32, pp. 277–283, feb 2007.
- [57] S. Pérot, O. Sperandio, M. A. Miteva, A.-C. Camproux, and B. O. Villoutreix, “Druggable pockets and binding site centric chemical space: a paradigm shift in drug discovery,” *Drug Discovery Today*, vol. 15, no. 15, pp. 656 – 667, 2010.
- [58] P. H. F. Hansen, S. Rödner, and L. Bergström, “Structural Characterization of Dense Colloidal Films Using a Modified Pair Distribution Function and Delaunay Triangulation,” *Langmuir*, vol. 17, pp. 4867–4875, aug 2001.
- [59] Y. Li, “Delaunay triangulation method for analysis of nearinfrared spectra of plant samples,” in *2010 4th Int. Conf. Bioinforma. Biomed. Eng. iCBBE 2010*, 2010.
- [60] J. L. Pascual-Ahuir and E. Silla, “GEPOL: An improved description of molecular surfaces. I. Building the spherical surface set,” *J. Comput. Chem.*, vol. 11, no. 9, pp. 1047–1060, 1990.
- [61] E. Ungersboeck, W. Gös, S. Dhar, H. Kosina, and S. Selberherr, “The effect of uniaxial stress on band structure and electron mobility of silicon,” *Math. Comput. Simul.*, vol. 79, no. 4, pp. 1071–1077, 2008.
- [62] S. Flodmark and E. Blokker, “A computer program for calculation of irreducible representations of finite groups,” *Int. J. Quantum Chem.*, vol. 1, no. 1 S, pp. 703–711, 1967.
- [63] V. Guillerm, Ł. J. Weseliński, Y. Belmabkhout, A. J. Cairns, V. D’Elia, Ł. Wojtas, K. Adil, and M. Eddaoudi, “Discovery and introduction of a (3,18)-connected net as an ideal blueprint for the design of metal-organic frameworks,” *Nat. Chem.*, vol. 6, no. 8, pp. 673–680, 2014.
- [64] SciPy Org, *scipy.signal.find_peaks — SciPy v1.4.1 Reference Guide*.

-
- [65] H. Coxeter, *Regular Polytopes*. Dover books on advanced mathematics, New York: Dover Publications, third ed., 1973.
- [66] J. Casey, *A treatise on Spherical Trigonometry*. London: Longmans Co, fifth ed., 1889.
- [67] H. S. Coxeter, “Wythoff’s construction for uniform polytopes,” *Proc. London Math. Soc.*, vol. s2-38, no. 1, pp. 327–339, 1935.
- [68] G. D. Tecnologías, *Manual de uso del supercomputador Quinde I*. Yachay EP, 2018.
- [69] S. Grimme, “Semiempirical gga-type density functional constructed with a long-range dispersion correction,” *Journal of Computational Chemistry*, vol. 27, no. 15, pp. 1787–1799, 2006.